1985

Low temperature thermodynamic properties of precipitation-hardening copper-beryllium alloys

Ronald L. Holtz
Iowa State University

Holtz, Ronald L.

LOW TEMPERATURE THERMODYNAMIC PROPERTIES OF PRECIPITATION-HARDENING COPPER-BERYLLIUM ALLOYS

Iowa State University PH.D. 1985

Low temperature thermodynamic properties of precipitation-hardening copper-beryllium alloys

by

Ronald L. Holtz

A Dissertation Submitted to the
Graduate Faculty in Partial Fulfillment of the
Requirements for the Degree of
DOCTOR OF PHILOSOPHY

Department: Physics
Major: Solid State Physics

Approved:

Signature was redacted for privacy.

In Charge of Major Work

Signature was redacted for privacy.

For the Major Department

Signature was redacted for privacy.

For the Graduate College

Iowa State University
Ames, Iowa

1985

TABLE OF CONTENTS

INTRODUCTION

Alloys of copper with approximately 2 weight percent beryllium have proven to be very useful technical materials. These alloys may be precipitation-hardened, which results in mechanical strengths comparable to stainless steels. For some applications requiring a high-strength material, copper-beryllium alloys have advantages over steels. Particularly important is that the copper-beryllium alloys are nonmagnetic, in contrast to the ferrous alloys. An important example of the use of precipitation-hardened copper-2 wt.% beryllium alloys is in the construction of diamond-anvil cells used for very high pressure experiments.

This Introduction gives a brief survey of topics which are discussed in detail in the following chapters. References are given in these later discussions.

Precipitation-hardening occurs in many alloys besides copper-beryllium, and two examples are copper-cobalt and copper-aluminum. This type of hardening may occur in an alloy when a supersaturated solid-solution of two or more component elements is allowed to decompose into a two-phase mixture. Controlled decomposition normally is accomplished by simple heat-treatment procedures. With appropriate combinations of heat-treatment times and temperatures, small and uniformly dispersed particles of a second phase form within the solid-solution. These precipitates may

strengthen the alloy by acting as obstacles to dislocation motion. In copper-beryllium, the solid-solution has the structure of pure copper and the precipitates are composed of the binary CuBe intermetallic phase.

Because of the importance of precipitation-hardening to materials applications, there has been much interest in the metallurgy of copper-beryllium alloys. The sequence by which decomposition and precipitation occurs has been studied extensively, as have precipitation-hardening mechanisms. The room temperature structures of the alloys in various conditions of hardness have been well characterized, as have the room temperature mechanical and elastic properties and their dependence on heat treatment. Very little work has been done on the low temperature metallurgical properties, however.

Previous work on the low temperature thermodynamic and transport properties of copper-beryllium alloys has been limited. Thermal expansivity, electrical resistivity, and thermal conductivity data have been reported, but in little detail and concerned only a few poorly characterized samples. Prior to the present work, no low temperature specific heat measurements have been reported.

The initial purpose of the present work was to provide precise thermal expansivity data required for a technical application of a commercial copper-2 wt.% beryllium alloy.

Data were obtained from 4 K to 300 K for a single precipitation-hardened sample of this alloy. The results were quite unexpected. Plots of the ratio of the alloy expansivity to that of pure copper as a function of temperature showed an anomalous 5 percent increase of the alloy expansivity peaking near 20 K. A second, unhardened, sample then was measured, and it was found that the magnitude of this expansivity enhancement appeared to depend on the state of hardness of the sample. Since this behavior was unfamiliar, and possibly an entirely new phenomenon, it was decided that further investigation was warranted.

Specific heat measurements from 1 K to 70 K were done on unhardened and precipitation-hardened samples of two commercially manufactured copper-2 wt.% beryllium alloys. A principal result of the specific heat studies was that the anomalous enhancement effect was found to be associated with the copper-beryllium solid-solution, rather than a feature of precipitation-hardening. Specifically, the specific heat of the solid-solution shows two main effects. One is that the contribution due to electrons is higher in the alloy than in copper, which may be partially attributed to the additional electrons contributed by the divalent beryllium. Secondly, the specific heat contribution due to lattice vibrations is nearly the same in both the alloy and copper. In fact, the solid-solution behavior is essentially the same

as for pure copper, but shifted to slightly lower temperatures. This slight shift of copper-like specific heat behavior shows up as a broad maximum in the ratio of the alloy to copper specific heats. It is believed that this specific heat shift is related to shifts of the frequencies of lattice vibrations caused by the presence of beryllium in copper.

The enhancement effect, then, actually is not an anomalous contribution to the specific heat of copper-beryllium alloys, but represents slight differences of the lattice dynamics between the alloys and copper. Such an effect may be present in other alloys, but has not been detected because of its relatively small magnitude and the broad temperature range over which it occurs.

There were several significant limitations to this work. Beryllium is toxic, which prevented the synthesis of pure samples since appropriate facilities were not available. This restricted the work to the use of technical-grade alloys, which were readily available. Such material is very impure, and in particular, iron and cobalt were present in all but one of the alloys studied. Large magnetic contributions to the specific heats can be associated with these two elements, and this prevented quantitative analysis of the results for most of the samples. The restriction to the use of commercially manufactured material

also prevented any study of the concentration dependence of the various properties.

Another problem was that quantitative comparisons of the experimental results with theoretical models were difficult. The beryllium is present in high concentrations, and has a quite different electronic structure from copper in addition to its much lighter mass. Simple models were used to account for the Debye temperature of the copper-beryllium solid-solution and its temperature dependence, but the effects of precipitation-hardening could not be entirely explained. The behavior of the electronic contribution to the specific heat was not resolved.

Still, this work is useful in that it reports the observation, characterization, and qualitative explanation of a previously unknown effect.

This paper is organized into four main sections besides this Introduction. The Background section gives a review of some very basic topics in solid state physics, and is intended to define parameters used later, and to discuss the principal contributions to the specific heat. The Copper-Beryllium Alloys section which follows describes the structure of the alloy and defines the terms used to describe the sample conditions. Precipitation-hardening and the sequence of precipitation are reviewed in that section.

The Experimental Results section first gives the

characteristics of the copper-beryllium samples, including the chemical compositions, heat-treatment conditions, densities, and Rockwell hardnesses. The thermal expansion results, which are published elsewhere, are then reviewed. The specific heat results on two copper-beryllium alloys are then discussed. Included are specific heat data for a pure copper sample which was used as a reference material, and a copper-cobalt alloy sample that provided an example of the effects of magnetic impurities. Electrical resistance measurements from 1 K to 80 K on one of the alloys are included, but are not discussed in detail.

In the Discussion section, qualitative arguments are given concerning the trends in the electronic specific heats, Debye temperatures, and lattice specific heats of the copper-beryllium alloys.

The Appendices include a review of the toxic properties of beryllium, some discussion of the experimental apparatus used, and tabulations of the experimental data.

BACKGROUND

Most of the topics discussed in this chapter are presented in a number of standard textbooks, so few references are given below. This author usually refers to Adkins (1) for topics in thermodynamics, Kubo (2) for statistical mechanics, and to Ashcroft and Mermin (3) for solid state physics. Useful reviews of the thermal expansivity and specific heat behaviors of solids are given, respectively, by Barron, Collins, and White (4), and by Gopal (5). References concerning particular experimental techniques are given in Appendix B of this work.

Thermodynamics

Simple thermodynamic systems are characterized by pressure (P), volume (V), and temperature (T). Two basic quantities that may be measured for such systems are the volume thermal expansivity, β, and the isothermal bulk modulus, B_T. These are given by

$$\beta = \frac{1}{V}\left(\frac{\partial V}{\partial T}\right)_P, \tag{1}$$

$$B_T = -V\left(\frac{\partial P}{\partial V}\right)_T. \tag{2}$$

This work reports measurements of linear thermal expansivity rather than volume expansivity. The linear expansivity, α, for a sample of length L, is defined as

$$\alpha = \frac{1}{L}\left(\frac{\partial L}{\partial T}\right)_P. \tag{3}$$

This quantity usually is simpler to measure than β. For materials with isotropic linear expansivities, $\beta = 3\alpha$. Anisotropic expansivities typically are related to anisotropies of the crystal structure, but can also be due to strains present in a material as the result of mechanical fabrication procedures such as extrusion or swaging. Such strains often may be relieved by annealing the material at high temperatures. The copper-beryllium alloys for which linear thermal expansivity measurements were done for the present work had been annealed.

Besides these equation of state properties, thermal properties may be measured. The heat capacity at constant volume, C_V, is defined in terms of the total energy, U, and the entropy, S, of the system as

$$C_V = \left(\frac{\partial U}{\partial T}\right)_V = T\left(\frac{\partial S}{\partial T}\right)_V. \tag{4}$$

The heat capacity data reported in this work were measured at constant pressure rather than constant volume. It is much simpler experimentally to maintain constant pressure than it is to hold the sample volume constant, while the constant volume heat capacity is easier to calculate theoretically. The relationship between C_P and C_V is

$$C_P = C_V + VT\beta^2 B_T. \tag{5}$$

At low temperatures, the difference between C_P and C_V is very small, and usually is neglected in comparisons between theory and experiment. As an example, for copper the magnitude of the correction term ($VT\beta^2B_T$) is only 0.0004% at 4 K, and rises smoothly to about 0.2% at 60 K. All of the materials studied have specific heats similar in magnitude to that of copper, and the corrections were of similar magnitude. The difference between C_P and C_V was neglected in the present work, since it was within the experimental uncertainty.

The bulk thermodynamic quantities described above can be related to the atomic details of a material through statistical mechanics analysis. The fundamental theoretical quantity is the partition function,

$$Z = \Sigma_S \exp(-E_S/k_BT), \tag{6}$$

where the sum is over all allowable states of the system. The total energy of the system in state S is E_S, and k_B is the Boltzmann constant. The Helmholtz free energy is then obtained from Z according to

$$F = -k_BT \ln Z. \tag{7}$$

The pressure and entropy may then be calculated from

$$P = -\left(\frac{\partial F}{\partial V}\right)_T, \tag{8}$$

$$S = -\left(\frac{\partial F}{\partial T}\right)_V . \tag{9}$$

The quantities B_T and C_V are obtained from P and S using the definitions in Eqns. 2 and 4, and β is found in terms of F by noting that

$$\beta B_T = \left(\frac{\partial P}{\partial T}\right)_V . \tag{10}$$

In certain simple systems, the free energy may be expressed as

$$F = U_0(V) + k_B T \Phi\left(\frac{\theta(V)}{T}\right) , \tag{11}$$

where U_0 is the total energy at zero temperature, and $\theta(V)$ is a characteristic temperature parameter that depends only on volume. The utility of this expression is that it leads to a simple relationship between the expansivity and heat capacity,

$$\beta = \frac{\Gamma C_V}{V B_T} . \tag{12}$$

This is known as the Grueneisen relation (4,6), with Γ the Grueneisen parameter, defined by

$$\Gamma = -\frac{\partial \ln\theta(V)}{\partial \ln V} . \tag{13}$$

This parameter is approximately a constant, with a magnitude near 2.

The Grueneisen relation may be generalized to multi-component systems for which there may be more than one characteristic temperature. A further generalization is to assume the validity of Eqn. 12, but to allow Γ to depend on temperature in addition to volume. Equations 11 and 13 are then no longer valid, but the phenomenological relationship thus obtained is very useful. For many solids, both Γ and B_T typically vary slowly with temperature, so that the expansivity is roughly proportional to the specific heat over wide ranges of temperature. If β, B_T, and C_V/V are all known, then Γ may be calculated, yielding information about the volume and temperature dependence of the energy levels of the system.

An elementary example of the application of statistical mechanics is to a collection of N independent particles, each of which has an energy that is one of a finite number of discrete energies. Specifically, if only 2 energies, 0 and ε, are allowed for each particle, the system is a two-level Schottky system, with heat capacity given by

$$C_{Schottky} = Nk_B\left(\frac{\Delta}{T}\right)^2 \exp(\Delta/T)[1+\exp(\Delta/T)]^{-2}, \qquad (14)$$

where Δ is a characteristic temperature defined by $\Delta = \varepsilon/k_B$. For temperatures much higher than Δ, this specific heat is approximately proportional to T^{-2}.

The principal contributions to the specific heats of

normal metals are due to electrons and lattice vibrations. For these systems, the distribution of energy levels generally is not simple, and the number of levels is essentially infinite. A useful formalism for such systems is in terms of the density of states, denoted by $g(\varepsilon)$ for electrons, and $D(\omega)$ for phonons. The density of states gives the number of one-particle energy levels per unit energy, per unit volume. In the case of phonons, it usually is expressed in terms of the phonon frequency ω, rather than energy, where $\omega = \varepsilon/\hbar$. A density of states function may be defined in terms of the number of atoms instead of the volume, but the volume density of states is used throughout this work.

Electrons

In the density of states formalism, the energy of a collection of electrons is

$$U = 2V_0 \int^{\infty} \varepsilon g(\varepsilon) f_{FD}(\varepsilon) d\varepsilon. \tag{15}$$

Here, $f_{FD}(\varepsilon)$ is the Fermi-Dirac distribution function,

$$f_{FD}(\varepsilon) = \left[\exp\left(\frac{\varepsilon-\mu}{k_B T}\right) + 1\right]^{-1}, \tag{16}$$

which describes the statistical probability that the state with energy ε is occupied, where μ is the chemical potential. The factor of 2 in front of the equation accounts for the spin degeneracy.

The Fermi energy, ε_F, is defined as the highest

occupied energy level of an electron gas in its ground state. At zero temperature, $\mu = \varepsilon_F$ and f_{FD} is a step function with value 1 for ε less than ε_F, and 0 for ε greater than ε_F. An important consequence of the functional form of $f_{FD}(\varepsilon)$ at nonzero temperatures is that, provided that $g(\varepsilon_F)$ is nonzero, the heat capacity of an electron gas is linear in temperature, and is given by

$$C_e = V\frac{\pi^2}{3} k_B{}^2 g(\varepsilon_F) T. \tag{17}$$

The simplest model of conduction electrons in a metal is the free-electron model. The energy of a free electron is just its kinetic energy $\varepsilon = \hbar^2 k^2/2m$, where $\hbar k$ is the electron momentum and m is the electron mass. The Fermi wavevector, k_F, is defined as the wavevector that corresponds to the Fermi energy. The only parameter in the free-electron model is the density of electrons, n_e. In terms of n_e, the Fermi wavevector is given by

$$k_F = (3\pi^2 n_e)^{1/3}. \tag{18}$$

The density of states for the free-electron model and its value at the Fermi level are given by

$$g_{free}(\varepsilon) = \frac{3}{2}\frac{n_e}{\varepsilon_F}\left(\frac{\varepsilon}{\varepsilon_F}\right)^{1/2}, \tag{19}$$

$$g_{free}(\varepsilon_F) = \frac{3}{2}\frac{n_e}{\varepsilon_F} = \frac{m}{\hbar^2\pi^2}(3\pi^2 n_e)^{1/3}. \tag{20}$$

The true value of $g(\varepsilon_F)$ for a metal, which is determined by specific heat measurements, often is very different from the free-electron value. A parameter that often is used to describe the difference is the effective mass, m^*, defined by

$$g(\varepsilon_F) = \frac{m^*}{m} g_{free}(\varepsilon_F). \tag{21}$$

As examples (3), the effective mass for pure copper is 1.3, and that for beryllium is 0.42.

Real metals contain atoms, of course, so the electrons are not free. In general, the actual dispersion relation, $\varepsilon(k)$, and the density of states are rather complicated functions, and cannot be fully described here. There are two effects that will be discussed. The first is that spatially periodic arrangements of the atoms in a metal produce gaps, or forbidden energies, in $\varepsilon(k)$. The density of states is zero for energies within these gaps, and may differ considerable from the free-electron model for energies near the gaps. The gaps occur at wavevectors given by $k = 2\pi/\lambda$, where λ is the wavelength of the periodic structure.

The second effect is that the energy levels associated with the valence electrons, which are discrete levels for free atoms, broaden into bands for atoms in a metal. The width in energy of the bands depends on the degree of

overlap of the wavefunctions of these states, or in effect, how close together the atoms are. The density of states for a narrow band can be quite high.

Pure copper is a relevant example of a real metal. The electronic density of states of copper (7) is smoothly varying, with no gaps, near ε_F (7.0 eV). The density of states near ε_F is approximately 30% higher than the free-electron prediction, and decreases with increasing energy (8). This is in contrast to the free-electron model, for which $g(\varepsilon)$ increases with ε, as shown by Eqn. 18. There also is a sharp peak in the density of states approximately 3 eV below the Fermi level, which is due to the band associated with the electron d-orbitals of the copper atom.

Phonons

The vibrations of the atoms in a solid also contribute to the heat capacity. A successful description of lattice vibrations, or phonons, is based on the harmonic approximation, which models the atoms as simple masses connected together by springs.

Even in the harmonic approximation, the dispersion relation, $\omega(k)$, and the density of states, $D(\omega)$, are complicated functions. Results for copper, as given by Sinha (9), serve as an example. One simple result, however, is that for long-wavelength, or acoustic, phonons the dispersion relation is approximately $\omega = ck$, where c is the magnitude

of the average sound velocity. The sound velocity depends on the direction of propagation and on the polarization, but very roughly depends on the lattice parameter a, some average spring constant κ, and an effective atomic mass M. For a periodic, one-dimensional monatomic chain, such a relation is exact and is given by $c = a(\kappa/M)^{1/2}$.

At low temperatures, only the lowest energy modes contribute significantly to the heat capacity. In view of this, a useful approximation is to use the linear dispersion relation, $\omega = ck$, for all values of k up to a maximum value k_D, given in terms of the density of atoms n_a by

$$k_D = (6\pi^2 n_a)^{1/3}. \tag{22}$$

This is the Debye approximation, and the density of states for this model is

$$D(\omega) = \frac{3}{2\pi^2}\frac{\omega^2}{c^3}. \tag{23}$$

The heat capacity due to lattice vibrations is given by

$$C_L = V\frac{\partial}{\partial T}\int_0^\infty D(\omega) f_{BE}(\omega)\hbar\omega d\omega, \tag{24}$$

where $f_{BE}(\omega)$ is the Bose-Einstein distribution function,

$$f_{BE}(\omega) = [\exp(\hbar\omega/k_B T) - 1]^{-1}. \tag{25}$$

The lattice heat capacity in the Debye model is given by the Debye function, which is tabulated in numerous

textbooks (5). A particularly simple result of the Debye model is that for sufficiently low temperature, the lattice heat capacity is given by

$$C_L = V \frac{12\pi^4}{5} n_a k_B \left(\frac{T}{\theta_o}\right)^3 . \qquad (26)$$

Here, θ_o is a characteristic temperature called the Debye temperature. For copper, θ_o is about 345 K, and for beryllium, it is about 1000 K (3). In terms of k_D and the sound velocity, it is given by

$$\theta_o = \frac{\hbar}{k_B} c k_D . \qquad (27)$$

The cubic temperature dependence is a good approximation to the lattice heat capacity of real materials for temperatures below about $\theta/30$. Above this, the full Debye function is a reasonable representation, with significant differences from Debye behavior typically appearing above $\theta/10$. The actual density of states usually increases more rapidly than ω^2, and a considerable amount of structure is present at high frequencies. The differences between observed heat capacity behavior and the ideal Debye model still may be described in the context of the model, however. This is done by representing the experimental lattice heat capacity with a Debye function, using a temperature-dependent Debye temperature as a fit parameter. Typically, $\theta(T)$ approaches the value θ_o at low temperatures, and then

decreases with increasing temperature. It reaches a minimum value of about $0.9\theta_0$ at temperatures near $\theta_0/5$, then approaches another constant value, θ_∞, at high temperatures. In general, θ_0 and θ_∞ are not equal.

Metals

Combination of the above results for electrons (Eqn. 17) and phonons (Eqn. 26), and division by the number of atoms, gives the low temperature molar specific heat of a normal metal as

$$C = \gamma T + \frac{12\pi^4}{5} R \left(\frac{T}{\theta_0}\right)^3 . \tag{28}$$

The electronic specific heat coefficient γ is related to $g(\varepsilon_F)$ by

$$\gamma n_a = \frac{\pi^2}{3} R k_B g(\varepsilon_F) . \tag{29}$$

A plot of C/T versus T^2 for a normal metal, for sufficiently low temperatures, is approximately a straight line. The $T^2 = 0$ intercept of the line is the coefficient γ, and its slope is proportional to θ_0^{-3}. Because of the Grueneisen relation, α/T versus T^2 also is nearly linear at low temperatures.

Specific heat data often are analyzed by performing linear least-squares fits of C/T versus T^2, using Eqn. 28, but including higher-order odd powers of T. This procedure provides a useful analytic representation of the data in

addition to the parameters γ and θ_0. Calculation of $\theta(T)$ may then be done by subtracting the electronic contribution from the total specific heat, and using the procedure outlined on page 17.

For the present study of copper-beryllium alloys, a useful method of displaying the specific heat results proved to be plotting the ratio C/C_{copper} versus temperature. The alloy specific heats are within ten percent of the specific heat of copper at all temperatures, so the ratio emphasizes small effects more clearly than any display of the alloy data alone.

Prior to the actual specific heat measurements, it was not known exactly what behaviors would be found. The beryllium concentration in the copper-beryllium alloys is high (2 wt.% is nearly 12 atomic percent) so that models based on low impurity concentrations were unlikely to be valid. In the solid-solution, the beryllium distribution was known to be disordered, so the alloy could not be thought of as an intermetallic compound. The two-phase mixture resulting from precipitation-hardening could be modeled simply as a two-phase material consisting of copper and the intermetallic compound CuBe, but no information on the properties of CuBe could be found.

Because beryllium is divalent and copper is monovalent, the number and density of electrons in the solid-solution

would be higher than in copper. This would increase the electronic density of states according to the free-electron model. However, since the electronic structure of beryllium is quite different from that of copper, the effects on the actual dispersion relation could not be predicted.

Beryllium has a much lighter mass than copper, and this would tend to increase the sound velocities and the Debye temperature in the solid-solution. The force constants associated with the beryllium, which were not known, would also cause some changes that could not be predicted.

One effect which was expected was the existence of local modes of oscillation (LMO) of the light beryllium atoms within the heavier copper host lattice (10). These vibrations occur with a single frequency, ω_{LMO}, and their molar specific heat contribution is given by the Einstein approximation,

$$C_{Einstein} = R(T_E/T)^2 \exp(T_E/T)[\exp(T_E/T)-1]^{-2}. \qquad (30)$$

The Einstein temperature, T_E, corresponding the the LMO frequency is given by $T_E = (\hbar/k_B)\omega_{LMO}$ and is approximately 490 K (10). The specific heat contribution due to these modes is negligible at low temperatures.

Magnetic Impurities

Most of the copper-beryllium alloy samples that were studied contained significant concentrations of iron and

cobalt. About 0.2 wt.% cobalt is added to commercial alloys intentionally for metallurgical reasons to be discussed later. The iron is present in roughly the same amount, but its presence is due to impure constituent materials. An undesirable result of the presence of cobalt and iron in the samples is the presence of large magnetic contributions to the specific heats. This prevented quantitative analysis of the results, except for two samples of a low iron concentration alloy.

Interaction of the magnetic moments of the cobalt and iron with external magnetic fields would produce a Schottky contribution to the specific heat, but this was not a consideration in the present work. Interaction of the moments with each other and with the conduction electrons results in more complicated magnetic specific heat contributions which cannot be fully considered here, but will be described briefly.

Cobalt tends to form clusters when present in copper, and the cobalt magnetic moments within the clusters arrange themselves antiferromagnetically at low temperatures (11). This causes a rapid rise of the specific heat as temperature decreases that becomes apparent below 10 K, and peaks below 1 K. This contribution may be nearly 50% of the total specific heat near 1 K for a copper-2.0 wt.% cobalt alloy. The precise magnitude of the contribution depends on the

sizes of the clusters and the cobalt concentration within the clusters, and these depend sensitively on sample preparation procedures. Since the contribution could not be calculated with confidence, it could not be accurately accounted for in the copper-beryllium alloy results.

Iron also tends to cluster when alloyed with copper, and the clusters could order ferromagnetically. This was not observed, but another effect was. Moments on isolated iron atoms interact with the conduction electron moments (12), and this also contributes to the specific heat (13). The temperature dependence and magnitude of this contribution is similar to that discussed above due to cobalt, but the source of the effect is quite different.

The interaction responsible for the magnetic specific heat contribution in copper-iron alloys also results in a minimum in the electrical resistivity near 20 K. The resistivity of normal metals arises from the scattering of electrons from impurities and from phonons. Scattering from nonmagnetic impurities is independent of temperature, and contributes a constant term, ρ_0, to the resistivity. Phonon scattering results in a resistivity contribution that is roughly proportional to T^5 at low temperatures, below approximately 40 K, and proportional to T at higher temperatures. Electron scattering from magnetic impurities is inelastic, involving changes in the electron and impurity

spins, and its temperature dependence is logarithmic above 1 K.

Between 1 K and 40 K, the resistivity for a metal containing a concentration c of magnetic impurities is given by Kondo (14) as

$$\rho(T) = aT^5 + \rho_0 - c\rho_1 \ln T \ . \tag{31}$$

The minimum in the resistivity occurs at the temperature

$$T_{min} = \left(\frac{c\rho_1}{5a}\right)^{1/5}, \tag{32}$$

and the depth of the minimum is given by

$$\rho(0)-\rho_{min} = c\rho_1\left[\ln\left(\frac{T}{T_0}\right)+\frac{1}{5}\right]. \tag{33}$$

In the above equation, T_0 contains details of the magnetic interactions, but may be taken as 1 K.

COPPER-BERYLLIUM ALLOYS

The equilibrium phase diagram (15) for the copper-beryllium binary alloy system is shown in Figure 1, with the principal solid phases denoted by α, β, γ, δ, and Be. Dashed lines in the diagram indicate estimated phase boundaries where information is incomplete or lacking.

The α phase is a disordered solid-solution of Be in Cu with the face-centered cubic (FCC) structure. The lattice parameter, a, depends linearly on Be concentration (16), with a = 3.615 A for pure copper, decreasing to 3.570 A at 13 atomic percent (2.1 weight percent) Be.

The β phase is a disordered solid-solution of Be and Cu with the body-centered cubic (BCC) structure and a = 2.79 A. The γ phase is the CuBe intermetallic compound with the CsCl-type BCC structure and a = 2.7 A. Above 880 ^{o}C the transition between β and γ is continuous, with γ representing an ordered version of β. γ sometimes is referred to as β', but recent convention has been the use of γ.

The δ phase is nominally the $CuBe_3$ intermetallic compound, although the homogeneity range is quite wide (70 to 80 at. % Be). It has the C15 structure (17), space group Fd3m, analogous to Cu_2Mg. The lattice parameter is 5.95 A for copper-rich compositions, decreasing to 5.90 A for beryllium-rich compositions.

At the Be end of the phase diagram, the structure is an

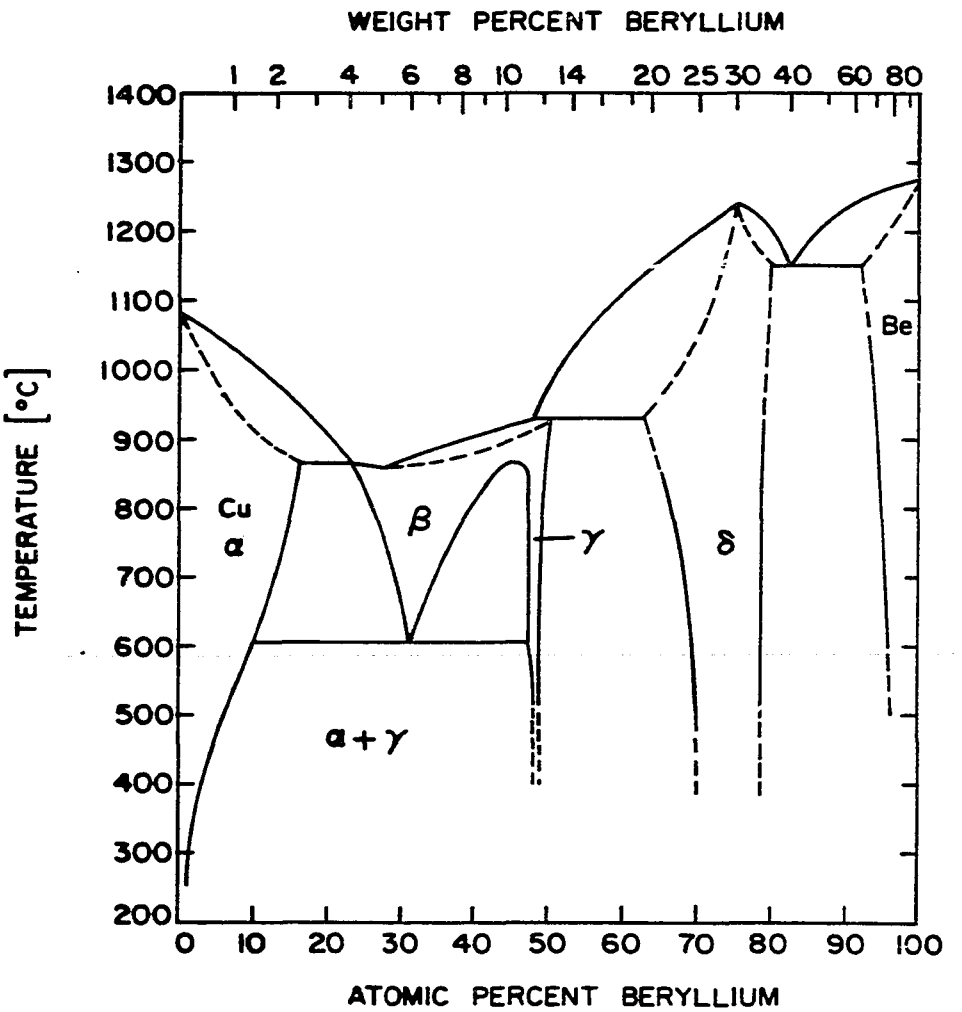

Figure 1. Copper-beryllium phase diagram, based on data given in Ref. 15

hexagonal close-packed (HCP) solid-solution of Cu in Be. For pure Be, the hexagonal lattice parameters a and c are 2.28 A and 3.58 A, respectively. Several types of cubic phases of Be, some of which are superconducting (18,19), have been stabilized with small concentrations of Cu.

The region of the phase diagram relevant to this work is the α solid-solution and the $\alpha + \gamma$ two-phase region for Be concentrations near 2 wt.% (12 at.%). Metastable supersaturated solid-solutions of Cu-2 wt.% Be are prepared by annealing between 750 ^{o}C and 850 ^{o}C, then rapidly quenching to room temperature. This procedure is referred to throughout this work as solution-annealing. Heat treatment of solution-annealed material below 600 ^{o}C results in the precipitation of regions of the γ-phase from the supersaturated solid-solution. Extensive literature exists on the precipitation process since it is of great interest to metallurgists.

Precipitation Sequence

Decomposition of the supersaturated solid-solution begins with the formation of Guinier-Preston (GP) zones (20). A single GP zone is a planar, monolayer accumulation of Be at sites along a {100} plane of the FCC lattice. The FCC lattice is preserved, but there is a local contraction of the lattice due to the smaller atomic size of Be than Cu. The Young's modulus of FCC metals is minimum in directions

perpendicular to {100} planes, so it is along these planes that the distortion is most easily accommodated (21).

The GP zones are disk-shaped, of monolayer thickness (2-3 A), and up to several hundred angstroms in diameter (22). The diameter depends on heat treatment time and temperature. For aging at 100 ^{o}C, the diameter is generally 10-30 A after 100 hours. At 200 ^{o}C, the zone diameters are about 70 A after 1 hour. The GP zones are stacked together in an ordered structure with a separation between disk faces of approximately 3 times the FCC lattice constant. This structure has been described as an "abutting stair-step" arrangement (23).

Crystal defects such as vacancies, impurities, dislocations, and grain boundaries are nucleation sites for zone formation (24). There is some evidence for the presence of spherical clusters of Be of 10-50 A diameter in solution-annealed material (25). These may be precursors to GP zone formation, but this is not certain since the clusters have been observed only at room temperature, and are not always present. Strain modulations of about 30 A periodicity are also present in solution-annealed Cu-Be (26). Such strain modulations apparently are common to many alloys that undergo martensitic phase transitions, but it is not known at present how this effect is related to the GP zones in Cu-Be.

As the GP zones grow in size, their crystal structure undergoes a series of modifications before the equilibrium γ-phase results. Two distinct intermediate phases have been identified (25), denoted γ' and γ''. These are metastable tetragonal distortions of the FCC parent lattice. For aging temperatures below 450 ^{o}C, the sequence of precipitation is GP zones $\rightarrow \gamma'' \rightarrow \gamma' \rightarrow \gamma$. At higher temperatures, the γ'' phase does not occur. At some stage during the precipitation process, regions of zones coalesce into larger precipitates.

The equilibrium structure of the decomposed Cu-Be solid-solution is an FCC matrix containing precipitates of γ. The matrix is an equilibrium, saturated solid-solution of Be in Cu. Because the decomposition occurs through a sequence of zone growth and structure changes, the γ-phase precipitates are structurally related to the matrix, with the relationship depending on the exact sequence of intermediate phases (25). Below 450 ^{o}C, the γ (100) plane is parallel to the matrix (110) plane and the [100] directions of both matrix and precipitate are parallel. For treatments above 450 ^{o}C, the relationship is $(111)_{\alpha} || (100)_{\gamma}$ and $[110]_{\alpha} || [111]_{\gamma}$.

Typical dimensions of the disk-shaped precipitates are 100 to 300 A thick, and 5000 to 10,000 A diameter. The separation between disk faces is generally several hundred

angstroms. Precipitates occupy approximately 20 percent of the volume of the alloy at equilibrium.

The highly distorted nature of the alloy crystal structure in both the solution-annealed and precipitated conditions is evident in the x-ray diffraction pattern. Figure 2 shows the (111) and (200) x-ray diffraction peaks which we obtained for solution-annealed Berylco-25 alloy, which is a commercial alloy containing 1.8 wt.% Be. The overall pattern (not shown) is that of an FCC lattice with a lattice parameter of 3.575 A. The peaks are rather broad, reflecting the lattice contraction around the Be atoms. These same two peaks are shown in Figure 3 for a sample that had been treated at 320 ^{o}C for 2 hours. The overall pattern still resembles FCC, but the peaks are now very broad and much reduced in maximum intensity, with the asymmetric line-shapes caused by the presence of two nearly overlapping, unresolved peaks (27). One peak is that of the FCC matrix, and the other is due to the tetragonal distortion of FCC representing the precipitate structure. A distinct BCC diffraction pattern corresponding to the equilibrium precipitate structure does not show up except for long treatment times at high temperatures, for which the precipitates become large.

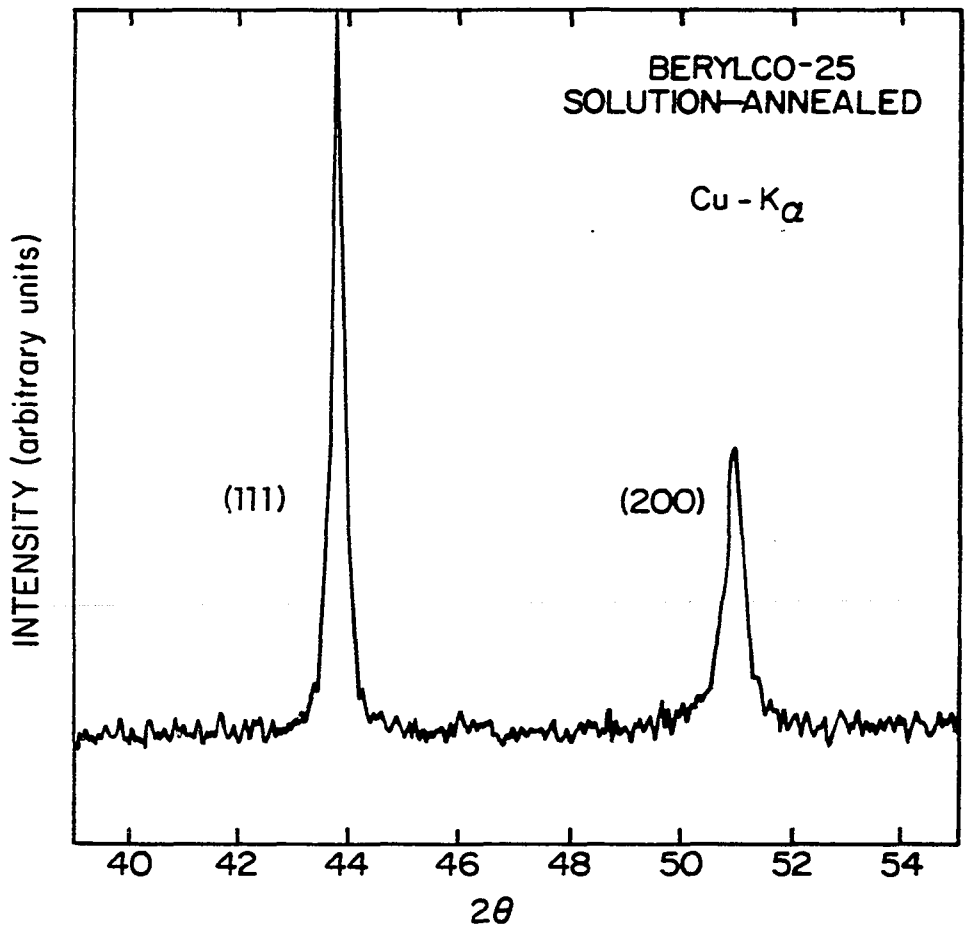

Figure 2. (111) and (200) x-ray diffraction peaks for solution-annealed Berylco-25

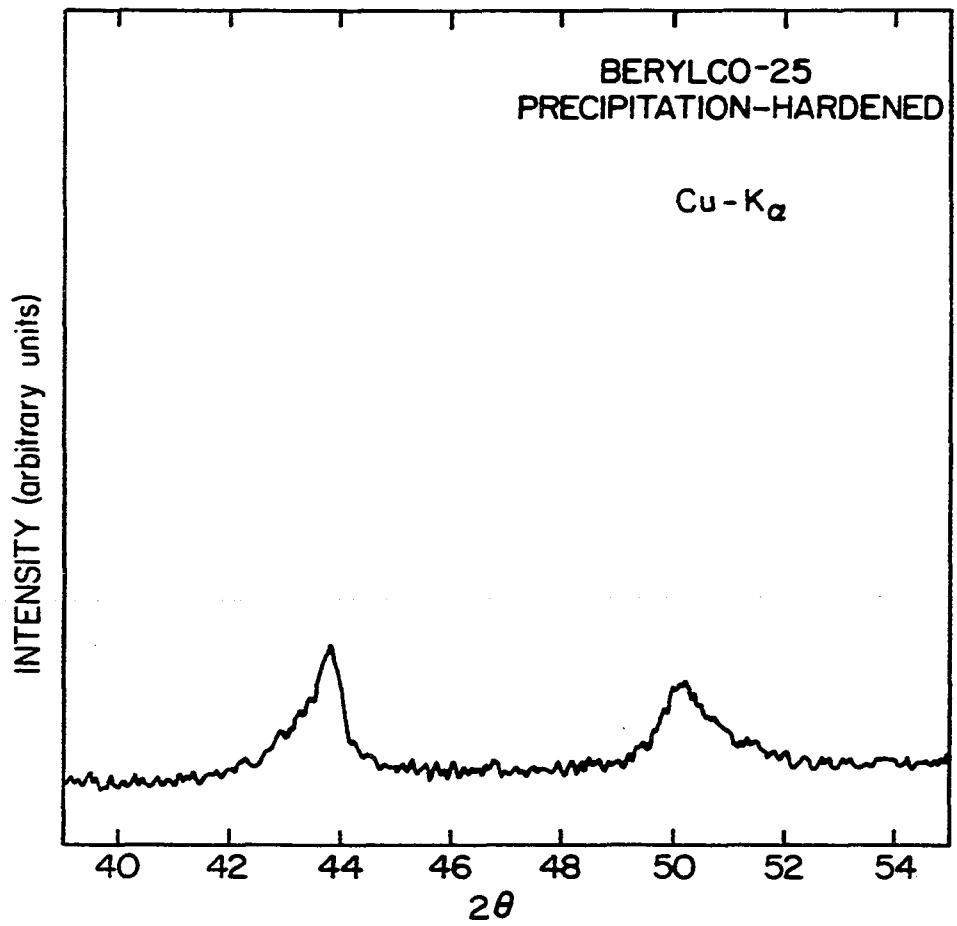

Figure 3. (111) and (200) x-ray diffraction peaks for precipitation-hardened Berylco-25

Precipitation-hardening

The presence of γ-phase particles results in the phenomenon of precipitation-hardening. Precipitates act as obstacles to line dislocation motion, strengthening the material. The particles do not necessarily have to be intrinsically hard. A review of precipitation-hardening is given by Kelly and Nicholson (24), and a more recent text is by Martin (28). Only a crude description is given below.

When a line dislocation encounters a precipitate on passing through a crystal, additional force may be required for it to proceed further. The dislocation must either slice through the particle or stretch around it. Resistance to shearing of a precipitate may come from several effects. If the precipitate lattice is coherent with the surrounding matrix, energy is required to destroy the coherency. This is the primary strengthening mechanism in copper-cobalt alloys (28). If the surface energy associated with a precipitate is high, shearing is resisted since it would create an additional precipitate-matrix interface. This effect is called chemical hardening, and is thought to be the important mechanism in copper-beryllium alloys (29).

Coherency and chemical hardening both involve the precipitate-matrix interface. Hardening may also depend on the bulk precipitate properties. Modulus hardening occurs if the precipitate is inherently harder than the matrix.

Stacking-fault hardening and order hardening both involve resistance to dislocation-induced changes in precipitate crystal structure.

If the energy required to shear a precipitate is very large, it may require less energy for a line dislocation to bypass the obstacle. This requires that the dislocation line stretch around it, and energy is required to increase the dislocation length. Large precipitates or closely spaced small ones are not easily bypassed, but small and widely spaced precipitates are. Another bypass mechanism, known as Orowan looping (28), is possible. This happens if a dislocation stretches completely around a precipitate, then tears away from it, leaving a dislocation loop around the obstacle.

In precipitation-hardened Cu-Be alloys, maximum strengthening results for a high concentration of small, closely spaced, precipitates. This configuration provides a large total precipitate surface area, enhancing the chemical hardening. Although the particle sizes are small, the close spacing resists dislocation stretching and looping.

For heat treatment at a fixed temperature, the strength of the alloy gradually increases with treatment time as the GP zones grow in size. At some time, maximum strength is attained when the optimal precipitate size and spacing is reached. Further treatment may result in the coalescing of

regions of small precipitates into a few larger ones. This is known as discontinuous precipitation. The strength is reduced since the total surface area of precipitates decreases. Commercial Cu-Be alloys contain small amounts of cobalt. This is known to inhibit discontinuous precipitation (28), but the mechanism is not understood. Trace impurities also provide additional nucleation sites for GP zone formation (24), thus improving the final strength.

Commercial Alloys

Commercial precipitation-hardening Cu-Be alloys are of two main types. Those with low Be concentration (less than 1 wt.%) are used for applications requiring moderate strength and moderate electrical and thermal conductivity. Alloys with approximately 2 wt.% Be have lower conductivities, but final heat treated strength comparable to stainless steel. Some advantages of Cu-Be alloys over steels are that they are nonmagnetic, ductile, and may be fabricated in a soft condition prior to precipitation-hardening. These 2 wt.% Be alloys are designated by the American Society for Metals (ASM) as Copper Alloys UNS #17200. The composition tolerances by weight percent are (30):

Be 1.8 - 2.0

Ni + Co 0.2 minimum

Ni + Co + Fe 0.6 maximum

Pb 0.1 maximum

all others 0.5 maximum

balance copper

A typical and widely used alloy of this class is Berylco-25, manufactured by Cabot Berylco (USA). Nominal composition by weight of this alloy is 1.9% Be and 0.2% Co. CUBE-250, made by Telcon Metals, LTD (UK) is similar, with 1.8% Be and 0.25% Co. There are many others, and a listing is given by Ross (31).

Iron often is present in commercial Cu-Be alloys, probably due to impure constituent materials. Iron increases the low temperature magnetic susceptibility, and for this reason its presence is not desirable for certain research applications. For most commercial applications, however, iron content is not a problem. Low-iron Cu-Be alloys may be specially ordered from various manufacturers, but are not standard commercial material.

Cu-Be alloys may be obtained in various tempers, or states of hardness. Fabrication of the alloy involves solution-annealing, followed by rolling, extrusion, or other processes that work-harden the material. Material that has been solution-annealed after all fabrication steps is designated as temper A in most commercial literature. The temper designation H, for hard, is for material that is not solution-annealed after, or at any stage during,

fabrication. Half-hard, 1/2-H, designates material that is solution-annealed after initial rough forming, but prior to final rolling. Other standard tempers are 1/4-H and 3/4-H. The temper designation for precipitation-hardened material is the letter T following the designation of the initial temper. For example, initially half-hard material that has been precipitation-hardened is designated 1/2-HT.

Temper A has the advantage that the alloy is fairly soft in this condition, and easy to machine. The work-hardened tempers 1/2-H and H are more difficult to machine, but have somewhat greater final strength after precipitation-hardening. This is because the work introduces a high dislocation density, and as mentioned before, these act as GP zone nucleation sites.

A typical solution-annealing treatment is 1 hour at 800 ^{o}C for each inch of part thickness. Rapidly quenching to room temperature after this treatment freezes in the high vacancy concentration associated with the high aging temperature. This allows for higher nucleation and diffusion rates during the precipitation process. An optimal precipitation-hardening treatment is 2 or 3 hours at 300 to 350 ^{o}C.

Detailed heat treatment procedures and data concerning mechanical properties are available from the manufacturers of Cu-Be alloys. An overview is given in the ASM Metals Handbook (30). A very detailed study of the mechanical

properties, including the effect of Be concentration, is given in the American Society for Testing and Materials (ASTM) Special Technical Publication No. 367 (32). Some of the low temperature mechanical properties have been reviewed by Richards and Brick (33).

EXPERIMENTAL RESULTS

Three Cu-Be alloys were studied, all of them from commercial sources. Linear thermal expansivity measurements from 4 K to 300 K were done on CUBE-250 and Berylco-25. CUBE-250 has a nominal composition of 1.8 wt.% Be and 0.25 wt.% Co, and is made by Telcon Metals, Ltd. (UK). The samples were provided in final heat-treated and machined form by J.E. Martin of the National Physical Laboratory, England. Berylco-25, manufactured by Cabot Berylco (USA), has a nominal composition of 1.9 wt.% Be and 0.2 wt.% Co.

Specific heat measurements from 1 K to 70 K were done on Berylco-25 and a low iron concentration alloy with 1.92 wt.% Be, produced by Kawecki Berylco (USA). The low-iron alloy samples were provided in heat-treated condition by J. Schilling of the Ruhr-Universitat, Bochum, West Germany. The specific heat and expansivity samples of Berylco-25 were made from material which was on hand, purchased from 1956 to 1959. Electrical resistance measurements from 1 K to 80 K were done on recently purchased Berylco-25 strip.

A copper sample, used as a specific heat and density standard, was made from 99.999 % pure ASARCO (American Smelting and Refining Company) copper. The material had previously been electron-beam melted into an ingot, then swaged to 5/8 inch diameter rod. The sample was strain-annealed for 2 hours at 300 ^{o}C after final machining.

A Cu-2 wt.% Co sample, used for thermal expansion measurements by Rehak (34), was included in the specific heat studies. The condition of this sample was not altered, and is believed to be an equilibrium Cu-Co solid-solution matrix containing precipitates of Co. Further details of the state of this sample are discussed by Rehak.

All of the experiments and data analysis employed standard techniques, and these are discussed in Appendix B. All of the experimental data are included in Appendix C.

Cu-Be Sample Characteristics

The Berylco-25 specific heat samples were made from two different lots of material. Samples made from 1/2 inch diameter round rod were designated with an "R", and those made from 5/8 inch thick hexagonal rod were designated with an "H". Numbers were also used in the Berylco-25 sample designations to distinguish individual specimens, but have no other significance. The 1/8 inch wide, 0.01 inch thick strip samples for resistance and x-ray diffraction measurements were designated with an "S". The low-iron alloy and CUBE-250 samples were designated simply as SA (solution-annealed) or PH (precipitation-hardened), since these were the only two conditions studied.

Table 1 lists the concentrations of Be, Co, and Fe in the Berylco-25 R, CUBE-250, and low-iron samples. The molecular weights listed were calculated from the

Table 1. Concentrations of principal constituents in the Cu-Be alloys

Alloy	Be	Co	Fe	Molecular Weight (gm/mole)
	Weight percent[a]			
Berylco-25	1.78	0.24	0.186	57.35
CUBE-250	2.03	0.348	0.0491	56.56
Low-iron Cu-Be	1.92[b]	0.04[b]	0.0013[c]	56.93
	Atomic percent			
Berylco-25	11.30	0.23	0.188	
CUBE-250	12.74	0.334	0.0497	
Low-iron Cu-Be	12.13	0.04	0.0013	

[a]Determined by atomic absorption spectroscopy unless noted otherwise.

[b]Determined by manufacturer, method unknown.

[c]From low-temperature magnetic susceptibility measurements.

concentrations. The exact Be, Co, and Fe concentrations in the Berylco-25 R and the CUBE-250 materials were determined by M. Tschetter (Ames Laboratory) using an atomic absorption spectroscopy method. The low-iron alloy composition was provided by the manufacturer (35), but the method of determination was not specified. The Fe concentration in the low-iron alloy was determined by low temperature magnetic susceptibility measurements (36). No chemical analysis was done on the H or S Berylco-25 samples.

The elemental composition of the Berylco-25 R samples was determined by an arc-source mass spectroscopy method (performed by R. Conzemius, Ames Laboratory), and is listed in Table 2. The manufacturer-determined low-iron alloy composition also is listed for comparison. The arc-source method is much less precise than the atomic absorption technique, so can be used only for qualitative comparisons. Discrepancies in the Berylco-25 Co and Fe concentrations between Tables 1 and 2 are due to this lack of precision, and so are of no significance.

The primary difference between the low-iron alloy and Berylco-25 is in the Fe concentration. Both alloys have roughly the same amounts of Al, Si, and Co. Apparently, the low-iron alloy has higher concentrations of Ni, Zn, Ag, and Sn than Berylco-25. Since the method of determination, and hence the precision, used by the manufacturer for the

Table 2. Impurity analysis for Berylco-25 and the low-iron alloy

Element	Concentration in atomic ppm	
	Berylco-25[a]	Low-iron Cu-Be[b]
B	10	
C	20	
O	300	
Mg	60	
Al	200	200
Si	400	300
P	20	
Cr	20	20
Mn	10	20[c]
Fe	600	13[c]
Co	600	400
Ni	37	100
Zn	40	200
Ag	6.5	110
Sn	34	200
Pb	20	20

[a]Arc-source mass spectroscopy.

[b]Manufacturer's determination, method not known.

[c]By low temperature magnetic susceptibility.

low-iron alloy is not known, the above comparison may not be meaningful.

Heat-treatment of all of the Berylco-25 samples was done with the samples sealed inside quartz tubes with a small amount of helium or argon gas. This was done to prevent oxidation of the samples, while allowing for better heat transfer than was possible in a vacuum oven. Oxidation of Cu-Be alloys during precipitation-hardening has very little effect on attainable strength, and is not a concern in commercial applications. Oxidation will also eliminate the Fe magnetic moment, with the desirable result of lowering the low temperature susceptibility (36). It was decided, however, that since the degree of oxidation could not be controlled, it would be prevented so as to avoid further complicating the sample conditions.

Solution-annealing treatment in all cases was 1 hour at 800 ^{o}C, followed by rapid quench to room temperature. Some of the samples were left in the half-hard condition so that the influence of cold-work on the specific heat could be studied. A standard precipitation-hardening treatment of 2 hours at 320 ^{o}C was given some of the samples. One sample was "overaged" for 21 hours at 450 ^{o}C, and its condition should represent equilibrium at that temperature. Another series of solution-annealed samples was treated at 250 ^{o}C for 1, 2, and 4 hours, to examine the evolution of changes

in the specific heat during precipitation. Table 3 lists all of the samples and their heat-treatment conditions. The density, Rockwell hardness, and experimental history for each sample are included.

Densities were determined by a standard hydrostatic method. A sample is weighed in air to obtain its "dry" weight, W_d, then is weighed while immersed in a liquid, to obtain its "wet" weight, W_w. The difference $W_d - W_w$ is the bouyant force $\rho_l V$, where ρ_l is the density of the liquid, and V is the sample volume. The sample density is then calculated from

$$\rho = \frac{\rho_l W_d}{(W_d - W_w)}. \qquad (34)$$

Performing the measurements on a reference sample of known density allows determination of ρ_l.

The pure copper specific heat sample density was determined using high purity water, and tabulated values of the density of water (37). The result was 8.94 ±0.01 gm/cm^3, with the uncertainty due primarily to uncertainty in the water density. The two CUBE-250 samples also were measured in this manner, and with the same accuracy, but in ordinary deionized water. The remainder of the samples, except for the Berylco-25 strips, were measured using the copper sample as a density reference. The precision of the sample densities relative to copper is about ±0.02%. The accuracy of

Table 3. Sample characteristics

Sample	Condition[a]	Density (ρ/ρ_{Cu})	Rockwell hardness	Exp[b]
Berylco-25				
R10	1/2-H	0.9227	C24	A
R11	A	0.9281	B61	C
R12	AT(1/250)	0.9311	B99	C
R13	AT(2/250)	0.9318	C23	C
R14	AT(4/250)	0.9322	C30	C
H1	1/2-HT(21.3/450)	0.9314	B95	C
H2	1/2-H	0.9289	B99	C
H4	A	-	-	T
H6	A	0.9294	B61	C
H7	AT(2/320)	0.9315	C36	C,T
H8	1/2-HT(2/320)	0.9361	C38	C
S1	A	0.9293	-	R,X
S2	AT(2/320)	-	-	R,X
CUBE-250				
SA	A	0.930	B61	A,T
PH	AT(4/330)	0.935	-	T
Low-iron Cu-Be				
SA	A	0.9244	B65	C
PH	AT(2/290)	0.9289	C32	C

[a]A denotes solution-annealed, 1/2-H denotes half-hard, and T(t/T) denotes precipitation-hardened t hours at T °C.

[b]Experiments done: A = chemical analysis, C = specific heat, T = thermal expansivity, R = electrical resistance, X = x-ray diffraction.

the absolute densities depends, of course, on the accuracy of the copper density.

X-ray diffraction lattice parameter measurements on the solution-annealed Berylco-25 strip gave a calculated density of 8.3265 ±0.0001 gm/cm^3. Compared to the hydrostatic density of other solution-annealed Berylco-25 samples, this figure is about 0.2 % high. The difference is not unusual, since the X-ray determination ignores vacancies.

The effect of heat-treatment on the density is shown in Figure 4. The solid curve through the data for the samples treated at 250 ^{o}C is the exponential function

$$\frac{\rho(t)-\rho(0)}{\rho(0)} = a[1 - \exp(-bt)], \qquad (35)$$

which describes the decomposition of the solid-solution as a simple decay process. This relation fits the data exactly with a = 0.0044 and b = 1.28 hr^{-1}, giving a time constant for precipitate growth at 250 ^{o}C of about 0.78 hours. In general, the density of a Cu-Be alloy sample will increase a few tenths of a percent during precipitation-hardening. It cannot, however, be accurately predicted, because the actual change is sensitive to treatment temperature and initial temper. In addition, the dimensional changes for half-hard material may not be isotropic due to the residual strain induced by the fabrication processes. For example, solution-annealing of half-hard samples typically resulted

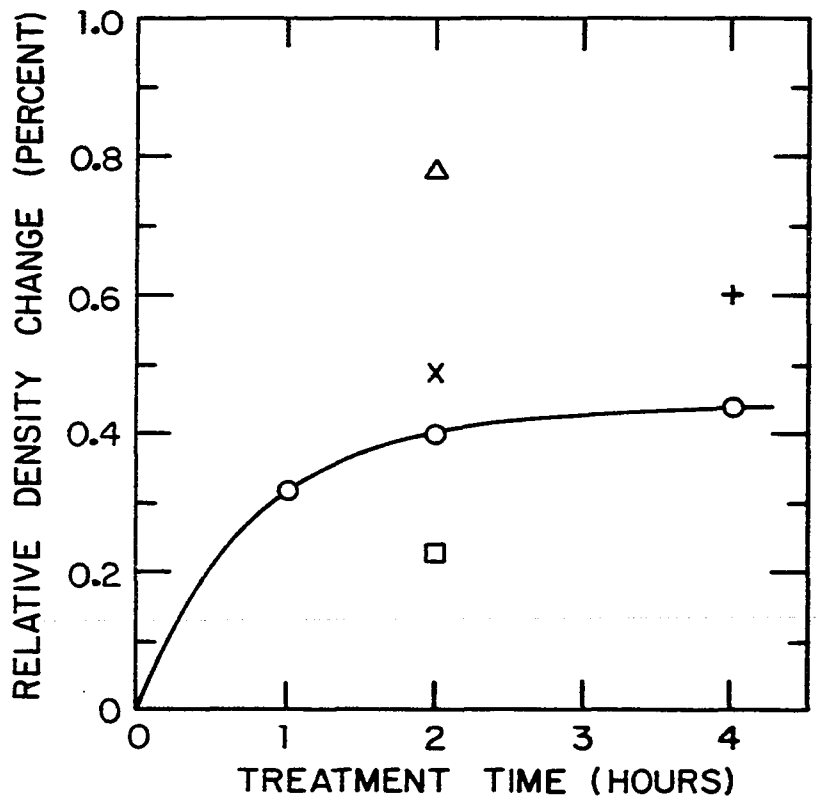

Figure 4. Relative density change during precipitation-hardening. The symbols indicate the alloy, temper, and precipitation-hardening temperature in ^{o}C as follows: o = Berylco-25, AT(250); □ = Berylco-25, AT(320); Δ = Berylco-25, 1/2-HT(320); x = low-iron Cu-Be, AT(290); + = CUBE-250, AT(330)

in a relative length decrease of about 0.1%, but no detectable change in the diameter.

Vegard's law (38) assumes that the density of a two-phase material is given by

$$\rho = \rho_1(1-f) + \rho_2 f, \qquad (36)$$

where ρ_1 is the density of phase 1, ρ_2 that of phase 2, and f is the volume fraction of the second phase. As an example, the equilibrium volume fraction of precipitates (f) is approximately 20% for an alloy with 12 at.% Be treated at 320 ^{o}C. The Be concentration in the equilibrium saturated solid-solution at this temperature is about 2 at.%. From lattice constant information (16), the density of the 2 at.% solid-solution is theoretically 8.863 gm/cm^3, which is taken as ρ_1 in Vegard's law. The density of the γ-phase (ρ_2) is theoretically 6.16 gm/cm^3. Using this information, Vegard's law predicts an equilibrium density after precipitation-hardening of 8.347 gm/cm^3. For the 12 at.% solid-solution, representing the solution-annealed condition, the theoretical density is 8.334 gm/cm^3. Vegard's law then predicts only a 0.16% increase in density during precipitation-hardening. Allowing a few tenths of a percent in the solution-annealed density to account for quenched-in vacancies raises the Vegard's law estimate to 0.4 to 0.5%. The conclusion is that Vegard's law can provide a crude

estimate of the densities of Cu-Be alloys, but does not agree in all the details with measured values.

The Rockwell hardnesses (39) were measured with a Wilson Model 3JR hardness tester. The results all agree with commercial specifications and other literature (30,32), and are sensitive enough to be used as a characterization of the samples. Figure 5 shows the Rockwell hardnesses, and it is seen that the trends agree with the general discussion of precipitation-hardening given in an earlier chapter. Hardness is improved with the presence of small concentrations of Co and Fe, as shown by the much greater hardnesses of Berylco-25 as compared to the low-iron alloy. Initially half-hard material is harder after treatment than initially solution-annealed material. The Rockwell hardnesses of the solution-annealed samples are not shown in Figure 5, but are typically B60 to B65, while half-hard samples are typically B95 to B100. The Rockwell C and B scales are not related in a simple manner, but B95 corresponds roughly to C20, and B60 is somewhat lower than C0. For comparison, the pure copper specific heat sample has a Rockwell hardness of E42, which corresponds roughly to B0.

Thermal Expansivity

Thermal expansion measurements on Cu-Be alloys have been done previously, primarily to provide technical

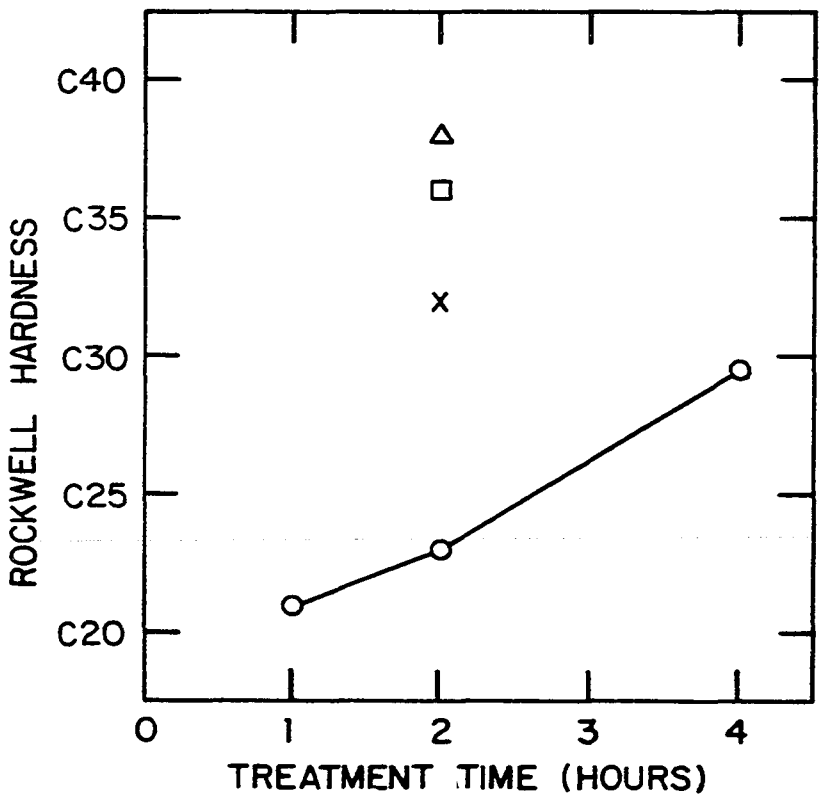

Figure 5. Rockwell hardness after precipitation-hardening. Refer to the caption of Figure 4 for the symbol definitions

reference data. Beenakker and Swenson (40) have reported linear thermal expansions for Berylco-25 measured with a dial-gauge dilatometer. They found a total relative contraction from 293 K to 0 K of $-3.31\times10^{-3} \pm 0.03\times10^{-3}$ for both 1/2-H and 1/2-HT conditions. Later measurements by Arp et al. (41) show differences due to heat treatment, with total contractions from room temperature to 20 K of -3.24×10^{-3} for solution-annealed, and -3.16×10^{-3} for precipitation-hardened samples. These measurements also were done with a dial-gauge dilatometer and have a stated accuracy of $\pm0.1\times10^{-3}$.

The present absolute measurements (42) of the linear expansivity of CUBE-250 were done to furnish much more accurate technical data than the earlier work. The experimental accuracy of the capacitance dilatometer apparatus was about ±0.1% in the expansivities, or roughly 1×10^{-5} in the absolute values of the contractions. For comparison with the earlier results, the total contractions from 293 K to 0 K were -3.09×10^{-3} for a solution-annealed sample and -3.07×10^{-3} for a precipitation-hardened sample. The differences between these results and those of Beenakker and Swenson, and Arp et al., are probably due to systematic experimental differences. Our relative measurements of the expansivity of Berylco-25 indicate that the contractions for that alloy should be within a few percent of those for CUBE-250.

In Figure 6, the ratio α/α_{Cu} is plotted versus temperature for solution-annealed and precipitation-hardened CUBE-250 (42). The copper expansivities used for reference are the smoothed results of Kroeger and Swenson (43). The ratio α/α_{Cu} is plotted rather than the expansivity itself in order to emphasize details of the behavior, since α for the alloy is close to that of copper.

Several features of the behavior shown in Figure 6 may be discussed in terms of the Grueneisen relation (Eqn. 12). Most of the temperature dependence of α/α_{Cu} is associated with the ratio of the specific heats.

The temperature dependences of Γ and B_T for Cu-Be alloys are not known, but the ratios of these quantities to the respective values for pure copper are expected to be roughly constant over wide ranges of temperature. It is also difficult to estimate the magnitudes of these various ratios. Room temperature sound velocity measurements (44) give a value of 1.3×10^{11} N/m^2 for the bulk modulus of half-hard Berylco-25, and the value for CUBE-250 is probably close to this since the two alloys are similar. The bulk modulus of copper, which is approximately 1.39×10^{11} N/m^2 (45), is nearly the same magnitude as that of the alloys. The dependence of B_T of the Cu-Be alloy on heat treatment is not known, but from trends in other elastic moduli (33), it is expected that B_T should be between 10 and 20 % higher for

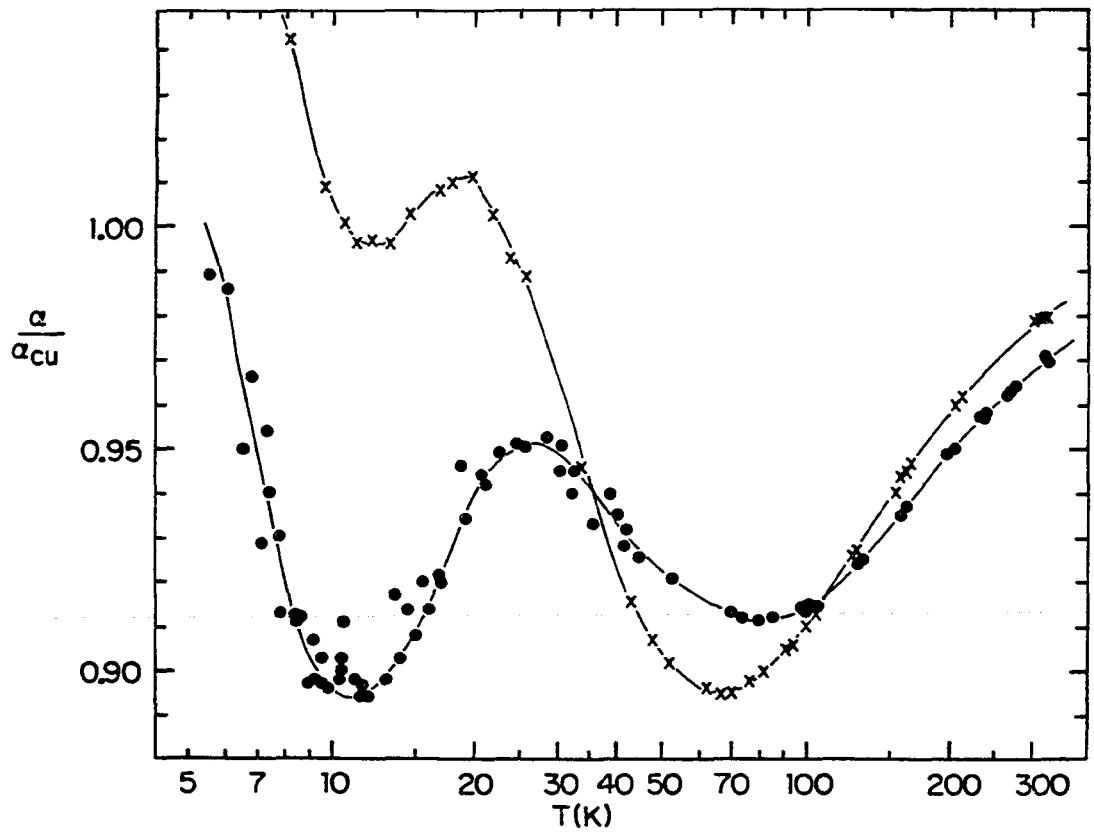

Figure 6. Ratio of the expansivity of CUBE-250 (from Ref. 42) to that of copper (from Ref. 43) for solution-annealed (x) and precipitation-hardened (●) conditions

precipitation-hardened material than for solution-annealed material.

Near room temperature, α/α_{Cu} in Figure 6 approaches unity for both heat-treated conditions of CUBE-250. The ratio α/α_{Cu} decreases as temperature decreases, indicating that both conditions of the alloy have slightly higher Debye temperatures than that of copper. At the other extreme, near 10 K, the ratios increase significantly as temperature decreases. This is because of the large magnetic impurity contribution that is present in the alloy, but not in copper. Figure 7 gives a plot of α/T vs. T^2 below 10 K for both CUBE-250 samples and for copper. Normally the slopes and intercepts of straight lines in such plots are associated with the lattice and electronic specific heat contributions, respectively. In the present case, however, the magnetic impurity contribution is also resembles a linear relationship in such a plot, so the standard interpretation is wrong.

The maximum near 20 K in the expansivity ratio for both samples in Figure 6 is unusual. The behavior in such a plot for most simple metals would be a smooth curve with a minimum near this same temperature instead of a maximum, and with the high and low temperature limiting behaviors discussed above. The magnitude of the enhancement effect possibly depends on sample condition, but this is ambiguous

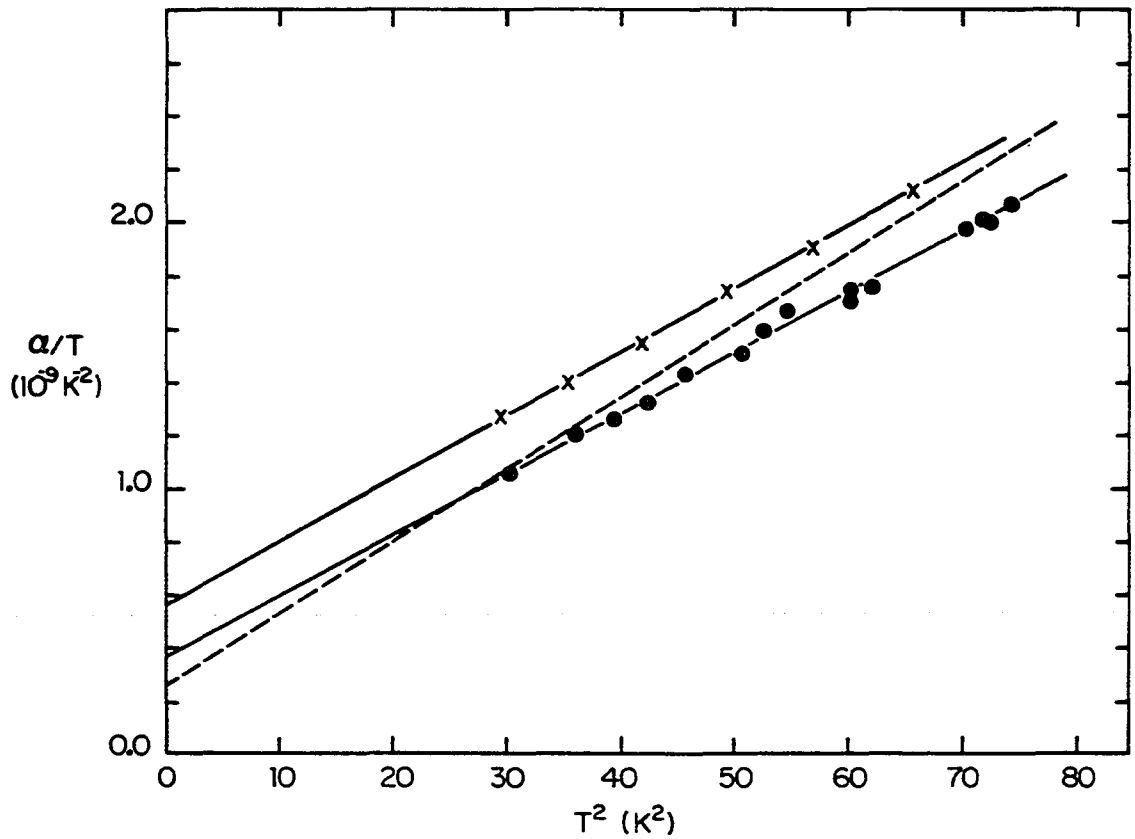

Figure 7. α/T vs. T^2 for solution-annealed (x) and precipitation-hardened (●) CUBE-250 (Ref. 42) and copper (dashed line). The copper expansivity is from Ref. 43

in the figure because the magnetic impurity effects below 15 K change drastically with precipitation-hardening.

Further interpretation of the thermal expansivity results is difficult, since it requires a detailed knowledge of three additional quantities, Γ, B_T, and C_v. For this reason, specific heat measurements were undertaken to more completely characterize the enhancement effect. The results of these measurements are discussed in the next sections.

The expansivities of solution-annealed and precipitation-hardened Berylco-25 also were measured, but with a relative expansivity apparatus. The ratio α/α_{Cu} for these samples is shown in Figure 8. Because of unresolved problems with the experiment, irreproducible, systematic errors of 10% or more are present in the data below 30 K, although the results above 50 K are probably of ± 1% accuracy. It is apparent that the qualitative behavior of Berylco-25 and CUBE-250 are the same, with an enhancement effect present and essentially the same high temperature limiting behaviors. This demonstrates that the effects noted in the discussion are not unique to CUBE-250. No expansivity measurements were done on the low-iron alloy, since samples of the appropriate size could not be obtained.

Specific Heat

To our knowledge, the specific heat of Cu-Be alloys has not been measured below room temperature before, except when

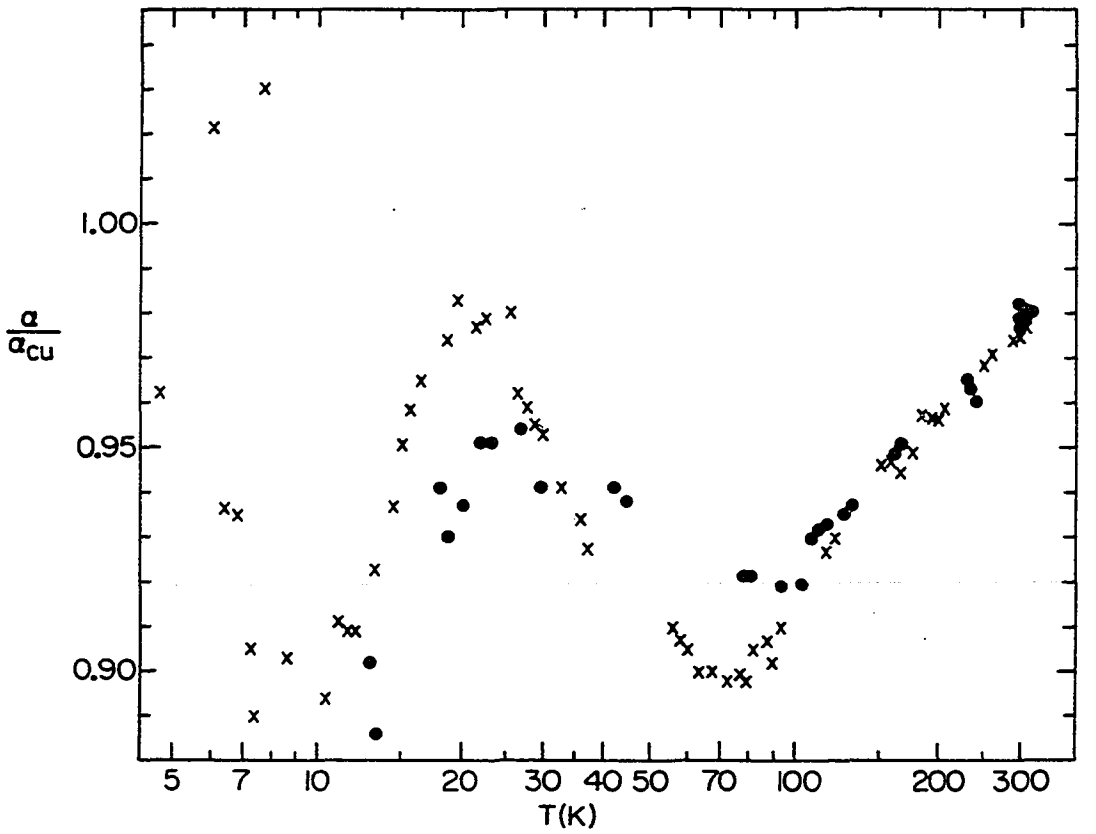

Figure 8. Ratio of the expansivity of Berylco-25 to that of copper (from Ref. 43) for solution-annealed (x) and precipitation-hardened (●) conditions

the material was present as part of calorimeters intended for other purposes. The high pressure calorimeters of Fugate (46), Krause (47), and Berton et al. (48) are examples, and provided initial crude estimates of the specific heats to be expected for Cu-Be alloys. The specific heats of Cu-1.8 wt.% Be alloys have, however, been studied at precipitation-hardening temperatures between 100 ^{o}C and 600 ^{o}C (49,50). This work provides no useful information about the low temperature properties of the alloy, so will not be discussed here.

Copper

Pure copper was chosen as a reference material since the Cu-Be specific heats are within 10% of that of copper below 70 K. Plots of the ratio of the Cu-Be specific heat to that of copper should therefore emphasize any small effects present.

The specific heat of copper, as carefully determined between 1 K and 30 K by Holste, Cetas, and Swenson (51), was chosen as the primary reference. These results are referred to as "HCS" copper in the following discussion. Satisfactory specific heat data covering the entire range of interest from 1 K to 70 K could not be found in the literature. Most reported data do not extend above 30 K, presumably because of the difficult nature of the experiment at higher temperatures. The popularly used reference data of

Furukawa et al. (52) cover the desired temperature range, but do not agree with HCS below 30 K. These are actually an average of many different determinations reported in the literature prior to 1968, some of doubtful accuracy. Stromberg et al. (53) report specific heat data for copper up to 50 K which could be extrapolated satisfactorily to 60 K. These data also have the problem of significant differences from HCS at low temperature, so were not used. It was decided to establish our own secondary reference for the copper specific heat up to about 70 K. These results are referred to as "RLH" copper throughout this work. "RLH" are the initials of this author's name, and have no other significance.

The sample was 99.999% pure ASARCO copper that had been electron-beam melted in vacuum, then swaged into a rod of 5/8 inch diameter. After final machining to a length of 1 inch, the sample was annealed for 2 hours at 300 ^{o}C to relieve internal strains. A thin layer of gold was sputtered onto the sample to help prevent corrosion due to handling.

The specific heat was measured from 4.4 K to 64 K initially, and the results were used for the least-squares fits described below. A second set of measurements from 1 K to 4 K were done later as a check on the experimental procedures. These low temperature data were not included in the

fits. The specific heat results for higher temperatures were not checked.

The temperature dependence of the specific heat was assumed to be of the form

$$C = A_1T + A_3T^3 + A_5T^5 + \text{---} \ . \qquad (37)$$

Least-squares fits of this function to the data were done, using standard numerical techniques (54), to furnish an analytical representation for the copper specific heat. The most accurate representation was obtained by fitting over several different ranges of temperature, with the fit ranges chosen so that the functions and their derivatives matched where the neighboring ranges overlapped. Four terms were used in each of the series because this was the lowest number of terms needed to obtain a root-mean-square deviation (RMSD) that was within the experimental uncertainty of about 0.2%. Inclusion of higher order terms did not improve the RMSD significantly, and only resulted in a more complicated representation. Table 4 lists the coefficients determined by the fits, and Table 5 is a tabulation of the copper specific heat evaluated from the fits.

The quality of the RLH copper specific heat representation is indicated in Figure 9 by the percent deviations of the data from the fits. Figure 10 shows the percent deviations of both the data and the RLH representation from that

Table 4. Fit coefficients for Eqn. 37 for the specific heat of copper (in mJ/gm-K)

Temperature range	Fit coefficients
4 - 12 K	$A_1 = 1.101955 \times 10^{-2}$
	$A_3 = 7.563931 \times 10^{-4}$
	$A_5 = -1.577611 \times 10^{-8}$
	$A_7 = 1.226453 \times 10^{-9}$
12 - 27 K	$A_1 = 1.639050 \times 10^{-2}$
	$A_3 = 6.478966 \times 10^{-4}$
	$A_5 = 7.128989 \times 10^{-7}$
	$A_7 = -4.035727 \times 10^{-10}$
27 - 63 K	$A_1 = -2.219474 \times 10^{-1}$
	$A_3 = 1.496702 \times 10^{-3}$
	$A_5 = -3.143035 \times 10^{-7}$
	$A_7 = 2.579002 \times 10^{-11}$

Table 5. Values of the copper specific heat using Eqn. 37 and the coefficients listed in Table 4

T (K)	C (mJ/gm-K)	T (K)	C (mJ/gm-K)
1[a]	1.178×10^{-2}		
2[a]	2.809	30	2.668×10^{1}
3[a]	5.348	32	3.228
4	9.249	34	3.835
5	1.497×10^{-1}	36	4.486
6	2.297	38	5.174
7	3.373		
8	4.775	40	5.895
9	6.555	42	6.643
		44	7.413
10	8.773	46	8.198
11	1.149×10^{0}	48	8.992
12	1.479		
13	1.876	50	9.792
14	2.348	52	1.059×10^{2}
15	2.905	54	1.139
16	3.555	56	1.219
17	4.308	58	1.298
18	5.174		
19	6.160	60	1.378
		62	1.458
20	7.276	64	1.541
22	9.927	66[a]	1.627
24	1.318×10^{1}	68[a]	1.719
26	1.704		
28	2.158		

[a]Outside of fit range.

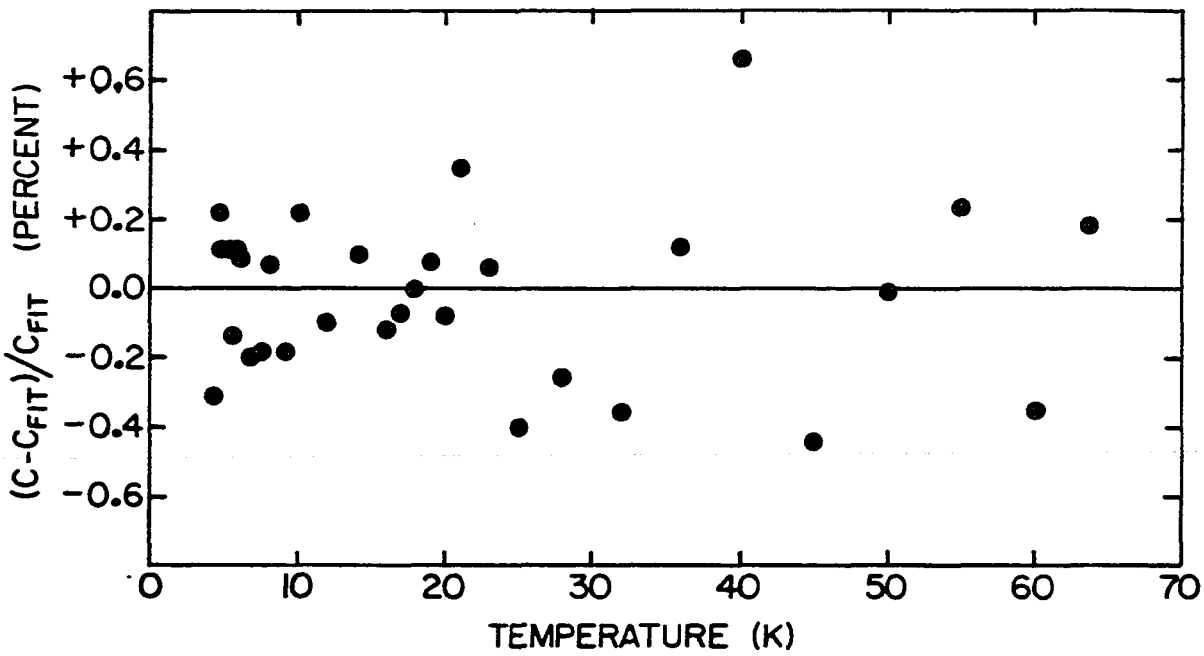

Figure 9. Percent deviations of the copper specific heat data from the RLH fits described in the text

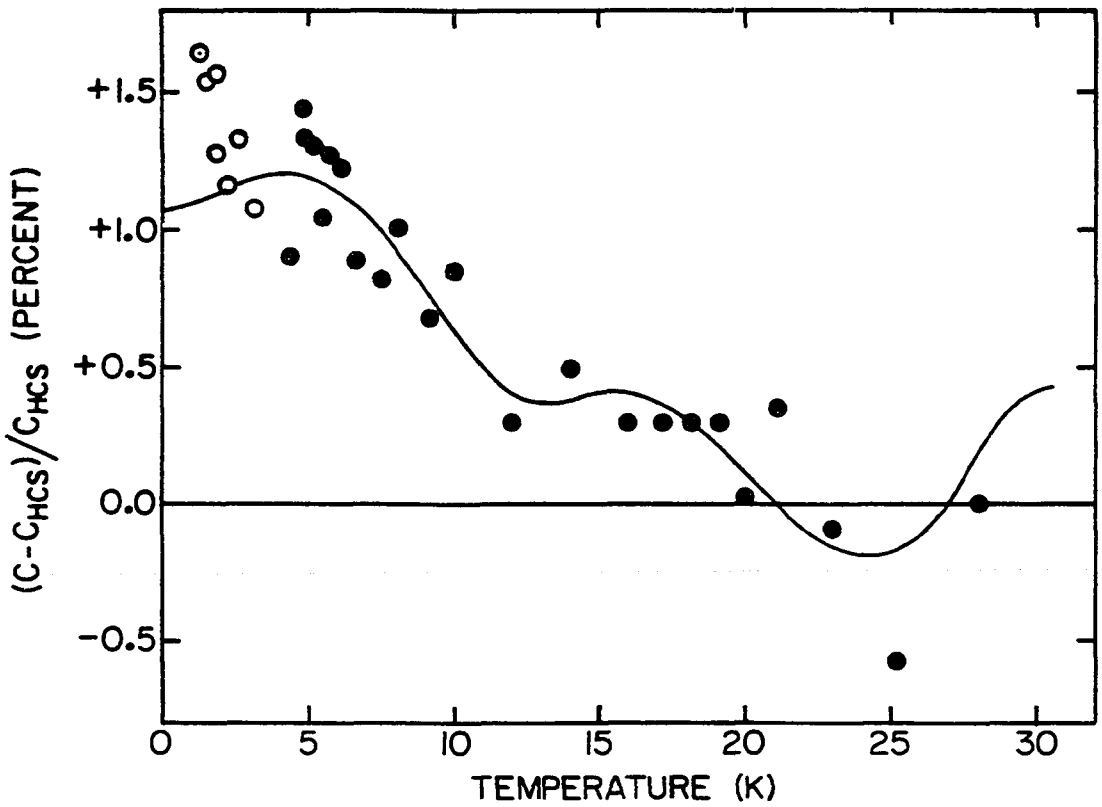

Figure 10. Percent deviations of the copper specific heat data and the RLH representation from the smooth fit of Holste, Cetas, and Swenson (51). Open circles are for data that were not included in the RLH fits

of HCS below 30 K. The 1 K to 4 K data are also shown in Figure 10. These low temperature data are about 0.5% higher than the representation (solid curve). This difference is probably a result of extrapolating the RLH representation to below 4 K, where it is not rigorously valid.

Both the RLH fits and the actual data differ from the HCS fit by approximately 1% at low temperatures. This was considered to be acceptable agreement. The difference probably represents slight differences between the RLH and HCS samples, such as strain-annealing procedure or the gold plating on the RLH sample.

In the following discussions of the specific heat results, the RLH copper specific heat representation is used as the reference in all of the figures.

Low-iron Cu-1.92 wt.% Be

The specific heats of solution-annealed and precipitation-hardened samples of the low-iron Cu-1.92 wt.% Be alloy were measured between 1 K and 50 K. These results are presented in Figure 11 as the molar specific heats of the two samples divided by that of RLH copper. At the highest temperatures measured, the specific heat ratios for both samples approach the same value of approximately 0.93. At higher temperatures, the ratios should increase, approaching 1.0, as the specific heats tend toward the Dulong-Petit value of 3R.

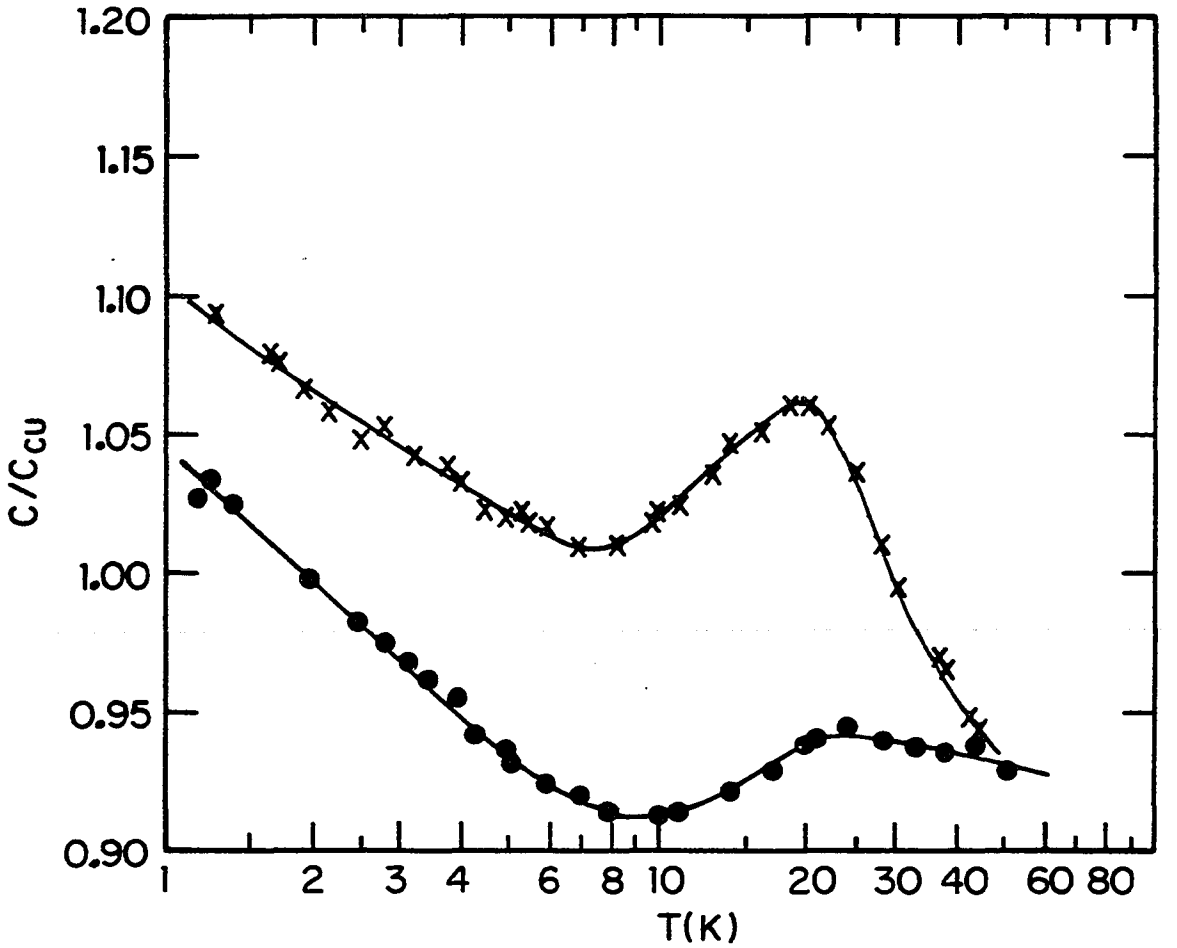

Figure 11. Ratio of the molar specific heats of the low-iron Cu-1.92 wt.% Be alloy to that of copper for solution-annealed (x) and precipitation-hardened (●) conditions

The unusual enhancement near 20 K seen in the thermal expansivity results (Figure 6) is also present in the specific heat ratios, so that both quantities behave similarly. Normal behavior of specific heat ratios, over the temperature range included in Figure 11, would appear as smooth curves that decrease monotonically with increasing temperature. For the alloy, the exact normal contribution is not known since the measurements could not be done to high enough temperatures to establish the trend. A simple straight line interpolation of the curves in Figure 11 between roughly 8 K and 50 K crudely represents the normal behavior, and allows estimates of the magnitude of the enhancement effect. For the solution-annealed sample, the specific heat ratio peaks at 20 K, and the enhancement represents about 10% of the sample specific heat at that temperature. For the precipitation-hardened sample, the effect is smaller, approximately 3%, and peaks at a slightly higher temperature near 25 K.

Since the enhancement is clearly greatest for the solution-annealed sample, it evidently is associated with the Cu-Be solid-solution. The smaller size of the enhancement for the precipitation-hardened sample is accounted for by the depletion of the Be concentration in the solid-solution matrix as precipitates form. The specific heat results therefore suggest that the enhancement effect is an

intrinsic property of the Cu-Be solid solution. Originally, it was suggested (42) that some interaction between dislocations and precipitates could be the source of the effect and could explain the expansivity results, but this idea now is known to be incorrect.

The shapes of the curves in Figure 11 suggest that the enhancement could be represented by a Schottky anomaly. Attempts were made to fit the data with various combinations of power series and Schottky functions, but satisfactory quantitative results were not obtained. A crude representation of the solution-annealed sample's specific heat could be obtained by assuming that it is equal to that of copper, with a slightly higher electronic specific heat, plus a two-level Schottky anomaly with a level splitting near 150 K. Curves qualitatively similar to those in Figure 11 could be generated in a variety of ways, but there was no definite and unique model. Various combinations of Debye, Einstein, and Schottky functions and electronic terms could be used to approximate the alloy and copper specific heats and produce maxima in the specific heat ratios near 20 K. However, quantitative agreement with the experimental results could not be arranged.

Below 5 K, the solution-annealed and precipitation-hardened Cu-Be samples both have normal metallic specific heats. Figure 12 shows C/T vs. T^2 for these samples, with

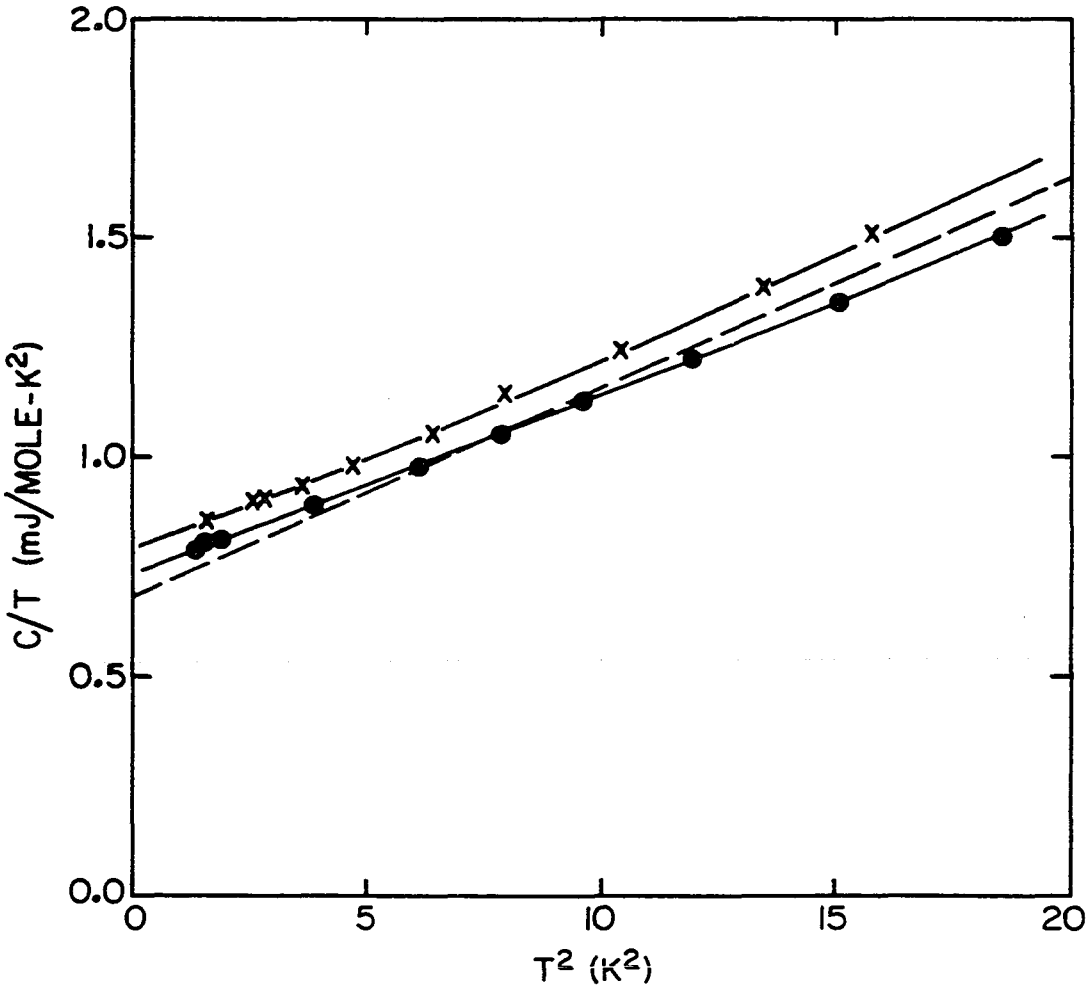

Figure 12. C/T vs. T^2 for the low-iron Cu-1.92 wt.% Be alloy in solution-annealed (x) and precipitation-hardened (●) conditions. The dashed line represents copper

the RLH copper results included for comparison. The electronic contribution to the specific heats, corresponding to the $T^2 = 0$ intercepts of the curves, is largest for the solution-annealed Cu-Be sample. It is reduced for the precipitation-hardened sample, and is smallest for copper. Comparing the slopes of the curves, it is apparent that the Debye temperatures of the solution-annealed alloy and copper are nearly the same, while that of the precipitation-hardened sample is slightly higher. Table 6 lists the electronic specific heat coefficients and Debye temperatures, determined by fitting C/T vs. T^2 to order T^4 for all three samples. The calculated electronic density of states and effective masses, defined by Eqns. 17 through 21 in the Background chapter, are listed in Table 7. For the free-electron density of states, it was assumed that Be is divalent in the Cu-Be solid-solution. The free-electron model was not applied to the precipitation-hardened alloy results since Be is monovalent in the γ-phase, and the amount of γ-phase present in the sample was not known.

The higher effective mass for the solution-annealed alloy than for copper indicates that simply accounting for the additional electrons contributed by the Be is insufficient to explain the experimental electronic specific heat. Possible changes in the band structure upon substituting Be in Cu are examined in the Discussion section.

Table 6. Electronic specific heat coefficients and Debye temperatures for the solution-annealed (SA) and precipitation-hardened (PH) low-iron Cu-1.92 wt.% Be samples and for copper

Sample	γ (mJ/mole-K^2)	θ_o (K)
RLH copper	0.7028	344.3
HCS copper	0.6926	344.9
SA Cu-Be	0.7691	348.4
PH Cu-Be	0.7304	362.1

Table 7. Experimental and free-electron density of states (in 10^{22} $ev^{-1}cm^{-3}$) and effective masses

Sample	$g(\varepsilon_F)$	$g_{free}(\varepsilon_F)$	m^*/m
RLH copper	2.50	1.81	1.38
SA Cu-Be	2.86	1.90	1.51
PH Cu-Be	2.73	-	-

The fact the the Debye temperatures of the solution-annealed Cu-Be alloy and of copper are nearly the same is coincidental. The effect on the Debye temperature of the light mass Be impurity is almost entirely cancelled by the smaller force constants associated with the Be-Cu interaction. This effect is considered in more detail in the Discussion section. Since the precipitation-hardened sample has a higher Debye temperature than both the solution-annealed and copper samples, it is clear that the γ-phase precipitates have an intrinsically higher Debye temperature. The magnitude of the γ-phase Debye temperature could not be determined because the amount of that phase present in the sample was not known.

Knowledge of the normal low temperature properties now allows a closer examination of the specific heat enhancement near 20 K. The contribution of the lattice only is calculated by subtraction of the electronic contribution from the total specific heat. A comparison of the alloy and copper lattice specific heat then can be made. A plot of the ratio of the alloy lattice contribution to that of copper is similar to the ratio of the total specific heats in Figure 11, and no additional information is gained. However, a comparison of the lattice specific heat to the ideal Debye model provides some interesting new information. Figure 13 shows the ratio of the lattice specific heats of the two

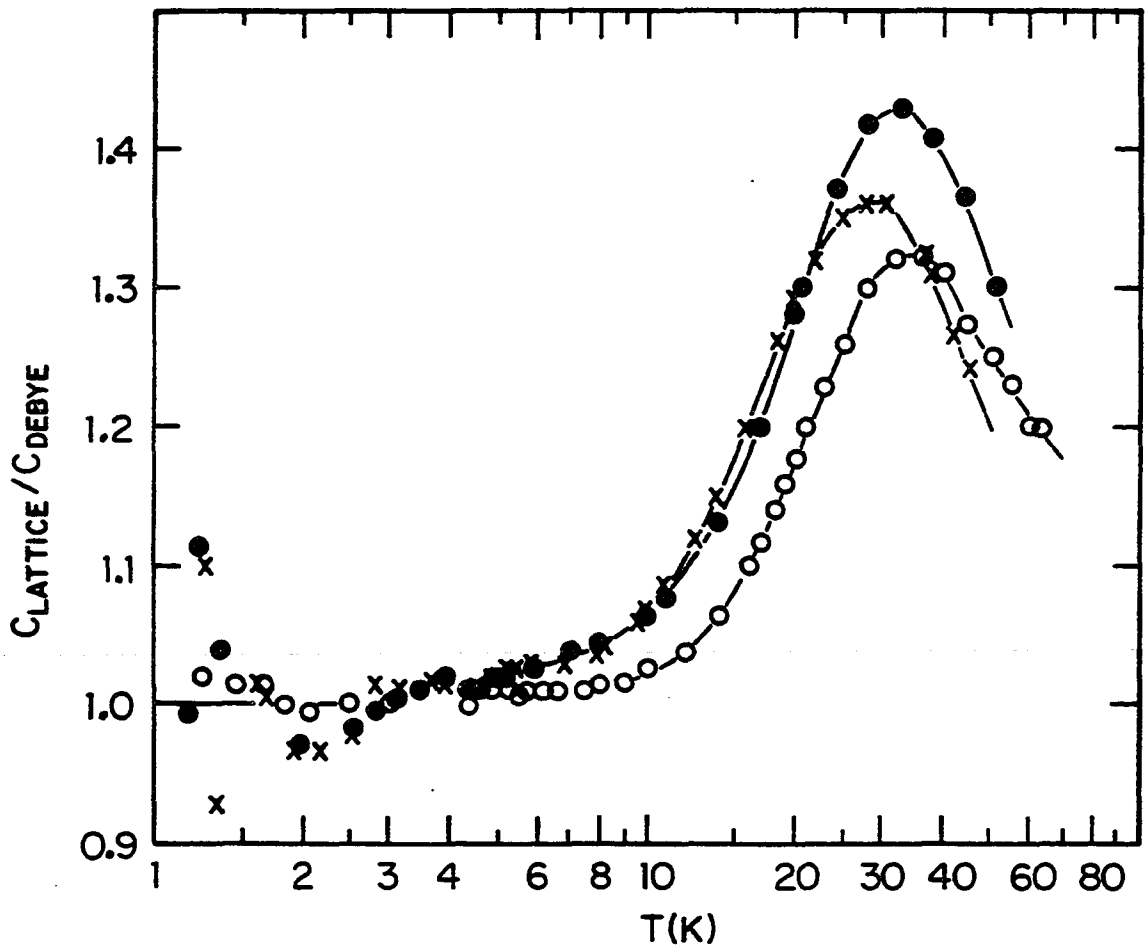

Figure 13. Ratio of the lattice specific heats to the Debye function for solution-annealed (x) and precipitation-hardened (●) Cu-1.92 wt.% Be samples, and copper (o). The Debye functions use the Debye temperatures listed in Table 6

alloy samples and of copper with respect to the Debye specific heats, using the Debye temperatures from Table 6. In this plot, all three samples show similar behavior, with a large positive deviation from the Debye model above 20 K. Such curves are completely normal and represent differences between the actual phonon density of states and the Debye model. It is apparent, therefore, that the enhancement in the specific heat ratios is due primarily to a shift of copper-like behavior to slightly lower temperatures. The ratio enhancement for the solution-annealed alloy is larger than that for the precipitation-hardened alloy because the shift is larger. These shifts of the deviations from Debye behavior correspond to changes in the phonon density of states upon alloying. This effect is considered in detail in the Discussion section.

Often, specific heat results are represented by fits of the lattice specific heat with the Debye function, using a temperature-dependent Debye temperature as a fit parameter. Such an analysis has little fundamental theoretical meaning, but can provide a useful reduction of data for comparison purposes. Figure 14 shows the ratio $\theta(T)/\theta_0$ vs. T/θ_0 for the two low-iron Cu-Be samples and for copper, where θ_0 is the appropriate value from Table 6 for each sample. The Debye temperature for copper has a minimum at higher temperatures than those plotted, so the Cu-Be behavior is again

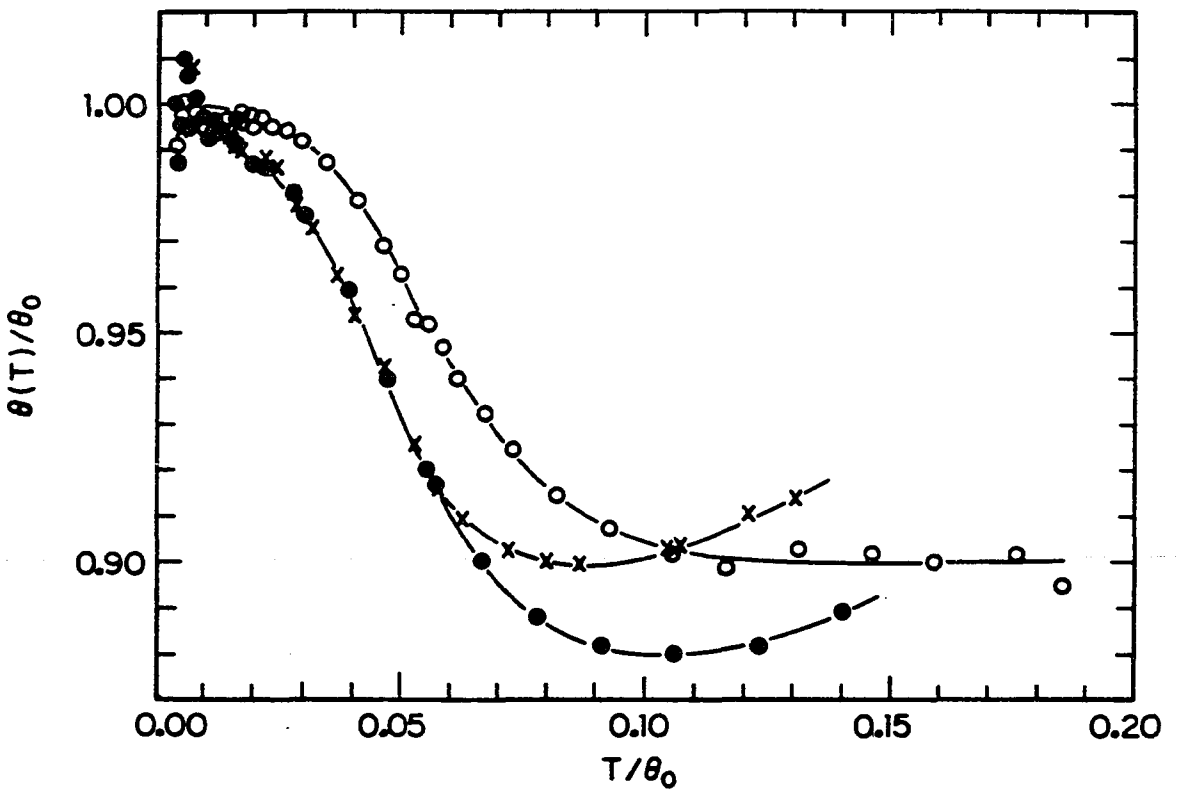

Figure 14. Reduced Debye temperature vs. reduced temperature for the solution-annealed (x) and precipitation-hardened (●) Cu-1.92 wt.% Be alloy, and for copper (o)

seen to be similar to copper, but shifted to lower temperatures.

Berylco-25

Several other features of the specific heat ratio enhancement effect are revealed by the Berylco-25 results described below. Samples of this alloy were easily obtainable and this allowed for study of a wider variety of heat-treatment conditions than was possible with the small amount of the low-iron alloy that was available. A major difference between Berylco-25 and the low-iron alloy is the presence in Berylco-25 of relatively high concentrations of Co (0.24 wt.%) and Fe (0.19 wt.%), which have large low temperature magnetic specific heats. The dependence of the magnetic contributions on heat-treatment is interesting in itself, but was not the intended object of study. The presence of these effects led to considerable frustration in the data analysis and interpretation before the low-iron alloy became available late in the work. We were unable to account quantitatively for the magnetic contributions in the Berylco-25 specific heats, so the results could only be qualitatively interpreted.

Figure 15 shows the specific heat ratio for solution-annealed and precipitation-hardened (2 hrs. at 320 ^{o}C) Berylco-25 samples. The behavior is similar to that shown in Figure 11 for the low-iron alloy, with the difference

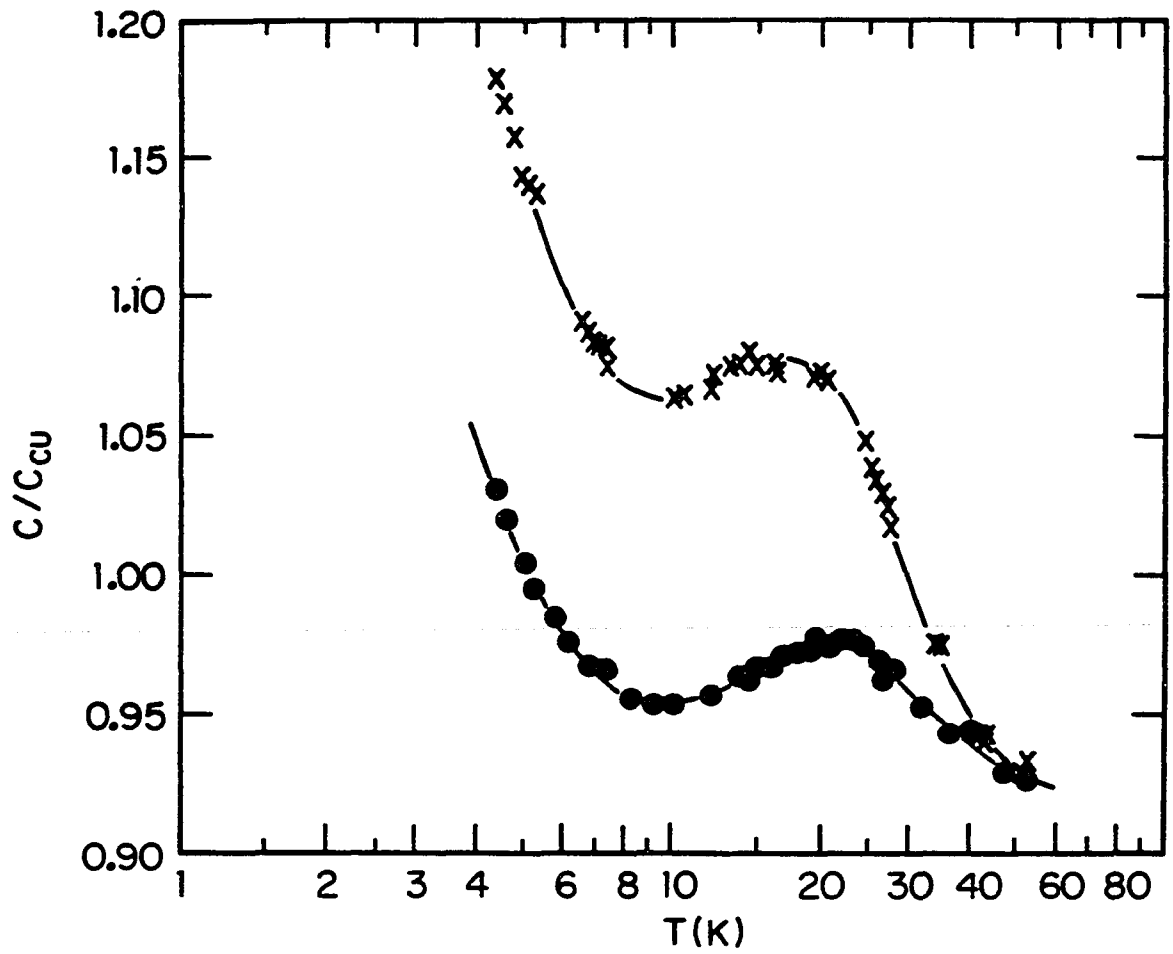

Figure 15. Ratio of the molar specific heat of Berylco-25 to that of copper for solution-annealed (x) and precipitation-hardened (●) conditions

that the ratios approach much larger values at low temperatures. This is a manifestation of the magnetic effects already mentioned. A plot of C/T vs. T^2 is shown in Figure 16 for these same two samples and for copper. Comparison with the corresponding results for the low-iron alloy in Figure 12 shows just how large the magnetic contribution is. The reduction in the low temperature specific heat with hardening is also much greater for Berylco-25 than for the low-iron alloy, indicating that these magnetic effects also change with heat-treatment.

The specific heat of half-hard material, as shown in Figure 17, is essentially the same as for the solution-annealed material shown in Figure 15. The limiting high and low temperature ratios are the same for both, but the half-hard sample has about a 1% higher contribution to the specific heat ratio in the region of the enhancement between 10 K and 30 K. The experimental accuracy is believed to be better than 1% in this temperature region, so the difference is probably real. It is possible that the enhancement effect is slightly increased by the residual strain present in the half-hard material.

Further comparison of Figures 15 and 17 shows that precipitation-hardening at 320 ^{o}C for 2 hours results in much greater reduction of the ratio enhancement for initially half-hard material than for initially solution-annealed

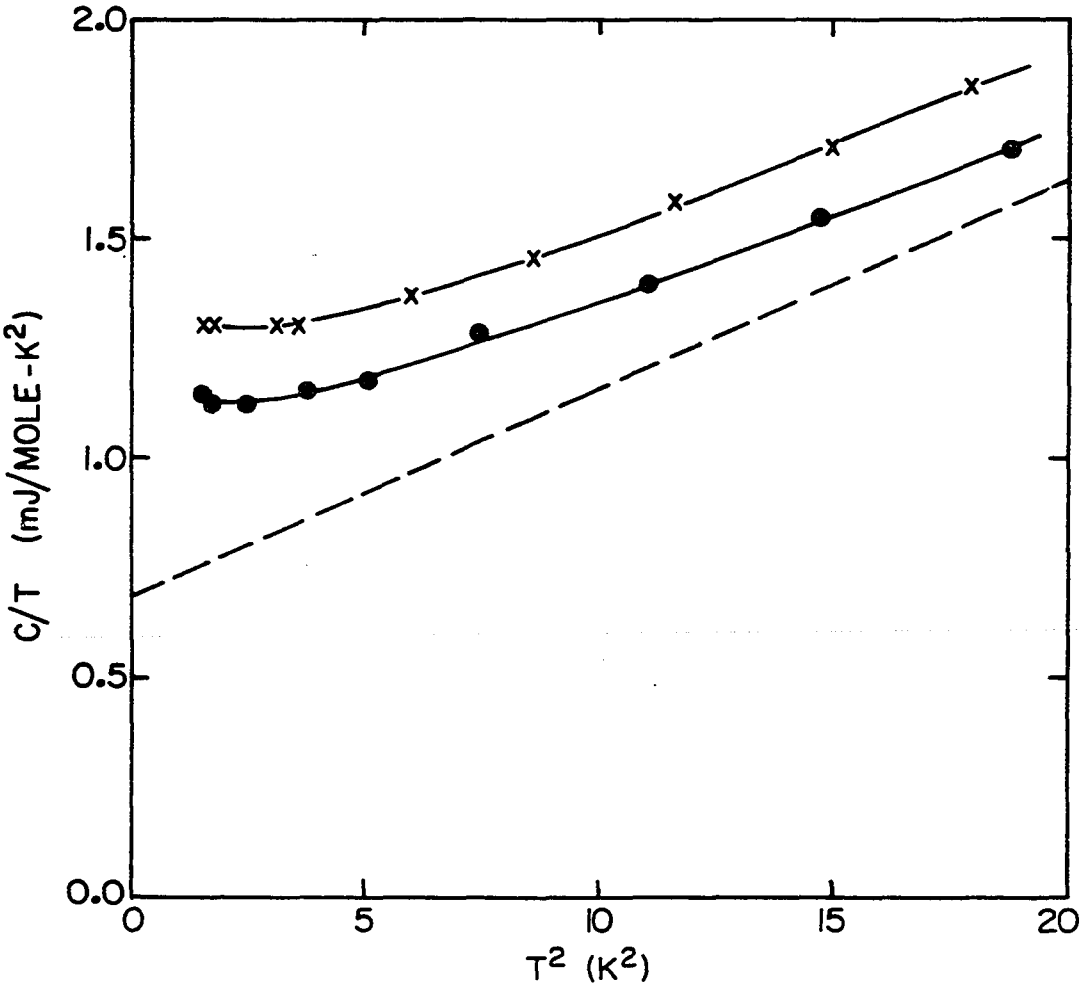

Figure 16. C/T vs. T^2 for solution-annealed (x) and precipitation-hardened (●) Berylco-25 and for copper (dashed line)

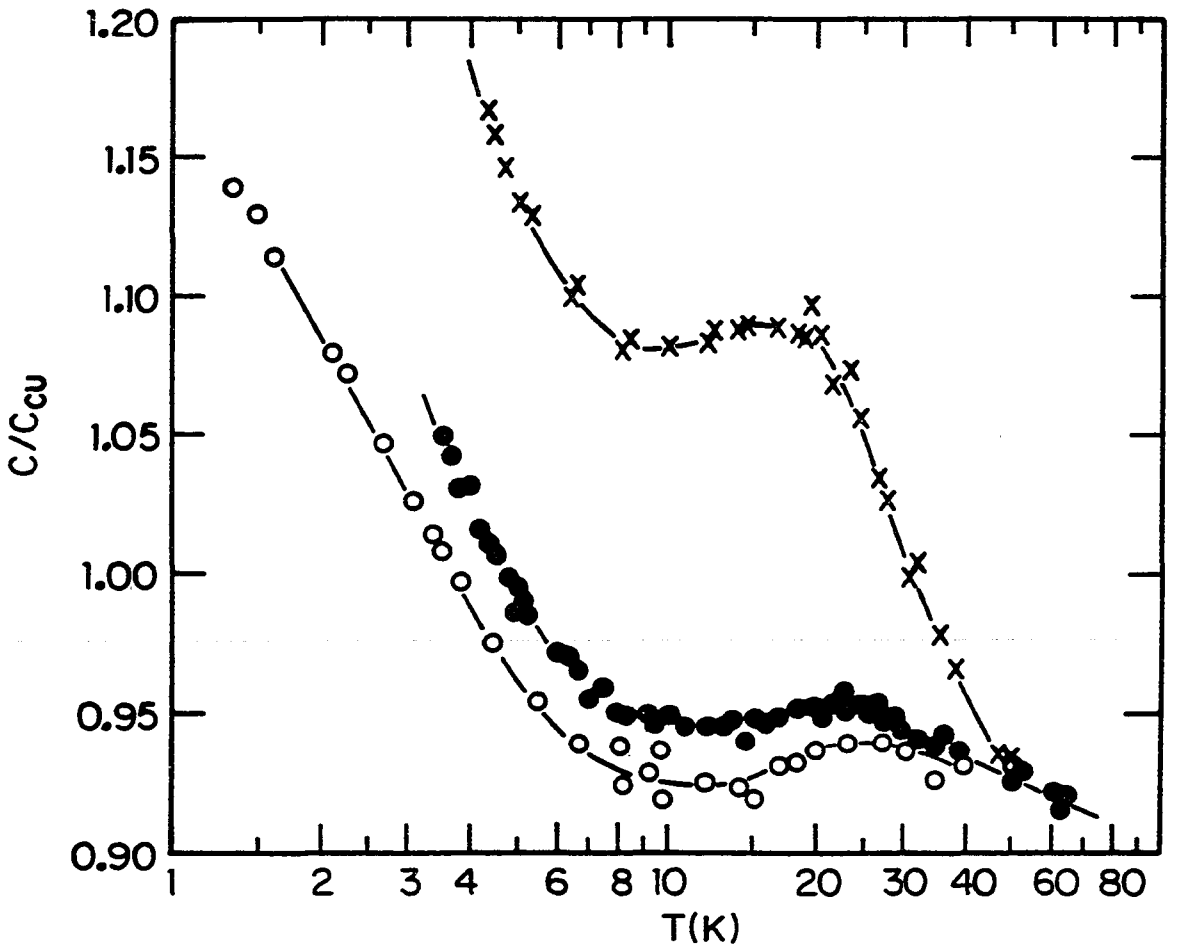

Figure 17. Ratio of the molar specific heat of Berylco-25 to that of copper for half-hard (x), an initially half-hard precipitation-hardened sample (●), and an "overaged" sample (o)

material. Cold-work prior to precipitation-hardening is known to result in greater final hardness by providing additional nucleation sites for precipitation at work-induced dislocations. It is thought that this effect results in the greater reduction of the ratio enhancement for half-hard material since the additional nucleation sites lead to more rapid precipitation. This in turn causes more rapid depletion of the Be concentration in the solid-solution matrix.

The bottom curve and data in Figure 17 are for a sample that was treated at 450 ^{o}C for 21.3 hours (overaged). This resulted in about a 1% decrease in the specific heat below 30 K, as compared to the 2 hour, 320 ^{o}C sample, although the size of the ratio enhancement is nearly the same. At 450 ^{o}C the equilibrium Be concentration in the Cu-Be matrix is about 0.4 wt.% , while at 320 ^{o}C it is near 0.2 wt.%. The overaged sample is closer to equilibrium, so the approximately equal sizes of the enhancements are probably due to incomplete precipitation in the 320 ^{o}C sample. The cause of the 1% difference below 30 K is not known, but could be due to oxidation of some of the iron in the overaged sample.

Three identical samples were treated at the lower temperature of 250 ^{o}C to determine how the specific heat changes during the early stages of precipitation. The results are displayed in Figure 18, where the actual data

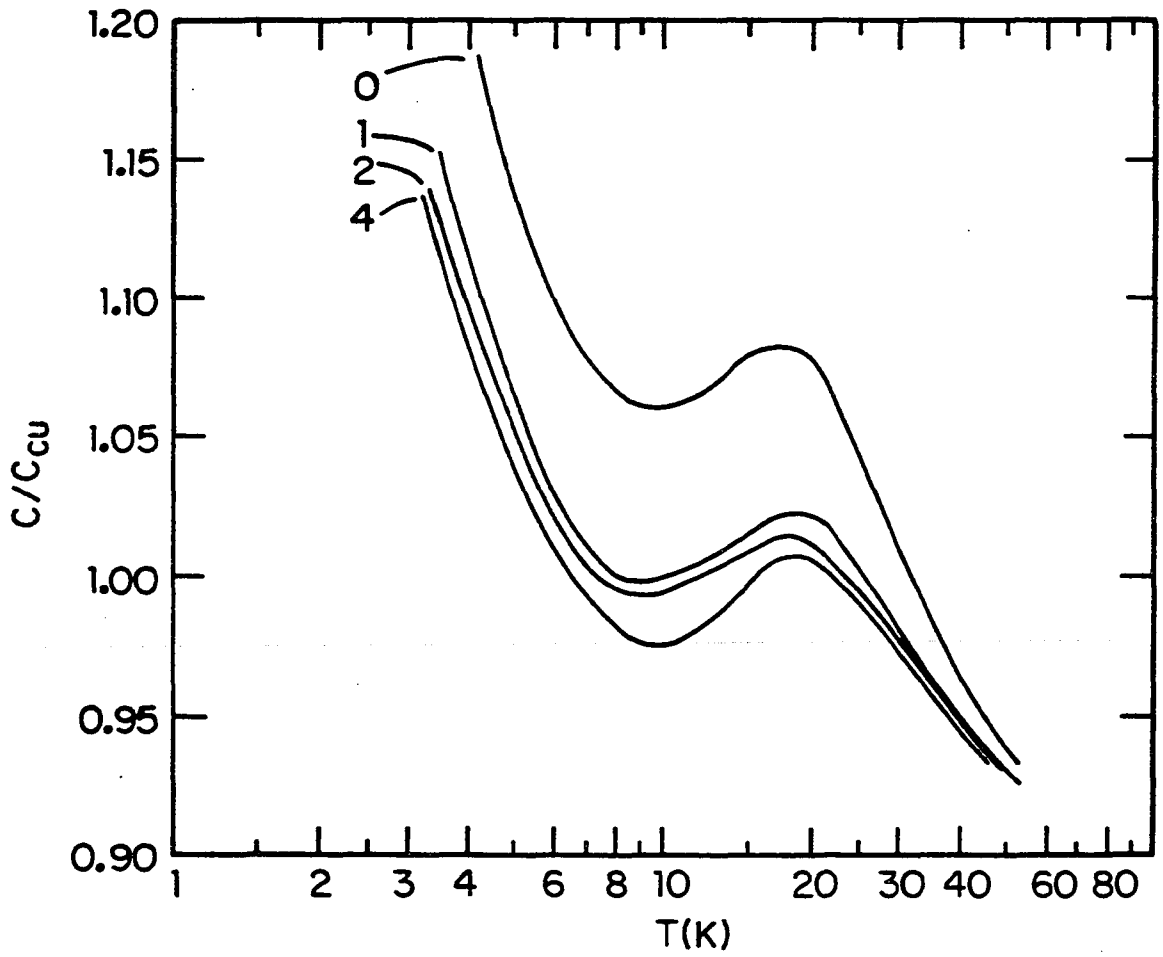

Figure 18. Ratio of the molar specific heat of Berylco-25 to that of copper for samples heat-treated at 250 °C. The numbers give the treatment times in hours

are omitted for clarity. The apparent size of the ratio enhancement does not seem to change during the early stages of precipitation, but the low temperature magnetic contributions decrease rapidly with treatment time. Most of the change occurs in the first hour of aging. As mentioned previously, the Co and Fe act as nucleation sites for zone formation, so that the specific heat contributions associated with these constituents should be expected to change earliest during hardening.

During the early stages of precipitation, the Guinier-Preston zones are essentially localized tetragonal distortions of the FCC parent solid solution around Be-rich regions. The lack of any significant change in the ratio enhancement effect during the early stages of hardening suggests that these small localized distortions have little effect on the phonon density of states. This in turn suggests that the interaction responsible for the shift in the phonon density of states, and hence the enhancement effect, is not very sensitive to interatomic distances. It is possibly fundamentally related to the crystal structure. This idea is consistent with the results in Figure 18, since the enhancement would not change significantly until later in the precipitation sequence when the precipitates take on a structure distinct from the FCC matrix.

Copper-2% Cobalt

Early in the study of Cu-Be alloys, the possibility that the ratio enhancement was a magnetic effect due to the Co or Fe constituents was considered. Solid solutions of Cu and Fe have been studied extensively both theoretically and experimentally, and no such effect has been found. Figure 19 shows the behavior of the ratio of the specific heats of Cu-Fe solid solutions (55) to that of copper for various Fe concentrations. More recent measurements by Tripplett and Phillips (13) examine the low temperature Cu-Fe specific heats more carefully, but the results are essentially the same. No enhancement of the specific heat ratio is seen.

Figure 19 also demonstrates the very large specific heat contribution of small quantities of Fe in Cu, as evidenced by the rapid increase of the ratio as temperature decreases. The contribution in Berylco-25, with 0.19 wt.% Fe, is only about one third of that shown in Figure 19 for the Cu-0.2wt.% Fe alloy. There are several possible explanations for the difference. Partial oxidation of the Fe could eliminate some of the magnetic moments, and hence reduce the magnetic specific heat contribution. Oxidation of the Fe could have occurred during manufacture of the Berylco-25. A more exotic possibility would be that the presence of Be near Fe in the alloy might fundamentally alter the Fe moments or the interaction responsible for the

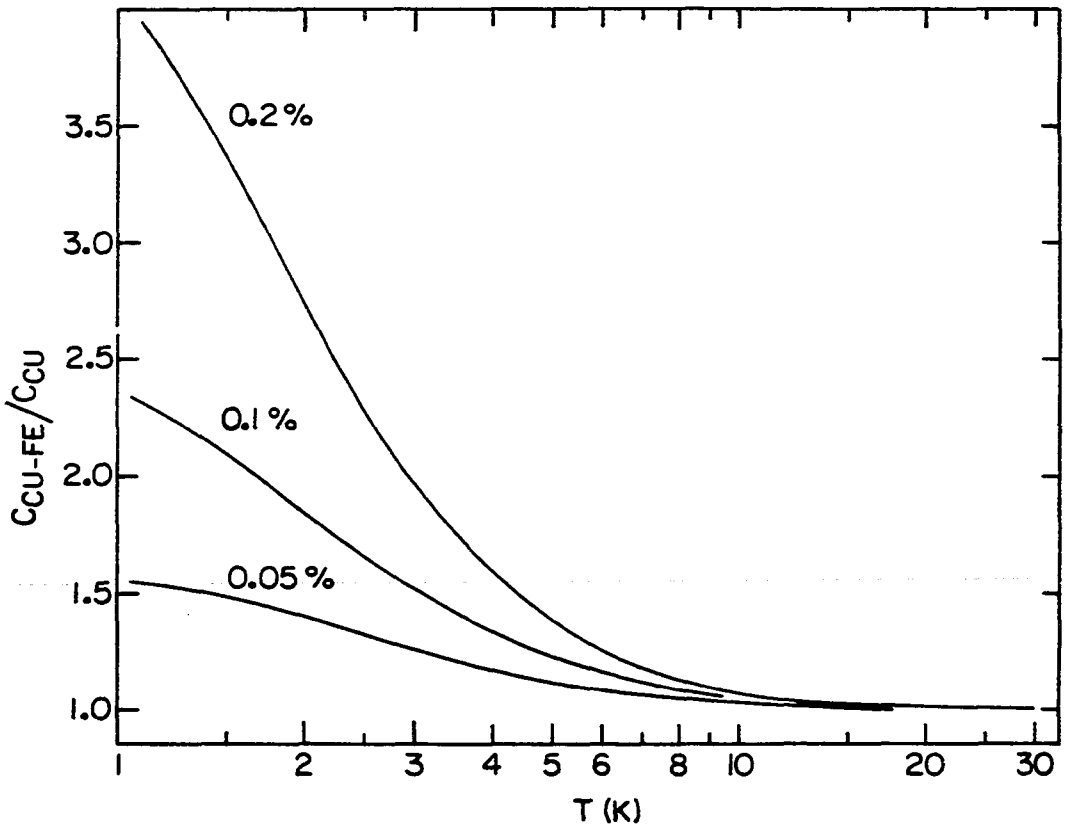

Figure 19. Ratio of the molar specific heats of Cu-Fe solid-solutions to that of copper. The concentrations are in weight percent. The Cu-Fe data were taken from Ref. 55

magnetic specific heat.

In order to determine if the ratio enhancement effect was due to the Co, specific heat measurements were done on the Cu-2wt.% Co sample used by Rehak for expansivity studies. This sample consists of a Cu-Co solid-solution matrix containing precipitates of Co. The specific heat ratio for this sample is shown in Figure 20, and no enhancement effect is present. The increase of the ratio toward lower temperatures is similar to the magnetic contribution in Cu-Fe and Berylco-25, and is due to magnetic interactions of the cobalt moments, as discussed on page 21. The plot of C/T vs. T^2 in Figure 21 for this sample also shows a slight upturn near 1 K, which also is present in the Berylco-25 results (Figure 16).

Electrical Resistance

Before the specific heat ratio enhancement effect was attributed to shifts in the phonon density of states, it was thought to be due to an anomalous structural distortion, or perhaps a phase transition. Precise electrical resistance measurements were carried out on samples of Berylco-25 strip to determine if any unusual effects were present, since phase transitions are often easily detected in the transport properties. In addition, resistance measurements could be done much more easily and to higher temperatures than could specific heat measurements.

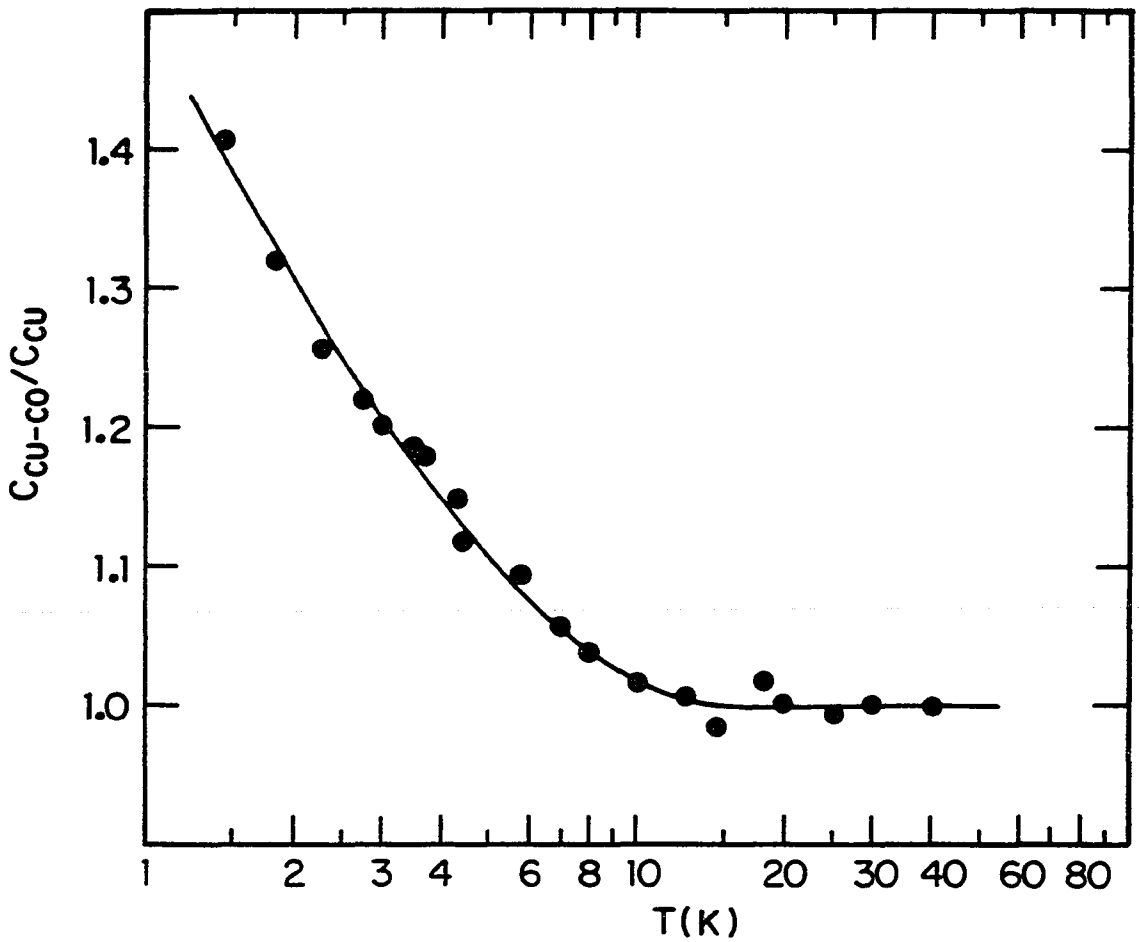

Figure 20. Ratio of the molar specific heat of the Cu-2 wt.% Co alloy to that of copper

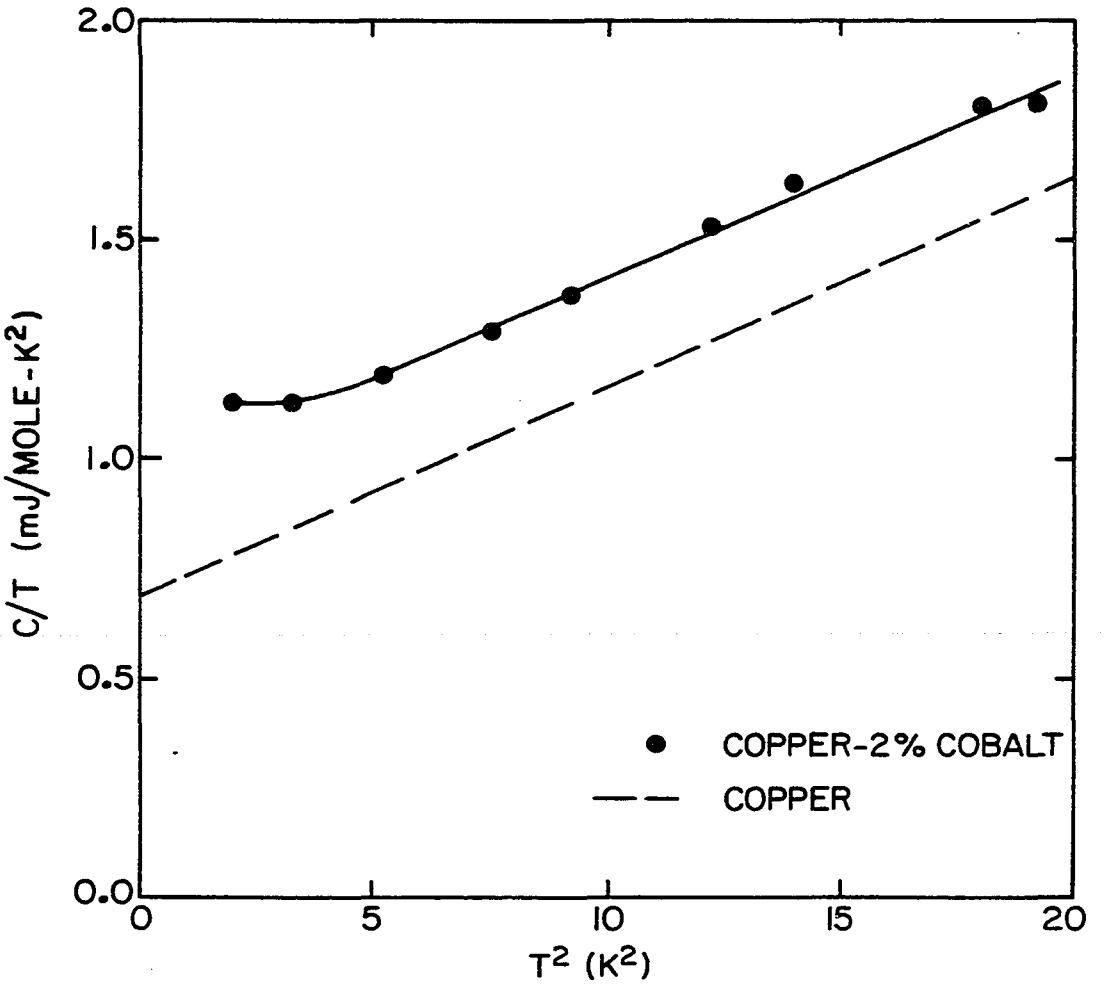

Figure 21. C/T vs. T^2 for the Cu-2 w.t% Co alloy (●) and for copper (dashed line)

The resistivity of precipitation-hardened Cu-1.82 wt.% Be alloy has been reported by Berman et al. (56) as 8.25 μΩ-cm at room temperature, 6.20 μΩ-cm at 77 K, and 5.54 μΩ-cm at 4.2 K. Their thermal conductivity measurements between 2 K and 80 K were reported in more detail, but no unusual effects were noted. Watson and Flynn (57) reported both resistivity and thermal conductivity results for half-hard Cu-1.83 wt.% Be samples from 133 K to 473 K in 50 K intervals, but also found nothing unusual. A room temperature (293 K) resistivity calculated from their data is 8.26 μΩ-cm, in agreement with Berman et al.

The Berylco-25 results reported here are much more precise than the earlier work, and have much finer temperature resolution. One set of measurements on a solution-annealed Berylco-25 sample were done from 1 K to room temperature in intervals of approximately 2 K, and it was determined that no unexpected effects were present. The actual data are not included here because the results include extraneous contributions due to the method used to attach leads to the sample.

Resistance results from 1 K to 80 K for solution-annealed and precipitation-hardened samples of Berylco-25 strip are shown in Figure 22. These data were obtained using an improved method of lead attachment and are believed to have a precision of better than 0.01%. The results are

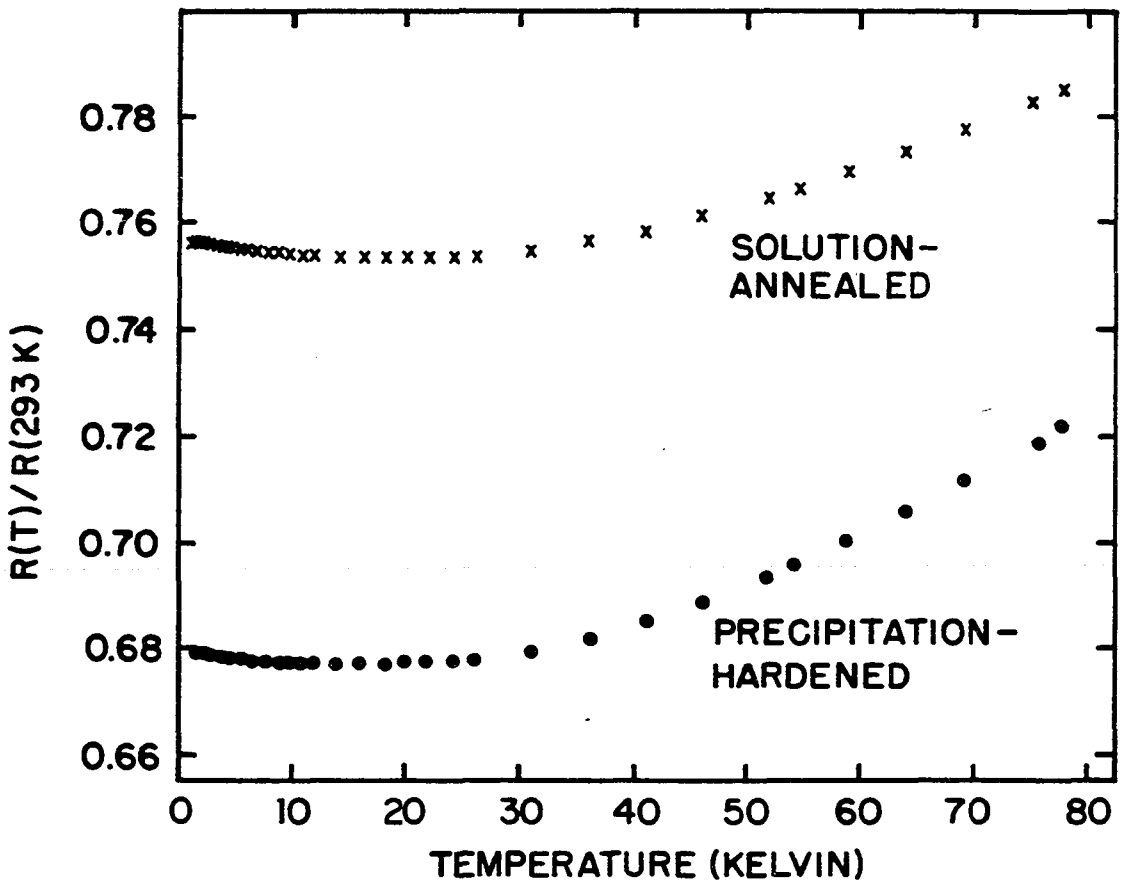

Figure 22. Resistance ratios for Berylco-25 strip samples

given as the ratio of the measured resistance to the value determined at 293 K. The absolute resistivities of the samples were not determined because their irregular cross-sectional area prevented an accurate analysis.

The resistance ratio for the precipitation-hardened sample is approximately 0.77 at 77 K and 0.68 at 4.2 K. The values calculated from the data of Berman et al. are 0.75 at 77 K and 0.67 at 4.2 K. The accuracy of Berman et al.'s results is not known, so the slight differences from the present results may not be significant.

Several effects are readily apparent in the resistance ratios in Figure 22. Both samples have rather large constant contributions to the resistance, which normally are associated with scattering of electrons by impurities. The constant resistance term of the solution-annealed sample is accounted for by the high density of Be "impurities". The constant contribution in the precipitation-hardened alloy is smaller, and this is thought to be due to the depletion of the Be concentration in the matrix as precipitates form. The effect of precipitates on the resistivity is not known.

It is also apparent in Figure 22 that the resistance of both samples has a minimum near 20 K. This is shown more dramatically in Figure 23, which is an expanded view of the data in Figure 22 below 40 K. As discussed in the Background chapter, the resistance minimum is due to electron

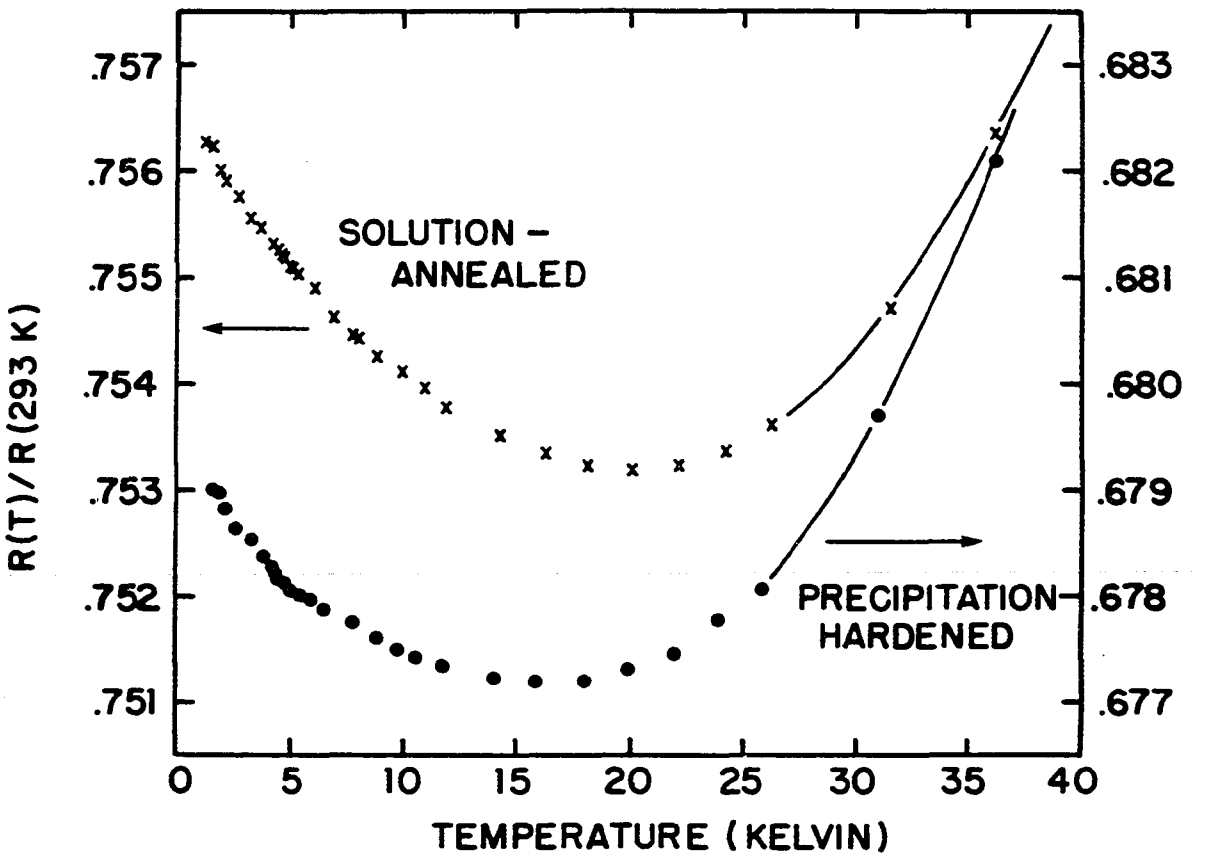

Figure 23. Resistance ratio for Berylco-25 strip below 40 K for solution-annealed (left scale) and precipitation-hardened (right scale) conditions

scattering by localized magnetic moments on Fe impurities, an effect originally explained by Kondo (14).

Kondo's expression (Eqn. 31) for the low temperature resistivity, including the magnetic impurity scattering, fits the Berylco-25 data very well below 30 K. The various parameters in Kondo's relation were determined by linear least-squares fits, and are given in Table 8. The magnetic Fe concentration may be estimated using these results and the assumption that the magnetic interactions in Berylco-25 are of the same nature and of the same strength as in Cu-Fe binary alloys. In addition, the value of 8.25 μΩ-cm was assumed for the room temperature resistivity of both sample conditions. The analysis gives a value of 0.03 wt.% for the Fe concentration in the solution-annealed sample and 0.02 wt.% for the precipitation-hardened sample. If the assumptions are valid, the results indicate that the magnetic moment of some of the Fe is eliminated during precipitation-hardening, possibly by oxidation during heat-treatment.

Further quantitative analysis of the resistance data was not attempted because of the rather complicated nature of both the theory of transport phenomena and of the alloy itself. The absence of anomalous effects was considered to be the essential experimental result.

Table 8. Parameters for the Kondo relations (Eqns. 31-33) for the Berylco-25 resistance data (in μΩ-cm)

Sample	ρ_o	$c\rho_1$	a	T_{min}	$\rho(0)-\rho_{min}$
SA	6.25	1.04×10^{-2}	5.2×10^{-10}	20.9	0.0036
PH	5.6	0.69×10^{-2}	8.9×10^{-10}	17.3	0.0022

DISCUSSION

Several features of the specific heats of copper-beryllium alloys have been described. The most notable of these is the existence of a maximum near 20 K in the ratio of the alloy specific heats to those of copper. This ratio enhancement was shown to be a manifestation of a slight shift to lower temperatures of the copper-like lattice specific heat of the Cu-Be solid-solution. In the discussion below, an attempt is made to relate this effect to changes in the phonon density of states as beryllium is substitutionally alloyed with copper. The Debye temperature of the Cu-Be solid-solution was found to be nearly the same as that of copper. This will be explained in terms of the adventitious cancellation of mass and force constant differences between the alloy and copper. The electronic specific heat coefficient of the Cu-Be solid-solution was found to be higher than that of copper. No definite explanation for this is given below, but several plausible sources for this behavior are examined.

This discussion concentrates on properties of the solid-solution. The structures of the precipitation-hardened samples were not well-characterized, but were assumed to represent an intermediate stage of precipitation rather than the equilibrium two-phase condition. However, a few comments are included below concerning possible effects

in the specific heats related to the presence of GP zones and the equilibrium two-phase configuration.

For this discussion, the low-iron Cu-1.92 wt.% Be alloy is assumed to be representative of the pure, binary Cu-Be system. The various magnetic specific heat contributions in the commercial alloys are regarded as experimental complications, and will be ignored.

Electronic Specific Heat

The experimental electronic density of states at the Fermi level for the solution-annealed low-iron sample is approximately 14% higher than that of copper, as is shown in Table 7. The free-electron model predicts a 5% increase in $g(\varepsilon_F)$ due to the higher electron density in the alloy as compared to copper. This prediction is in the right direction, but is not of the correct magnitude.

The poor agreement between the free-electron prediction and the experimental result is not surprising, since this simple model does not take into account the actual band structure of the metal. The rigid band model (58) does partially account for band structure effects. This model assumes that an alloy has the electronic structure of the host metal (copper), and that the only difference is in the electron density. As was mentioned in the Background chapter, the density of states for copper decreases uniformly with energy near the Fermi level, so that $g(\varepsilon_F)$ decreases

with increasing electron density. A rigid band model based on copper therefore predicts a trend which is opposite to that observed, so it is even less adequate than the free-electron model.

Other theoretical models consider the electronic properties of single, isolated impurities. A well-known result of such a theory is that the conduction electrons act to screen the impurity potential (59). The distance over which the electron density is disturbed by an impurity is on the order of $2\pi/k_F$, or typically several angstroms. This distance, however, is of the same magnitude as an average distance between the Be atoms in the 12 at.% solid-solution. The impurities, therefore, cannot be regarded as isolated, which destroys the validity of single impurity theories in the present case.

Any precise theoretical interpretation of the experimental electronic specific heat results must involve more detailed models, and more complicated calculations, than can be given here. There are, however, some very basic ideas which may be applied to the high concentration alloys under consideration.

A basic and important concept in the theory of metals is that the presence of spatially periodic potentials results in gaps in the electronic density of states (3). For a potential of wavelength λ, the gap occurs in the

dispersion relation at a wavevector $2\pi/\lambda$. If the Fermi energy is near a gap, the electronic density of states at the Fermi level could be very different from the free-electron prediction.

The primary example of a periodic potential is the crystal structure of an alloy. In particular, if an ordered, periodic arrangement of Be atoms existed in the Cu-Be solid-solution, this would be expected to produce a gap at a wavevector of $2\pi/d$, where d is equal to the Be-Be interatomic distance.

For an FCC crystal structure with lattice parameter a, the density of atoms is given by

$$n_a = 4/a^3. \tag{38}$$

For an FCC solid-solution of Be and Cu, with Be concentration x, the Be density, n_{Be}, is given by

$$n_{Be} = xn_a. \tag{39}$$

The concentration dependence of the lattice parameter (16) for the alloy is given approximately by

$$a = 3.615 - 0.346x. \tag{40}$$

The average Be-Be separation in the 12 at.% alloy then is approximately d = 4.6 A, corresponding to a wavevector $k_{Be} = 1.38\times10^{8}cm^{-1}$.

The Fermi-wavevector, defined for free electrons by

$$k_F = (3\pi^2 n_e)^{1/3}, \tag{41}$$

may be calculated from the electron density, n_e, given by

$$n_e = [(1-x)+2x]n_a, \tag{42}$$

where the Be is assumed to be divalent in the solid-solution. For a 12 at.% Be alloy, k_F is found to be approximately $1.42 \times 10^8 cm^{-1}$. It is emphasized here that this is the magnitude of the Fermi wavevector for a free-electron model. In a real metal, k_F depends on direction in momentum space since the Fermi surface generally is not a sphere, but the free-electron k_F does provide a rough measure of the its size. The Fermi surface of copper (7) is roughly spherical, but has flat areas and bulges.

The wavevector associated with the average Be-Be separation is seen to be nearly equal to the Fermi wavevector. The two wavevectors would be equal for a Be concentration of 13.6 at.%, which incidentally is nearly equal to the maximum solubility limit of Be in Cu (15).

If the Be distribution were ordered in the alloy, there certainly would be a gap in the density of states near the Fermi level. This would easily account for the observed electronic specific heat behaviors.

The Be distribution in a typical solution-annealed

Cu-Be alloy is thought to be disordered rather than periodic. It is not clear what effect disorder would have on the above gap arguments, although it possibly could introduce localized resonance states within the gap if the disorder were not too severe. The result of complete disorder (random distribution of Be) is not known, but may completely smear any gap in the density of states (60).

The fact that k_F and k_{Be} are nearly the same for the 12 at.% alloy is interesting, and cannot be ignored even though the Be is thought to be disordered. This property, along with the observed electronic specific heat behavior, suggests that short-range order may exist in the solution-annealed low-iron alloy sample. Small regions of ordered Be distribution in the alloy could exhibit a gap in the density of states, and hence account for the experimental results. There is, in fact, tentative support for the existence of short-range order in the alloy in the form of clusters of Be (25). These have been observed in a few samples, but do not seem to be a normal feature of the structure of these alloys. The sample preparation conditions for which these clusters occur also are not known. The presence of such clusters in the samples used for the present work cannot be ruled out, since no structural studies of these samples were done, and their exact condition is not known.

A definite explanation of the observed electronic

specific heat of the solution-annealed alloy requires more complete and detailed structural characterization of the samples. Neutron scattering or X-ray diffraction studies could be done to search for short-range order. The dependence of the electronic specific heat contribution on Be concentration would be another interesting study. Since both k_F and k_{Be} depend on concentration, these could be varied, and anomalous changes in the electronic specific heat coefficient could appear as a function of concentration. A more complete study of the conditions leading to Be clusters also would be useful.

The effects on the electronic properties of the alloy due to GP zones and precipitates are also unknown. It was observed experimentally that precipitation-hardening reduced the electronic specific heat coefficient. A simple explanation for this is that in the CuBe intermetallic phase, the Be is monovalent and the density of states is of similar magnitude to copper (61). At some stage during precipitate growth, therefore, there must be an electronic transition between the divalent state of Be in the solid-solution and the monovalent form in the equilibrium precipitates. We speculate that this transition would occur for one of the intermediate precipitate stages. A more refined study of the evolution of specific heat as a function of precipitation-hardening time and temperature is suggested.

Debye Temperature

The Debye temperature may be written as

$$\theta = \frac{\hbar}{k_B} c k_D, \tag{43}$$

where c is an average magnitude of the sound velocity, and k_D is the magnitude of the Debye wavevector defined by

$$k_D = (6\pi^2 n_a)^{1/3}. \tag{44}$$

The sound velocity depends on the polarization of the lattice vibrations and on their direction of propagation, but for a monatomic lattice c may be written as

$$c = a \left(\frac{\kappa}{M}\right)^{1/2} \tag{45}$$

where a is the lattice parameter and M is the atomic mass. The parameter κ represents the interatomic force constants in the harmonic approximation, averaged over direction and polarization. The Debye temperature then is proportional to $(\kappa/M)^{1/2}$, and for a monatomic FCC lattice may be expressed as

$$\theta = \frac{\hbar}{k_B}(24\pi^2)^{1/3}\left(\frac{\kappa}{M}\right)^{1/2}. \tag{46}$$

Although Eqn. 46 is appropriate for a monatomic lattice, a crude understanding of the Debye temperature of a high concentration solid-solution may be obtained by regarding κ and M as atomic averages of the effective force constant and

mass, respectively. This approximation is reasonable since the the sound velocity describes the propagation properties of phonons with wavelengths that are much larger than the distances between solute atoms.

It was found experimentally that the Debye temperature of the Cu-12 at.% Be solid-solution is nearly the same as that for pure copper. The average atomic mass in this alloy is approximately 90% of the atomic mass of pure copper, which implies, according to Eqn. 46, that the average effective force constant κ in the alloy must be about 90% of its value in pure copper. In effect, the change in force constant is cancelled by the change in mass, resulting in virtually no change in the Debye temperature.

The local mode of oscillation of the light Be atoms in Cu-Be solid-solutions has been studied by inelastic neutron scattering (10,62), and these results have been used to calculate the Be-Cu interatomic force constants (63). The values thus obtained depend sensitively on the theoretical model used to describe the local mode behavior, but range from 40% to 60% of the Cu-Cu force constant. A reasonable average value is assumed to be 50%.

For a large number of atoms, therefore, the average effective force constant should be lower in the alloy than for copper. Although this average could not be calculated, it is clear that the experimental Debye temperature behavior

is qualitatively consistent with the neutron scattering results.

A detailed theoretical calculation of the Debye temperature of a pure metal containing isolated impurities has been given by Agrawal (64). The mass of the substitutional impurity (Be) is denoted m′, and the host lattice atoms (Cu) have mass m. The impurity-host force constant is κ′ and that for the host-host interaction is κ. For an impurity concentration x, the Debye temperature is given by

$$\theta(x) = \theta(0)\left[\, 1 - \frac{x}{2}\left(\alpha - \frac{2\beta}{1+\eta\beta}\right)\right] , \qquad (47)$$

where α is the mass defect parameter,

$$\alpha = \frac{m'-m}{m} , \qquad (48)$$

and β is the relative force constant difference given by

$$\beta = \frac{\kappa'-\kappa}{\kappa} . \qquad (49)$$

The parameter η in Eqn. 47 is a numerical constant characteristic of the crystal structure only. Its value for an FCC lattice has not appeared in the literature (65), but should be between 0.10 and 0.15. For the following calculations, the value of 0.13 was assumed.

For the Cu-12 at.% Be solid-solution, x = 0.12 and α = -0.86. The force constant κ′ is assumed to be 0.5κ, consistent with the neutron scattering results mentioned

above. Equation 47 then gives $\theta = 0.99\theta(0)$, a 1% decrease in the Debye temperature upon alloying. The experimental result, given in Table 6, is an approximate 1% increase. This can be considered to be reasonable agreement between the model and observed behavior. Both show that the Debye temperature remains essentially unchanged upon alloying. More precise values for κ and η could improve the numerical agreement.

Alternately, using the experimentally determined values of θ from Table 6, the force constant change β is found from Eqn. 47 to be -0.34. This gives $\kappa' = 0.66\kappa$, which is in reasonable agreement with the value of 0.63κ given by Kesharwani (63), which was obtained from neutron diffraction data using a model that partially accounts for the effects of high impurity concentration.

The presence of GP zones is not expected to have a great effect on the Debye temperature. The zones are essentially localized distortions of the FCC lattice with dimensions that are comparable to the Be-Be separation in the solid-solution. The Be concentration is slightly higher in the neighborhood of a zone, so that impurity-impurity interactions would be more important, but this effect should remain small except for large zones. In the early stages of precipitation, therefore, the arguments given above concerning the force constant and mass differences between the

alloy and copper should still have some validity. The principal effect on θ should be the change in the average atomic volume associated with the density increase upon precipitation-hardening.

Assuming that the Grueneisen parameter for the alloy is equal to the value for pure copper, approximately 2, the effect of the volume change due to zone formation may be estimated from

$$\Gamma = -\frac{d\ln\theta}{d\ln V}. \qquad (50)$$

The density change with precipitation-hardening, given in Table 3 for the low-iron alloy, is approximately +0.5% which is equivalent to a volume change of -0.5%. Equation 50 then predicts a change in θ of +1%. Experimentally, θ is indeed seen to increase with precipitation-hardening, but the magnitude of the change is larger, about 5%. Most of this change for the low-iron alloy samples could be related to an intrinsically higher Debye temperature for large precipitates.

Phonon Spectrum Changes

In the Debye model, the phonon density of states $D(\omega)$ is proportional to ω^2, and the Debye temperature is constant and equal to θ_o. For real materials, $D(\omega)$ typically varies more rapidly than ω^2 and the Debye temperature consequently depends on temperature, approaching θ_o at very low

temperatures. In particular, if $D(\omega)$ increases more rapidly than ω^2, $\theta(T)$ decreases with increasing temperature. This is the behavior exhibited in Figure 14 for copper and both conditions of the low-iron Cu-1.92 wt.% Be samples. The initial decrease of $\theta(T)$ with temperature is equivalent to the positive deviations from the Debye specific heat shown in Figure 13. It is apparent that the initial decrease of $\theta(T)$ is more rapid for the solution-annealed Cu-Be alloy than for copper. This indicates that the substitution of Be in Cu results in an increase in the phonon density of states for low frequencies.

A simple model (66) of the low-frequency density of states which describes the experimental specific heat behavior is given by

$$D(\omega) = a_2\omega^2 + a_4\omega^4. \tag{51}$$

The coefficient a_2 is given by the Debye model as

$$a_2 = \frac{3}{2\pi^2 c^3} = 9n_a \frac{\hbar^3}{k_B{}^3 \theta_o{}^3}, \tag{52}$$

and $a_4\omega^4$ represents the deviations of $D(\omega)$ from Debye behavior. A calculation of the low temperature specific heat for this model gives an approximation for $\theta(T)$ as

$$\theta(T) = \theta_o\left[1 - \left(\frac{T}{\theta_1}\right)^2\right], \tag{53}$$

with

$$\theta_1 = \left(\frac{21\hbar^2 a_2}{20\pi^2 k_B^2 a_4}\right)^{1/2} , \qquad (54)$$

which is valid for T much less than θ_1. The parameter θ_1 gives a measure of the temperatures for which the ω^4 term in Eqn. 51 contributes significantly to the specific heat. Specifically, deviations from the Debye model due to this term are approximately +1% for a temperature of $\theta_1/17$, and +12% at $T = \theta_1/5$.

Least-squares fits of Eqn. 53 to the experimental data represented in Figure 14 give θ_1 as 97 K for copper, 66 K for the solution-annealed Cu-Be alloy, and 69 K for the precipitation-hardened alloy. The uncertainties of these figures are ±10%.

These results indicate that the ω^4 contribution to the phonon density of states is nearly twice as large for the Cu-Be alloy as it is for copper, while the Debye contributions (ω^2 terms) are essentially the same in both materials. This difference may be stated in another way by rewriting Eqn. 51, using Eqn. 54, as

$$D(\omega) = a_2\omega^2\left[1 + \frac{21}{20\pi^2}\left(\frac{\hbar\omega}{k_B\theta_1}\right)^2\right] . \qquad (55)$$

which is dimensionally more transparent than Eqn. 51. The difference between Eqn. 55 and the Debye density of states is about 10% for a frequency given by $\hbar\omega = k_B\theta_1$. For the

Cu-12 at.% Be solid-solution, this frequency is only 68% of the corresponding frequency for pure copper.

For a given crystal structure, with a fixed number of atoms, the total number of phonon modes is fixed. Any change in the density of states upon substitutional alloying may therefore be regarded as shifts of the phonon frequencies rather than the appearance or disappearance of modes. The above arguments and the results for copper and the Cu-Be solid-solution indicate that for the low frequencies for which Eqn. 51 is valid, the phonon modes shift to lower frequencies upon alloying. It was shown above that the relative shift apparently is quite large for low ω.

At higher frequencies the density of states differs considerably from the Debye model, and the details of the specific heat behavior cannot be understood with simple arguments such as those given above. A few qualitative comments may be made, however, using the density of states of copper (9,67) shown in Figure 24 as an example. The Debye model is indicated in the figure by the dashed line. The frequency of the first Van Hove singularity, denoted ν_1, is 3.43 THz, or 165 K in temperature units. The Debye frequency ν_D corresponds to a temperature of 345 K, and the maximum frequency of the spectrum ν_M, is 7.3 THz (350 K). Note that the frequencies in the figure (ν) are related to those given in the earlier equations (ω) by $\nu = \omega/2\pi$.

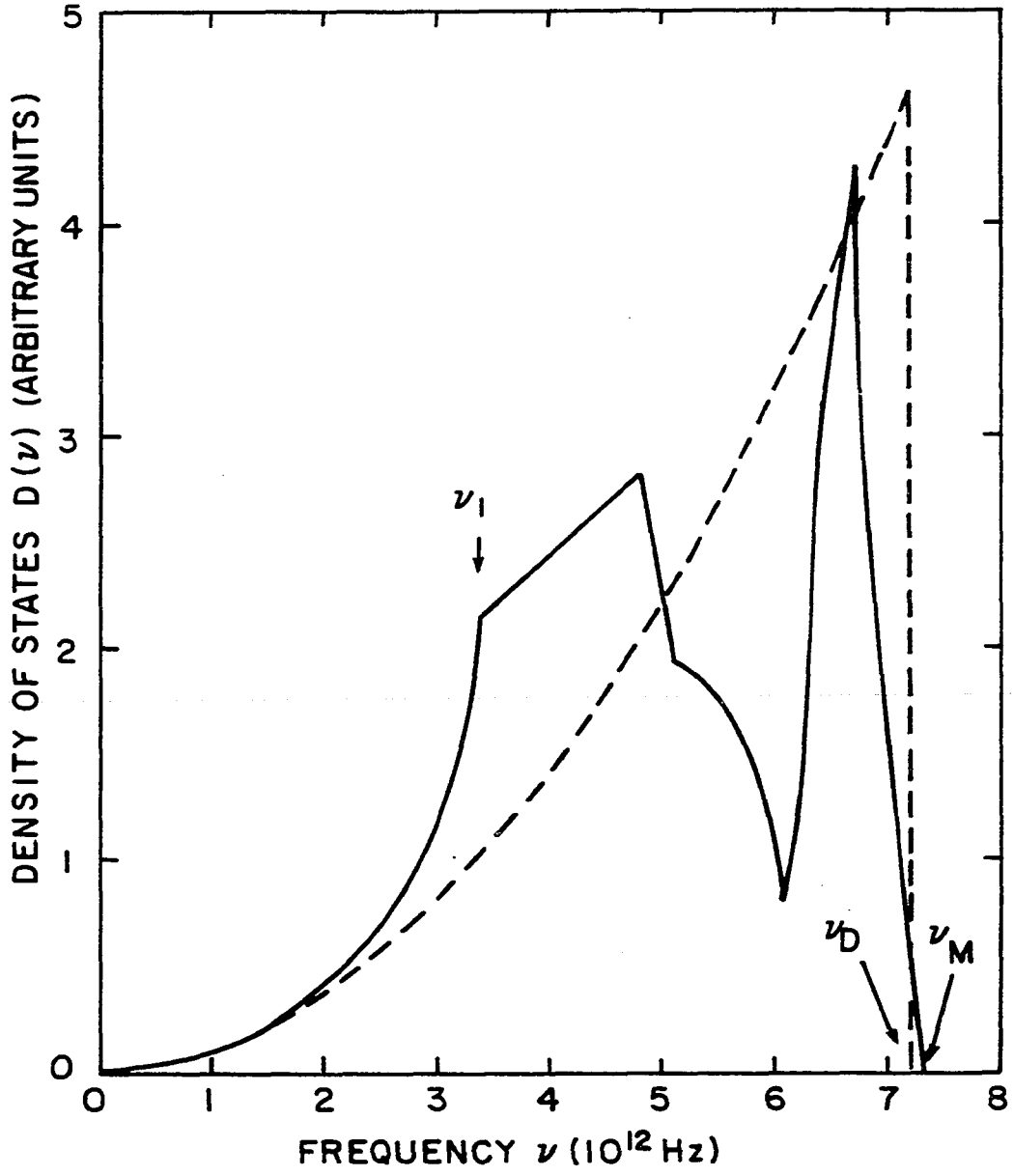

Figure 24. Phonon density of states for copper, based on data given in Ref. 67. The dashed line represents the Debye model, with ν_D the Debye frequency. The frequency of the first Van Hove singularity is ν_1, and the maximum frequency of the spectrum is ν_M

If the negative shifts of the phonon mode frequencies persist to higher frequencies, the location of the first Van Hove singularity would also be shifted downwards. The specific heat results do not positively state that such a shift occurs, but are consistent with this possibility. Neutron diffraction measurements of the location of this singularity would provide a direct test of this speculation.

The behavior of the phonon density of states of Cu-Be solid-solutions for high frequencies has been well-characterized as a result of the neutron scattering studies of the light impurity local modes (62). These modes have frequencies which are above ν_M, and would appear in Fig. 24 as an additional sharp peak in $D(\nu)$ at approximately 10.2 THz (490 K). The appearance of these modes is accompanied by a decrease in $D(\nu)$ for frequencies near ν_M, and an upward shift of ν_M. For a Cu-12 at.% Be solid-solution, ν_M increases to 7.75 THz (372 K), or a change of +6% from its value for copper.

The changes in the phonon density of states due to the substitution of Be in Cu are summarized as follows. The specific heat results of the present work are consistent with a shift to lower frequencies of low frequency phonon modes. The neutron scattering literature clearly indicates an upward shift of frequencies near ν_M, along with the existence of local modes. The behavior for intermediate

frequencies is not known, but could present interesting possibilities for further study. This would be accomplished most directly through neutron scattering measurements of the density of states.

SUMMARY

Specific heat measurements from 1 K to 70 K have been reported for alloys of copper with approximately 2 wt.% beryllium. These results have been used to characterize the behavior of the electronic density of states, the Debye temperature, and the low-frequency phonon density of states for solution-annealed and precipitation-hardened conditions of the alloy. The principal differences in these quantities between the copper-beryllium solid-solution and pure copper were shown to be slight increases in both the electronic density of states at the Fermi level and the low frequency phonon density of states. The Debye temperature remains unchanged. The principal effect of precipitation-hardening is to reverse the density of state changes, and to increase the Debye temperature by several percent. This seems to be related to the depletion of the beryllium concentration in the matrix as precipitates form.

The increase in the electronic density of states at the Fermi level upon alloying may be partially explained by the increase in the electron density. A full explanation of the electronic behavior could not be presented, but there may be effects present due to possible short-range order of the beryllium distribution in the solid-solution. The approximate equality of the Debye temperature for both the solid-solution and for copper is more easily explained in terms of

cancellation of changes in average atomic mass and interatomic force constants.

The behavior of the lattice contribution to the specific heat of the copper-beryllium solid-solution is consistent with an increase in the low-frequency phonon density of states upon alloying. This is associated with deviations of the density of states from the ideal Debye model, which can be related to shifts of the phonon frequencies to lower frequencies.

These changes in the phonon density of states are manifested in the specific heat of the alloy as a maximum, or enhancement, near 20 K in the ratio of the alloy specific heat to that of copper. This method of displaying the data was very important for the present work, since the subtle lattice specific heat effects might otherwise have gone unnoticed.

Specific heat measurements on the standard commercial alloy Berylco-25 revealed very large magnetic contributions due to the presence of small amounts of iron and cobalt in this material. The Debye temperatures and electronic specific heat coefficients could not be calculated for these samples because the precise magnitude of the magnetic effects could not be determined. Qualitative interpretation of the Berylco-25 results suggested that the principal role of work-hardening in this alloy is to provide additional

nucleation sites for precipitate formation. This in turn leads to a more rapid decrease in the magnitude of the ratio enhancement upon hardening. These results also suggest that very little change occurs in the lattice specific heat of the alloy for early stages of precipitation-hardening.

Thermal expansivity results for the alloy CUBE-250 also show an enhancement effect. These results are qualitatively consistent with the specific heat results, but were not quantitatively analyzed. In particular, the Grueneisen parameter could not be derived.

Electrical resistance measurements on Berylco-25 samples show very large constant resistivity contributions, which are to be expected for a highly disordered alloy. The Kondo effect, due to the iron in the alloy, was also found. Precipitation-hardening reduces this magnetic resistivity contribution, consistent with an effective decrease in the magnetic iron concentration.

The specific heat of pure copper was obtained between 1 K and 65 K. The least-squares fits of these data, and the tabulated values obtained from these fits, provided a useful representation of the specific heat of copper for reference purposes. Previously published copper reference data of comparable accuracy cover only the temperature range from 1 K to 30 K. The present work, therefore, roughly doubles the range for which copper may be used as a specific heat

reference material.

Several possibilities for further experimental work on this class of copper-beryllium alloys are suggested. A study of the dependence of the electronic specific heat coefficient on beryllium concentration for copper-beryllium solid-solutions could help to resolve the unexplained density of states behavior. More detailed characterization of the structure of the solid-solution could determine if some form of short-range order exists in the beryllium distribution. Neutron scattering studies could verify the suggested negative shifts of the phonon frequencies, in addition to determining changes which may occur in the density of states that cannot be resolved through specific heat measurements. For these suggested studies, the use of high-purity, binary copper-beryllium alloys is strongly recommended.

REFERENCES

1. C. J. Adkins, Equilibrium Thermodynamics, 2nd ed. (McGraw-Hill, New York, 1975).

2. R. Kubo, Statistical Mechanics (North-Holland, New York, 1965).

3. N. W. Ashcroft and N. D. Mermin, Solid State Physics (Holt, Rinehart and Winston, New York, 1976).

4. T. H. K. Barron, J. G. Collins, and G. K. White, Adv. Phys. 29, 609 (1980).

5. E. S. R. Gopal, Specific Heats at Low Temperatures (Heywood, London, 1966).

6. E. Grueneisen, Handbook der Physik (Springer-Verlag, Berlin, 1926), Vol. X, pp.1-59.

7. G. A. Burdick, Phys. Rev. 129, 138 (1963).

8. B. N. Harmon, Physics Department, Iowa State University (private communication).

9. S. K. Sinha, Phys. Rev. 143, 422 (1966).

10. I. Natkaniec, K. Parli'nski, A. Bajorek, and M. Sudnick-Hrynkiewicz, Phys. Lett. 24A, 517 (1967).

11. R. Tournier, J. J. Veyssie', and L. Weil, in Metallic Solid Solutions, edited by J. Friedel and A. Guinier (W. A. Benjamin, New York, 1963), Chap. XVI, pp. 1-8.

12. P. B. Wiegmann, J. Phys. C 14, 1463 (1981).

13. B. B. Triplett and N. E. Phillips, Phys. Rev. Lett. 27, 1001 (1971).

14. J. Kondo, Prog. Theor. Phys. 32, 37 (1964).

15. M. Hansen, Constitution of Binary Alloys, 2nd ed. (McGraw-Hill, New York, 1958), p.281.

16. R. Reinbach and H. G. Baer, Z. Metallkd. 60, 453 (1969).

17. W. B. Pearson, A Handbook of Lattice Spacings and Structures of Metals and Alloys (Pergamon, New York, 1958), Vol. 1, p. 98.

18. C. E. Olsen, B. T. Matthias, and H. H. Hill, Z. Phys. 200, 7 (1967).

19. V. I. Tutov, E. E. Semenenko, and A. A. Chupikov, Sov. J. Low Temp. Phys. 8, 340 (1982).

20. V. Gerold, Z. Metallkd. 45, 593 (1954).

21. D. J. Millar, G. Sines, and J. W. Goodman, Acta Metall. 23, 245 (1975).

22. S. Yamamoto, M. Matsui, and Y. Murakami, Trans. Japan Inst. Metals 12, 159 (1971).

23. V. A. Phillips and L. E. Tanner, Acta Metall. 23, 441 (1973).

24. A. Kelly and R. B. Nicholson, Prog. Mat. Sci. 10, 151 (1963).

25. R. J. Rioja and D. E. Laughlin, Acta Metall. 28, 1301 (1980).

26. L. E. Tanner, A. R. Pelton, and R. Gronsky, J. Phys. (Paris) 43, C4-169 (1982).

27. M. I. Gitgarts and A. V. Tolstoy, Phys. Met. Metallogr. (USSR) 45, 133 (1979).

28. J. W. Martin, Micromechanisms in Particle-Hardened Alloys (Cambridge University Press, Cambridge, 1980).

29. L. M. Brown and R. K. Ham, Strengthening Methods in Crystals, edited by A. Kelly and R. B. Nicholson (Elsevier, Amsterdam, 1971), p.12.

30. American Society for Metals, Metals Handbook, 9th ed. (American Society for Metals, Metals Park, Ohio, 1979), Volume 2, pp..303-305.

31. R. B. Ross, editor, Metallic Materials Specification Handbook (Spon, London, 1980), Section 14D, pp. 125-128.

32. G. R. Gohn, G. J. Herbert, and J. B. Kunh, The Mechanical Properties of Copper-Beryllium Alloy Strip, American Society for Testing and Materials Special Technical Publication No. 367 (ASTM, Philadelphia, 1964).

33. J. T. Richards and R. M. Brick, J. Metals, May 1954, 574.

34. D. J. Rehak, M.S. Thesis, Iowa State University, 1972 (unpublished).

35. Kawecki Berylco Corp., Report of Analysis 406065A0, 1976 (unpublished).

36. J. Schilling, Ruhr-Universitat, Bochum, West Germany (private communication).

37. R. C. Weast, editor, CRC Handbook of Chemistry and Physics, 59th ed. (CRC Press, West Palm Beach, Florida, 1978), p. F-11.

38. S. N. Maiti and D. Roy, Phys. Status Solidi B 122, 449 (1984).

39. V. E. Lysaght, Indentation Hardness Testing (Reinhold, New York, 1949).

40. J. J. M. Beenakker and C. A. Swenson, Rev. Sci. Instrum. 26, 1204 (1955).

41. V. Arp, J. H. Wilson, L. Winrich, and P. Sikora, Cryogenics 2, 230 (1962).

42. R. L. Holtz and C. A. Swenson, J. Appl. Phys. 54, 2844 (1983).

43. F. R. Kroeger and C. A. Swenson, J. Appl. Phys. 48, 853 (1977).

44. H. Kandil, Ames Laboratory, Iowa State University (unpublished work).

45. H. M. Ledbetter and E. R. Naimon, J. Phys. Chem. Ref. Data 3, 897 (1974).

46. R. Q. Fugate, Ph.D. Thesis, Iowa State University, 1970 (unpublished).

47. J. K. Krause, Ph.D. Thesis, Iowa State University, 1978 (unpublished).

48. A. Berton, J. Chaussy, B. Cornut, J. Odin, J. Paureau, and J. Peyrard, Cryogenics 19, 543 (1979).

49. L. G. Gavrilenko, A. V. Gavrilova, B. M. Mogutnov, and Yu. D. Tyapkin, Phys. Met. Metallogr. (USSR) 26, 179 (1968).

50. K. Hirano, J. Phys. Soc. Japan 10, 721 (1955).

51. J. C. Holste, T. C. Cetas, and C. A. Swenson, Rev. Sci. Instrum. 43, 670 (1972).

52. G. T. Furukawa, W. G. Saba, and M. L. Reilly, Critical Analysis of the Literature and Evaluation of Thermodynamic Properties of Copper, Silver, and Gold from 0 to 300 K (U. S. Govt. Printing Office, Washington, D.C., 1968), NSRDS-NBS18.

53. T. F. Stromberg, R. J. Balestri, and W. C. Overton Jr., J. Chem. Phys. 57, 1502 (1972).

54. P. R. Bevington, Data Reduction and Error Analysis for the Physical Sciences (McGraw-Hill, New York, 1969).

55. J. P. Franck, F. D. Manchester, and D. L. Martin, Proc. Roy. Soc. (London) A263, 494 (1961).

56. R. Berman, E. L. Foster, and H. M. Rosenberg, British J. Appl. Phys. 6, 181 (1955).

57. T. W. Watson and D. R. Flynn, Trans. Metall. Soc. AIME, 242, 876 (1968).

58. M. H. Cohen and V. Heine, Adv. Phys. 7, 395 (1958).

59. J. Friedel, Adv. Phys. 3, 446 (1954).

60. B. N. Harmon, Physics Department, Iowa State University (private communication).

61. V. L. Moruzzi, A. R. Williams, and J. F. Janak, Phys. Rev. B 10, 4856 (1974).

62. Yu. L. Shitikov, M. G. Zemlyanov, G. F. Syrikh, and N. A. Chernoplekov, Sov. Phys. JETP 51, 752 (1980).

63. K. M. Kesharwani, Phys. Status Solidi B 93, 691 (1979).

64. B. K. Agrawal, J. Phys. C 2, 252 (1969).

65. A. K. Srivastava and B. K. Agrawal, J. Phys. C 3, L20 (1970).

66. A. A. Maradudin, E. W. Montroll, G. H. Weiss, and I. P. Ipatova, Theory of Lattice Dynamics in the Harmonic Approximation, 2nd ed. (Academic, New York, 1971), p. 469.

67. E. C. Svensson, B. N. Brockhouse, and J. M. Rowe, Phys. Rev. 155, 619 (1967).

68. "Speaking Out: Heath Hazard Information for Users of Beryllium Alloys", pamphlet available from Cabot-Berylco Corporation, Reading, Pennsylvania (1981).

69. I. R. Tabershaw, editor, The Toxicology of Beryllium, Public health service publication no. 2173, (U.S. Department of Health, Education and Welfare, 1972).

70. Code of Federal Regulations, Revised July 1983, Volume 29, Chapter XVII, Part 1910.1000, Subpart Z.

71. G. K. White, Experimental Techniques in Low Temperature Physics, 3rd ed. (Clarendon, Oxford, 1979).

72. C. A. Swenson, High Sensitivity Expansivity Measurement Techniques (unpublished).

73. F. R. Kroeger, Ph.D. Thesis, Iowa State University, 1974 (unpublished).

74. K. G. Lyon, Ph.D. Thesis, Iowa State University, 1978 (unpublished).

75. M. Wun and N. E. Phillips, Cryogenics 15, 36 (1975).

ACKNOWLEDGEMENTS

The author wishes to thank the following persons who contributed to the completion of this work:

Dr. C. A. Swenson for suggesting the problem, and for his continual support, patience, and understanding;

J. Ostenson and R. Brown for their technical assistance during the initial stages of the experimental work;

T. Freidmann for the beautifully done electrical resistance measurements, and K. Hagen for performing preliminary resistance measurements;

and Dr. W. Kamitakahara for suggesting phonon frequency shifts as the explanation for the lattice specific heat behavior.

APPENDIX A. BERYLLIUM TOXICITY

A significant disadvantage of Cu-Be alloys is that Be is toxic. Inhalation of Be or Be compounds may result in a form of irreversible lung damage known as Berylliosis (68,69). This condition can be serious enough to cause death, but seems to depend on individual sensitivity.

Inhalation of Be or Be compounds is the known source of the hazard. Ingestion or exposure through wounds is not thought to pose a risk. For this reason, exposure standards have been established for airborne Be concentrations only. The OSHA standard (70) for occupational exposure to airborne Be is a time-averaged, maximum exposure to 2 μg per cubic meter of air. The acceptable ceiling is 5 $\mu g/m^3$, and the allowable one time peak exposure is to 25 $\mu g/m^3$ for 30 minutes. Monitoring of airborne Be concentrations presents somewhat of a problem, however.

Appropriate precautions must be taken when working with any potentially dangerous substance. Section 1910.1000 of the Code of Federal Regulations (70) prescribes the use of local exhaust ventilation for commercial working of most beryllium-containing material. Respirators and disposable clothing are recommended when large amounts of contamination cannot be avoided, such as in large scale grinding or welding operations.

Pure beryllium and beryllium oxide require extreme precautions. The beryllium in the standard Cu-2 wt.% Be alloys is chemically bonded to the copper, so most ordinary small scale machining operations with normal ventilation should pose little risk provided fine dust is not generated. Beryllium will dissociate from the alloy if heated above 860 ^{o}C, so overheating during solution-annealing must be avoided. Welding also poses a risk. Beryllium oxide may form during heat treatment in air, so solution-annealing and precipitation-hardening are best done in inert atmospheres, vacuum, or standard salt-baths. Acid is often used to etch or clean parts, and is effective in removing any oxide layer after heat treatment in air. The liquid waste generated by this is hazardous, as it contains free beryllium in solution.

Another area of concern is waste disposal. Standards exist (68) for industrial users of alloys containing more than 5 wt.% Be, but the standard 2 wt.% Be alloy is not covered by these regulations. Small amounts of solid Cu-Be waste may be disposed of without special precautions. Larger amounts may be returned to the manufacturer for recycling. Any dust or liquid waste involving the commercial alloys ought to be handled by an appropriate agency.

APPENDIX B. EXPERIMENTAL DETAILS

All of the thermal expansion, heat capacity, and electrical resistance measurements were done using standard methods and apparatus of standard construction. These are well-described elsewhere. An overview of low temperature experimental techniques is given by White (71). Below, references for each experiment are given, rather than lengthy descriptions. The following discussion concentrates on significant differences of the present work from more typical experimental arrangements, and on problems that were encountered.

Thermal Expansion

A very useful review of experimental thermal expansivity measurement techniques is given by Swenson (72). A less detailed description is given by Barron, Collins, and White (4).

The linear thermal expansivities of the CUBE-250 samples were determined with the absolute thermal expansion apparatus used previously by Kroeger (73) for studies of copper and aluminum. No changes were made to either the procedures or to the equipment, which are well-described by Kroeger.

Measurements of the linear expansivities of several of the Berylco-25 samples were attempted using the relative expansion apparatus described by Lyon (74). The intention

was to determine the Grueneisen parameter for these samples, for which specific heat data had also been obtained. Reliable results were not obtained due to a number of unresolved experimental problems.

In a basic relative thermal expansion experiment, a sample with flat, parallel ends is mounted inside a "cell". The cell consists of a cylindrical shell surrounding the sample, with a flat plate across the bottom and one at the top. One end of the sample is secured to the bottom plate. The top plate of the cell contains a smaller, concentric insulated plate, which forms a parallel plate capacitor arrangement with the top end of the sample. The distance between the end of the sample and the top plate is the gap of the capacitor, and is equal to the difference in lengths of the cell and the sample. The gap is determined by a measurement of the capacitance. The thermal expansion coefficient of the sample is determined by measuring the change in the gap with changes in temperature, and knowledge of the temperature dependence of the cell length. The cell length may be calibrated against a reference sample of known expansivity.

The Lyon apparatus (74) has provisions for simultaneous measurements on four independent samples. According to the original design, one of the samples would be a reference of known expansivity, and the expansivities of three unknown

samples could be determined during each experimental run. In practice, however, it has been necessary to use three reference samples with only one unknown in this apparatus. Anomalously large, and irreproducible cell expansions have been encountered, in addition to an apparent tilt of the top plate with respect to the bottom plate. Three reference samples are required simply to define the geometry of the cell, so that only one unknown could be measured. The cause of the anomalous cell expansions is not known.

In attempts to improve the behavior of the cell, numerous changes have been made in its construction. Originally, the cell used three separate support posts to separate the top and bottom plates. These were replaced with a single machined unit. Different methods of insulating the capacitor plates were also tried. These included the spring-loaded mechanical construction of the original design, the use of epoxy for both insulation and support, and the pressed-in plate method used by Kroeger for the absolute apparatus. In addition to the design changes, all of the cell parts were replaced with sturdier pieces of strain-annealed, high quality copper.

Although, in effect, the entire cell had been replaced, the problems were not cured, and in fact appeared to worsen in some cases. A different design, based on that of Barron et al. (4), has been tried, with similar unusual results.

Since the difficulties were not resolved by the cell changes, it has been suggested that the copper reference samples that have been used for all of the studies have anomalous expansivities. These samples were made from the same rod, and in the same way, as the copper specific heat sample described in the Experimental Results section. The specific heat of this material was found to be well-behaved. It is difficult to reconcile this fact with the suggestion of anomalous expansivities for the other samples, but the possibility will be investigated.

Heat Capacity

Heat capacities were measured by the conventional heat-pulse technique with the same electrical systems and procedures as used previously by Fugate (46) and Krause (47) for their work on solidified gases. The metal dewars and fixed cryostat used for that work were replaced with a glass dewar system and a removable insert of standard design.

The addenda and sample were suspended with nylon thread within a temperature-controlled "shield" consisting of a copper vacuum can and a 67 cc capacity liquid helium "pot". The shield, in turn, was contained inside a main vacuum can immersed in the liquid helium bath.

Three different addenda were used, designated "December", "April", and "September" according to the month in which each was put into service. All three were of the

same basic configuration as that shown in Figure B1. The flat bottom of a round or hexagonal rod sample rests on a copper platform within a frame of copper wire. The heater assembly, of approximately 550 ohms of Pt-8%W wire wound noninductively on a small copper form, is in contact with the top of the sample. Apiezon-N grease was used at both ends of the sample to ensure good thermal contact with the addenda. Most conventional addenda designs use a mechanical clamp of some sort to secure the sample. For the present work, the samples were large enough that their own weight acted to hold them in place. This allowed for less massive addenda, since a clamp was not necessary.

Germanium thermometer GR15698 was inserted into a holder consisting of copper foil silver-soldered to the frame for the December and April addenda, or into a hole drilled into the frame itself for the September addenda. A copper wire attached to the frame leads to a mechanical "jaws"-type heat switch mounted on the shield. All electrical connections on the addenda were made with nonsuperconducting cadmium-bismuth solder. All mechanical construction was done with silver-solder. Electrical leads were thermally and mechanically anchored to the addenda with GE 7031 varnish. The support threads were tied to the addenda in various locations, but were not varnished into place because they would occasionally have to be replaced due to

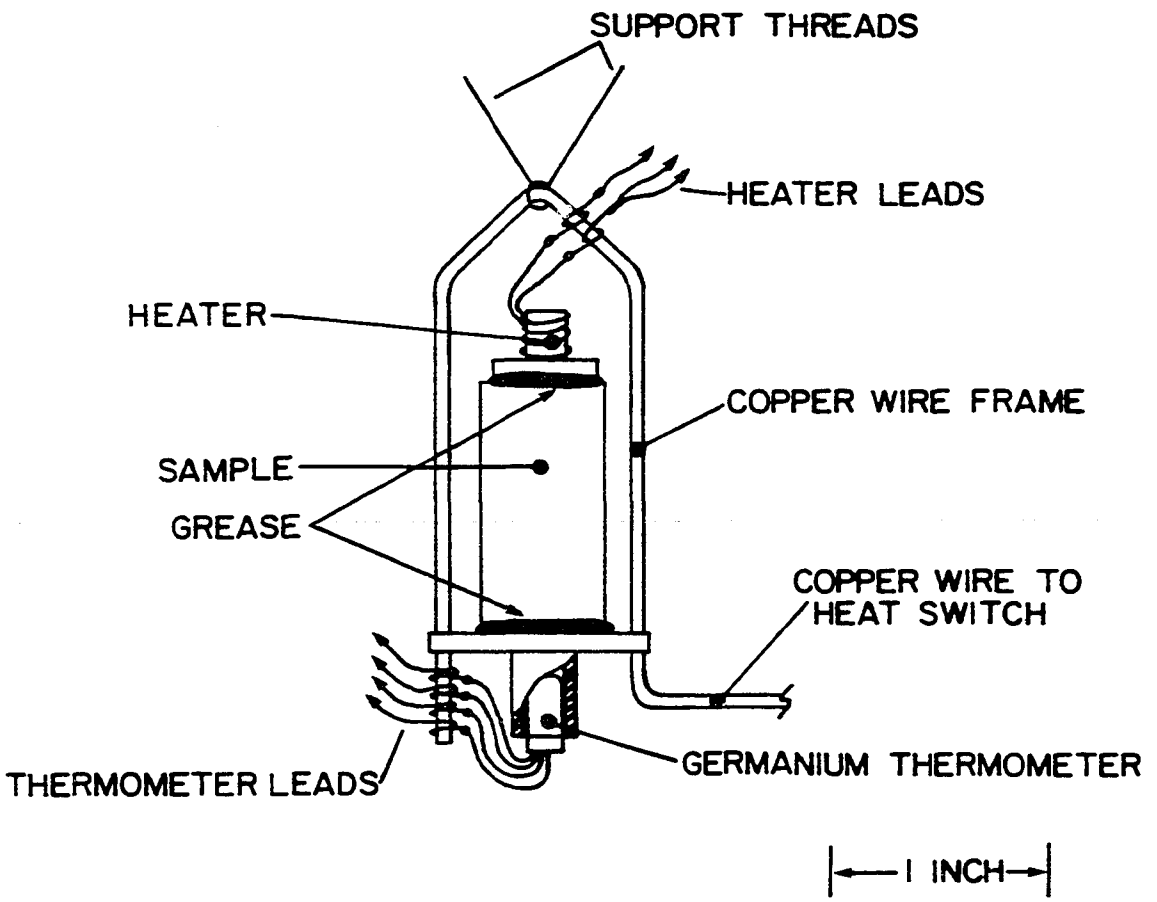

Figure B1. Addenda configuration

stretching or breakage. It was decided to avoid changing the addenda heat capacity by the addition of any new varnish in each instance of thread replacement.

Analysis of the heat capacity data was conventional, and is described by both Fugate and Krause. Least-squares fits of an odd power series in temperature were used to determine an analytic representation of the addenda heat capacities. The fits were used to subtract the addenda contribution to the heat capacity for each measurement. Corrections were done to the data to compensate for the effect of finite temperature interval, but the effect was negligible.

Figure B2 shows the contribution of the addenda to the total heat capacity for two extreme cases, and for the more typical case. The maximum in the addenda contribution is caused by the very large heat capacities of the grease and varnish used on the addenda. The ratio of the specific heat of Apiezon-N grease (75) to that of copper is shown in Figure B3. Small amounts of grease and varnish have considerable effect on the addenda heat capacity, and could cause serious error in the final sample specific heat determinations if not properly accounted for.

Care had to be taken to ensure that any grease that adhered to the samples was correctly replaced when samples were changed. Typically, 2 to 4 mg of grease would adhere

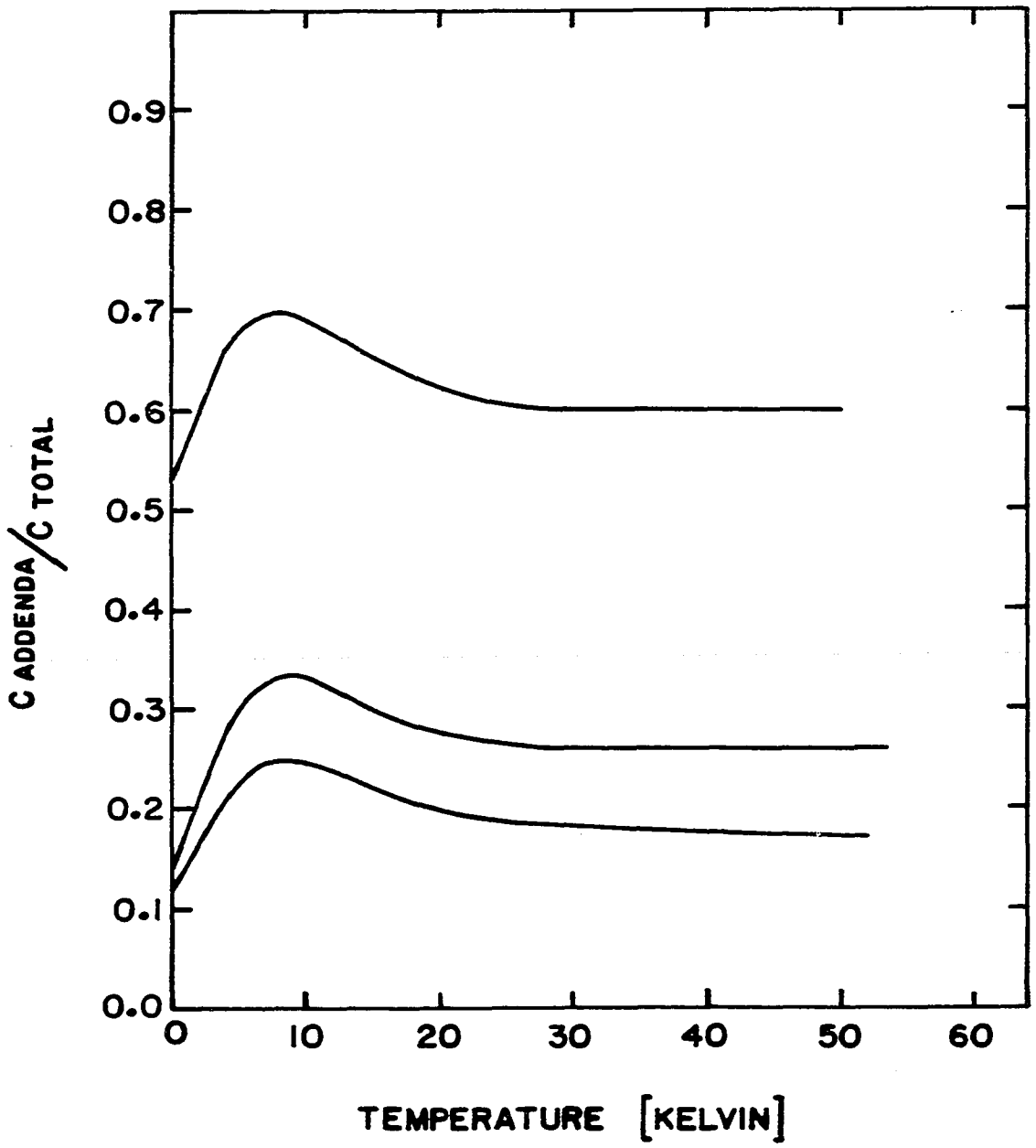

Figure B2. Addenda contribution to the measured heat capacities, shown as the ratio of the addenda to total heat capacities. The top and bottom curves represent the extreme cases and the middle curve represents the more typical case

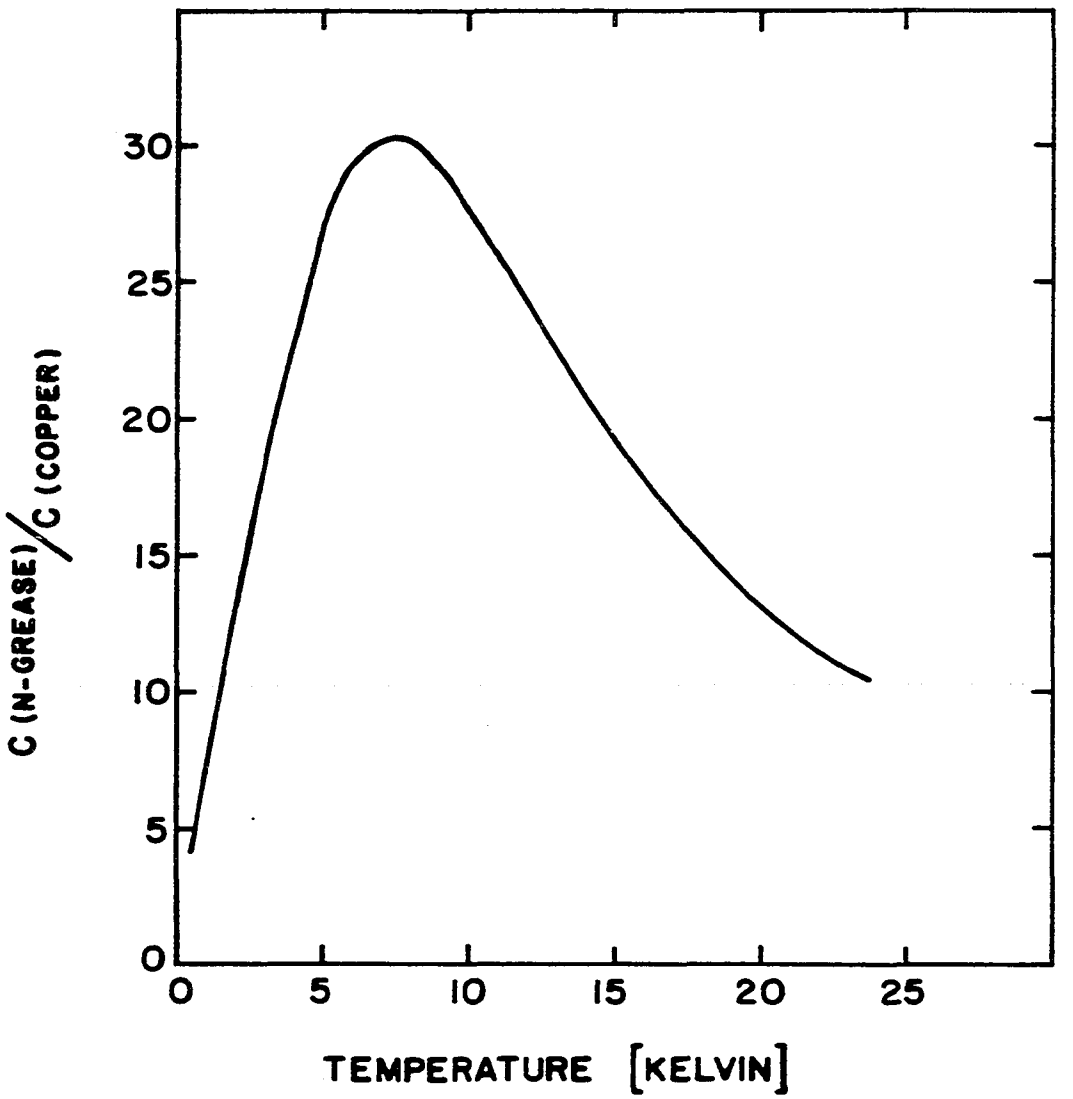

Figure B3. Ratio of the specific heats (per gram) of Apiezon N grease to copper. The grease data were taken from Ref. 75, and the copper data from Table 5

to the samples, as determined by measuring the sample mass both before and after the run. This amount of grease was then applied to the next sample to be run. In all cases, the grease was replaced to within 0.1 mg of the correct value. Figure B4 indicates the possible percent error in a final sample specific heat determination if grease replacement were in error by 1.0 mg. The top curve is the worst case possible (smallest sample), while the two lower curves are representative of nearly all of the samples. Since grease replacement was better than 0.1 mg, the actual errors were probably less than 1/10 of those shown, perhaps 0.02 % at most.

Measurements on the pure copper sample designated RLH copper, discussed in the Experimental Results section, provided a consistency check on the procedures. The same copper sample was run twice, first with the December addenda, and these are the data used for the RLH fits. The second run was done after a series of six Berylco-25 samples had been measured with the April addenda. The deviations of the data for this second run from the first, as described in the Experimental Results section, were insignificant. This consistency between runs, and the close agreement of the results with those of Holste, Cetas, and Swenson (51), indicate that the procedures, including grease replacement, were correct.

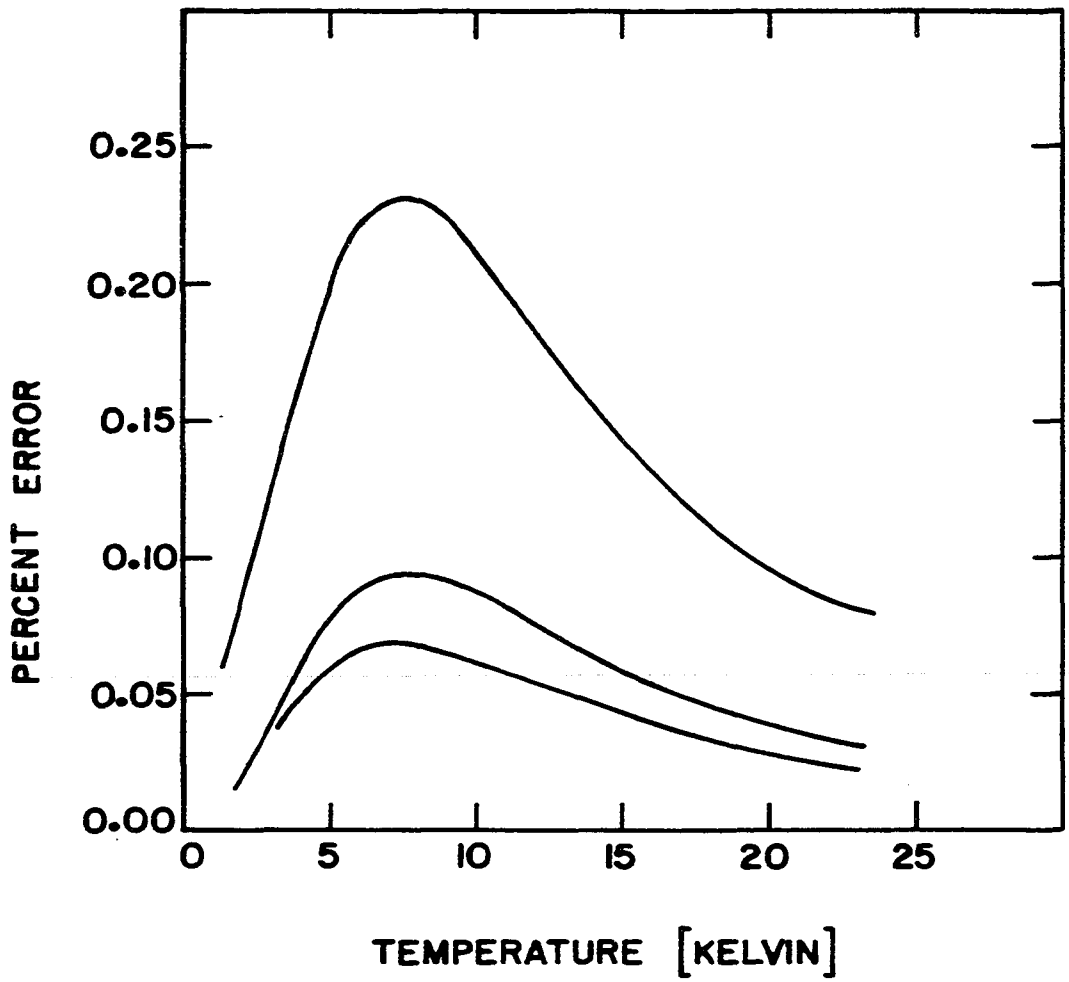

Figure B4. Percent error possible in the sample specific heats for a 1 mg error in grease replacement. The top curve is for the solution-annealed low-iron Cu-Be sample, and represents the worse case. The bottom curve represents the large hexagonal rod samples and the copper sample. The middle curve is for the other samples

Several strange effects were noticed during the course of the heat capacity work. One was the occurrence of excessive random noise levels of up to 20 μV, and sudden shifts of up to 200 μV of the zero-point voltage in the GR15698 thermometry measurements. These were eventually found to correlate with the times that a local AM radio station operating at 1.43 MHz was broadcasting. Unsuccessful attempts were made to deal with the problem by using a low-pass filter in the measuring circuit. In desperation, measurements were done only at night when the station was off the air. The effect was later attributed to RF rectification in the germanium thermometer itself. Krause, and the present author, have previously noted heating effects at temperatures near 1 K due to RF pickup, which corresponded to power inputs of about 5 nW. The very high noise levels and zero shifts at all temperatures was a new effect and caused considerable frustration until the source was understood.

Vibrations at low temperatures are often a major source of extraneous sample heating, in particular those vibrations resulting from the operation of mechanical heat switches. With the first two addenda used for this work, data could not be reliably obtained below 2 K, even though temperatures below 1 K were easily reached before opening the heat switch. With the third addenda, however, the vibrational

heating was very much reduced and data could be taken to 1.1 K with little difficulty. This was unexpected, and it is thought that by attaching the heat switch wire near the bottom of the frame, rather than at the top, accidentally resulted in a more stable configuration. It also is possible that a different jaw arrangement on the September addenda was responsible for the reduced level of vibrations. With the last addenda the heat switch was closed by pushing the wire down under light spring tension rather than forcibly pulling it up. These changes were made simply because there was no room on the September addenda to locate the heat switch at the top, so the results were pleasantly surprising.

Electrical Resistance

For the resistance measurements, the heat capacity addenda was replaced with a 5/8 inch diameter, 2 inch long copper rod. The Berylco-25 strip samples were wound noninductively onto this rod, and held in place with GE 7031 varnish. Thermometer GR15698 was inserted into a hole in the center of the rod, and this unit was secured to the shield.

The samples were cut from 0.01 inch thick, 0.125 inch wide strip. The lengths of approximately one foot were chosen since this was the most that could conveniently wound onto the form. The widths were trimmed with shears to about

1/32 inch, to increase the total resistance of the samples to approximately 0.5 ohms.

The current leads for the four-terminal dc resistance measurements were soft-soldered to the very ends of the sample strips, and the voltage leads attached with small alligator clips a few millimeters away from the current leads. This arrangement was used because it was found that conventional methods of lead attachment, such as soft-soldering, silver-soldering, welding, and the use of conducting paints all produce some contribution to the measured resistance. Any solder used would tend to flow along the sample a short distance, thus short-circuiting part of it. This is an important source of error when the sample resistance is very small. The high temperatures needed for silver-soldering and welding would have affected the physical state of the alloy, so these methods were rejected. Conducting paint inherently results in a weak mechanical joint, and is subject to high noise levels.

The resistance was measured with the same potentiometer system as was used for the heater resistance measurements during the heat capacity experiments. Initially, several currents ranging from 100 μA to 10 mA were tried. This was done in order to determine if local heating of the sample or leads would affect the measured resistance, or if high currents in the vicinity of the germanium thermometer would

disturb the temperature measurements. No current-dependent effects were noted in either case, so all subsequent measurements were done using the highest available currents to obtain maximum sensitivity. Sensitivity of 0.01%, or about 5×10^{-5} ohms for the 0.5 ohm samples, was obtained. These figures probably also represent the accuracy of the results, although no standard samples were measured to verify this. The only problem encountered involved heating of the manganin leads due to the high currents used. This heating increased the boil-off rate of liquid helium condensed in the pot, reducing the running time to only a few hours as compared to 20 hours endurance during a typical heat capacity run. When this was first noticed, a leak in the pot was suspected, and much time and effort was spent trying to locate the leak before the true source of the problem was realized.

The tremendous increase of strength of precipitation-hardened Berylco-25 over that of the solution-annealed condition was very apparent when attempts were made to wind the hardened sample strip around the copper post. Heat treatment had to be done with the sample strip wound around another copper form of 1/2 inch diameter to approximate the desired final shape.

APPENDIX C. EXPERIMENTAL DATA

The following tables list the experimental specific heats in mJ/gm-K for all the samples measured, and the resistance ratios for the two Berylco-25 strip samples. Included in each table are the sample designation, condition, and the sample density and Rockwell hardness if these are known.

The sample conditions listed for the copper-beryllium alloy samples give the temper designation. These are coded as follows: A = solution-annealed; 1/2-H = half-hard; AT(x/y) = initially solution-annealed, precipitation-hardened for x hours at y ^{o}C; 1/2-HT(x/y) = initially half-hard, precipitation-hardened x hours, y ^{o}C.

Table 3 on page 45 summarizes the copper-beryllium alloy sample characteristics. Tables 1 and 2 give the chemical compositions.

Table C1. Copper specific heat

Sample: January copper ("RLH" copper)
Condition: Strain annealed, gold sputtered
Density: 8.94 gm/cc

T (K)	C (mJ/gm-K)	T (K)	C (mJ/gm-K)
4.36	1.104E-01	18.20	5.361E+00
4.66	1.282E-01	19.11	6.281E+00
4.84	1.393E-01	20.10	7.389E+00
5.26	1.683E-01	21.11	8.706E+00
5.52	1.879E-01	23.03	1.153E+01
5.71	2.041E-01	25.21	1.538E+01
6.12	2.413E-01	28.13	2.184E+01
6.63	2.934E-01	32.11	3.249E+01
7.49	4.009E-01	36.22	4.565E+01
8.04	4.842E-01	40.13	5.982E+01
9.11	6.771E-01	45.03	7.781E+01
10.04	8.891E-01	50.28	9.903E+01
12.02	1.485E+00	54.88	1.177E+02
13.96	2.330E+00	60.44	1.390E+02
16.06	3.593E+00	63.61	1.527E+02
17.17	4.444E+00		

Table C2. Copper specific heat

Sample: June copper ("RLH" copper, second run)
Condition: same as January copper,but gold removed

T (K)	C (mJ/gm-K)	T (K)	C (mJ/gm-K)
1.25	1.533E-02	2.11	3.028E-02
1.48	1.886E-02	2.49	3.909E-02
1.66	2.181E-02	3.02	5.406E-02
1.83	2.482E-02		

Table C3. Cu - 2 wt.% Co specific heat

Sample: Cu-Co
Condition: see text, page 37
Density: 8.933 gm/cc

T (K)	C (mJ/gm-K)	T (K)	C (mJ/gm-K)
1.45	2.569E-02	8.07	5.077E-01
1.81	3.229E-02	7.02	3.593E-01
2.28	4.288E-02	10.06	9.090E-01
2.74	5.597E-02	12.58	1.718E+00
3.03	6.545E-02	14.63	2.644E+00
3.49	8.398E-02	18.02	5.295E+00
3.74	9.538E-02	19.77	7.023E+00
4.25	1.208E-01	25.18	1.528E+01
4.38	1.254E-01	30.20	2.726E+01
5.84	2.359E-01	40.17	5.961E+01

Table C4. Low-iron Cu-1.92 wt.% Be specific heat

Sample: SA
Condition: A
Density: 8.264 gm/cc
Rockwell: B65

T (K)	C (mJ/gm-K)	T (K)	C (mJ/gm-K)
1.27	1.894E-02	6.88	3.640E-01
1.33	1.979E-02	7.96	5.297E-01
1.42	2.094E-02	8.17	5.694E-01
1.62	2.532E-02	9.46	8.543E-01
1.69	2.668E-02	9.79	9.411E-01
1.91	3.124E-02	10.99	1.311E+00
2.17	3.732E-02	12.81	2.078E+00
2.17	3.691E-02	13.96	2.723E+00
2.59	4.737E-02	16.04	4.203E+00
2.53	4.704E-02	18.52	6.720E+00
2.82	5.637E-02	20.13	8.796E+00
3.23	7.096E-02	22.07	1.178E+01
3.66	8.966E-02	25.06	1.752E+01
3.98	1.055E-01	27.94	2.416E+01
4.51	1.363E-01	30.31	3.060E+01
4.97	1.679E-01	36.49	5.034E+01
5.17	1.843E-01	37.52	5.400E+01
5.47	2.095E-01	42.09	7.069E+01
5.89	2.490E-01	45.51	8.436E+01

Table C5. Low-iron Cu-1.92 wt.% Be specific heat

Sample: PH
Condition: AT(2/290)
Density: 8.304 gm/cc
Rockwell: C32

T (K)	C (mJ/gm-K)	T (K)	C (mJ/gm-K)
1.16	1.606E-02	8.00	4.867E-01
1.22	1.713E-02	10.03	9.002E-01
1.37	1.951E-02	10.99	1.168E+00
1.97	3.068E-02	14.04	2.436E+00
2.48	4.257E-02	17.09	4.547E+00
2.80	5.175E-02	20.06	7.696E+00
3.10	6.136E-02	20.74	8.585E+00
3.45	7.391E-02	24.10	1.409E+01
3.89	9.314E-02	28.26	2.327E+01
4.31	1.135E-01	33.08	3.707E+01
4.95	1.524E-01	38.24	5.491E+01
5.09	1.619E-01	44.53	7.969E+01
5.91	2.285E-01	50.68	1.041E+02
6.97	3.426E-01		

Table C6. Berylco-25 specific heat

Sample: H6
Condition: A
Density: 8.309 gm/cc
Rockwell: B61

T (K)	C (mJ/gm-K)	T (K)	C (mJ/gm-K)
4.34	1.432E-01	14.56	3.173E+00
4.52	1.550E-01	14.87	3.368E+00
4.71	1.679E-01	16.34	4.530E+00
4.90	1.810E-01	16.63	4.775E+00
5.07	1.949E-01	19.74	8.272E+00
5.23	2.078E-01	20.06	8.729E+00
6.59	3.497E-01	20.43	9.258E+00
6.74	3.690E-01	24.72	1.684E+01
6.90	3.905E-01	25.16	1.764E+01
7.08	4.165E-01	25.58	1.854E+01
7.26	4.438E-01	26.51	2.067E+01
7.44	4.696E-01	27.12	2.210E+01
10.27	1.114E+00	27.75	2.365E+01
10.57	1.210E+00	34.18	4.201E+01
12.02	1.758E+00	34.74	4.395E+01
12.39	1.931E+00	42.12	6.982E+01
13.27	2.374E+00	42.61	7.161E+01
13.54	2.524E+00	43.16	7.406E+01
13.84	2.700E+00	51.54	1.070E+02
14.18	2.908E+00	52.15	1.102E+02

Table C7. Berylco-25 specific heat

Sample: H7
Condition: AT(2/320)
Density: 8.328 gm/cc
Rockwell: C36

T (K)	C (mJ/gm-K)	T (K)	C (mJ/gm-K)
4.41	1.296E-01	19.03	6.671E+00
4.58	1.391E-01	19.63	7.400E+00
5.10	1.741E-01	20.09	7.997E+00
5.26	1.854E-01	20.77	8.879E+00
5.81	2.317E-01	21.42	9.838E+00
6.19	2.680E-01	22.09	1.089E+01
6.89	3.470E-01	23.15	1.269E+01
7.39	4.145E-01	23.59	1.337E+01
8.29	5.557E-01	24.27	1.474E+01
9.10	7.130E-01	26.06	1.843E+01
10.19	9.777E-01	26.96	2.037E+01
12.10	1.606E+00	28.21	2.362E+01
13.61	2.298E+00	32.31	3.505E+01
14.38	2.718E+00	36.59	4.888E+01
15.11	3.184E+00	40.16	6.226E+01
15.96	3.773E+00	47.23	8.920E+01
17.03	4.657E+00	52.03	1.087E+02
17.96	5.525E+00		

Table C8. Berylco-25 specific heat

Sample: H2
Condition: 1/2-H
Density: 8.304 gm/cc
Rockwell: B99

T (K)	C (mJ/gm-K)	T (K)	C (mJ/gm-K)
4.33	1.412E-01	18.04	6.267E+00
4.48	1.507E-01	18.85	7.215E+00
4.69	1.648E-01	19.24	7.789E+00
5.06	1.933E-01	20.27	9.143E+00
5.29	2.128E-01	21.43	1.079E+01
6.36	3.230E-01	23.04	1.371E+01
6.51	3.427E-01	24.11	1.565E+01
8.09	5.897E-01	26.49	2.072E+01
8.43	6.586E-01	27.35	2.279E+01
10.13	1.091E+00	30.58	3.133E+01
11.99	1.771E+00	31.07	3.293E+01
12.15	1.848E+00	36.55	5.066E+01
13.89	2.765E+00	38.10	5.573E+01
14.10	2.899E+00	47.12	8.960E+01
16.60	4.818E+00	49.73	1.002E+02

Table C9. Berylco-25 specific heat

Sample: H8
Condition: 1/2-HT(2/320)
Density: 8.369 gm/cc
Rockwell: C38

T (K)	C (mJ/gm-K)	T (K)	C (mJ/gm-K)
3.50	8.250E-02	16.81	4.368E+00
3.68	9.030E-02	17.52	4.987E+00
3.85	9.780E-02	18.21	5.656E+00
4.01	1.063E-01	18.89	6.377E+00
4.17	1.135E-01	19.58	7.169E+00
4.33	1.221E-01	20.23	7.973E+00
4.61	1.393E-01	20.50	8.294E+00
4.76	1.484E-01	20.96	8.927E+00
4.93	1.600E-01	21.49	9.718E+00
4.98	1.623E-01	22.07	1.062E+01
5.12	1.732E-01	22.67	1.158E+01
5.28	1.852E-01	23.14	1.233E+01
5.29	1.861E-01	23.80	1.352E+01
6.07	2.542E-01	24.45	1.477E+01
6.36	2.849E-01	25.17	1.635E+01
6.65	3.169E-01	25.89	1.769E+01
7.09	3.689E-01	26.63	1.942E+01
7.53	4.326E-01	27.37	2.106E+01
7.91	4.877E-01	28.06	2.276E+01
8.30	5.537E-01	28.69	2.444E+01
8.80	6.484E-01	29.45	2.639E+01
9.27	7.467E-01	30.33	2.881E+01
9.49	7.946E-01	31.27	3.149E+01
9.80	8.693E-01	32.10	3.391E+01
10.17	9.671E-01	35.10	4.357E+01
10.28	9.932E-01	36.13	4.723E+01
10.79	1.139E+00	37.31	5.114E+01
10.83	1.153E+00	37.98	5.354E+01
11.25	1.283E+00	38.69	5.612E+01

Table C9. (Continued)

11.67	1.427E+00	51.15	1.050E+02
12.22	1.634E+00	51.71	1.076E+02
12.88	1.909E+00	52.27	1.100E+02
13.59	2.249E+00	61.00	1.446E+02
14.26	2.585E+00	61.66	1.468E+02
14.96	3.021E+00	62.31	1.494E+02
15.74	3.540E+00	62.96	1.514E+02

Table C10. Berylco-25 specific heat

Sample: H1
Condition: 1/2-HT(21.3/450)
Density: 8.327 gm/cc
Rockwell: B95

T (K)	C (mJ/gm-K)	T (K)	C (mJ/gm-K)
1.33	2.066E-02	9.32	7.405E-01
1.49	2.374E-02	9.63	8.203E-01
1.60	2.550E-02	9.93	8.752E-01
2.08	3.557E-02	12.15	1.569E+00
2.26	3.990E-02	13.79	2.295E+00
2.65	5.023E-02	14.98	2.945E+00
3.08	6.367E-02	16.69	4.189E+00
3.36	7.374E-02	18.07	5.405E+00
3.51	7.984E-02	19.95	7.473E+00
3.86	9.533E-02	23.07	1.204E+01
4.47	1.261E-01	26.99	1.996E+01
4.96	1.640E-01	30.51	2.910E+01
5.40	1.884E-01	34.96	4.244E+01
6.55	2.966E-01	39.91	6.059E+01
8.07	5.082E-01	49.06	9.742E+01
8.19	5.193E-01		

Table C11. Berylco-25 specific heat

Sample: R11
Condition: A
Density: 8.297 gm/cc
Rockwell: B61

T (K)	C (mJ/gm-K)	T (K)	C (mJ/gm-K)
1.24	2.825E-02	7.94	5.523E-01
1.34	3.022E-02	8.78	7.134E-01
1.78	4.015E-02	9.92	1.010E+00
1.90	4.309E-02	12.34	1.896E+00
2.46	5.809E-02	15.00	3.476E+00
2.94	7.439E-02	15.70	4.016E+00
3.42	9.407E-02	20.09	8.822E+00
3.88	1.150E-01	22.36	1.238E+01
4.24	1.363E-01	25.33	1.813E+01
4.47	1.503E-01	30.06	2.993E+01
4.92	1.819E-01	35.11	4.549E+01
5.96	2.759E-01	39.76	6.233E+01
6.95	3.968E-01	50.80	1.048E+02

Table C12. Berylco-25 specific heat

Sample: R12
Condition: AT(1/250)
Density: 8.324 gm/cc
Rockwell: B99

T (K)	C (mJ/gm-K)	T (K)	C (mJ/gm-K)
1.21	2.440E-02	7.90	5.128E-01
1.35	2.596E-02	8.94	7.119E-01
2.08	4.297E-02	10.06	9.847E-01
2.56	5.663E-02	12.55	1.887E+00
2.97	6.981E-02	15.18	3.393E+00
3.59	9.451E-02	17.82	5.665E+00
4.33	1.323E-01	21.19	9.925E+00
4.48	1.415E-01	25.06	1.682E+01
4.97	1.743E-01	30.02	2.903E+01
5.97	2.587E-01	39.86	6.055E+02
6.92	3.674E-01	52.16	1.095E+02

Table C13. Berylco-25 specific heat

Sample: R13
Condition: AT(2/250)
Density: 8.330 gm/cc
Rockwell: C23

T (K)	C (mJ/gm-K)	T (K)	C (mJ/gm-K)
1.19	2.303E-02	7.39	4.306E-01
1.32	2.556E-02	8.48	6.147E-01
1.84	3.698E-02	10.94	1.246E+00
2.08	4.200E-02	14.02	2.626E+00
2.74	6.098E-02	17.07	4.912E+00
3.42	8.576E-02	19.62	7.657E+00
3.96	1.104E-01	22.00	1.116E+01
4.29	1.283E-01	26.99	2.116E+01
4.95	1.706E-01	31.27	3.271E+01
5.97	2.569E-01	36.23	4.847E+01
6.11	2.727E-01	43.52	7.591E+01

Table C14. Berylco-25 specific heat

Sample: R14
Condition: AT(4/250)
Density: 8.334 gm/cc
Rockwell: C29.5

T (K)	C (mJ/gm-K)	T (K)	C (mJ/gm-K)
1.22	2.439E-02	7.02	3.731E-01
1.31	2.571E-02	8.42	5.933E-01
1.55	3.041E-02	8.75	6.554E-01
1.93	3.887E-02	10.99	1.239E+00
2.25	4.613E-02	12.00	1.607E+00
2.72	6.137E-02	14.94	3.173E+00
3.33	8.138E-02	17.64	5.403E+00
3.84	1.037E-01	20.20	8.388E+00
4.33	1.293E-01	22.23	1.139E+01
4.62	1.466E-01	25.12	1.681E+01
5.32	1.963E-01	30.33	2.974E+01
6.08	2.639E-01	36.47	4.933E+01

Table C15. Berylco-25 resistance

Sample: S1
Condition: A
Density: 8.308 gm/cc (x-ray density)

T (K)	R(T)/R(293)	T (K)	R(T)/R(293)
1.206	0.75625	10.939	0.75397
1.505	0.75623	11.924	0.75376
1.884	0.75600	14.300	0.75352
2.165	0.75590	16.414	0.75333
2.641	0.75575	18.043	0.75321
3.262	0.75557	20.125	0.75318
3.738	0.75546	22.067	0.75321
4.291	0.75532	24.242	0.75335
4.427	0.75526	26.223	0.75362
4.593	0.75521	31.467	0.75472
4.768	0.75519	36.213	0.75633
4.959	0.75513	41.321	0.75853
5.158	0.75509	46.236	0.76120
5.378	0.75503	52.068	0.76468
6.013	0.75490	54.720	0.76646
6.910	0.75463	59.101	0.76949
7.894	0.75445	64.091	0.77346
7.975	0.75443	69.232	0.77750
8.829	0.75426	75.380	0.78272
9.956	0.75412	77.882	0.78502

Table C16. Berylco-25 resistance

Sample: S2
Condition: AT(2/320)
Density: not known

T (K)	R(T)/R(293)	T (K)	R(T)/R(293)
1.636	0.67900	13.980	0.67724
1.784	0.67897	15.843	0.67721
2.052	0.67882	18.075	0.67721
2.635	0.67864	19.955	0.67732
3.222	0.67853	21.975	0.67746
3.759	0.67838	24.040	0.67776
4.204	0.67827	25.926	0.67809
4.300	0.67823	31.190	0.67970
4.479	0.67816	36.318	0.68208
4.729	0.67812	41.233	0.68505
5.067	0.67805	46.181	0.68868
5.459	0.67801	51.673	0.69348
5.959	0.67798	54.360	0.69597
6.507	0.67787	58.705	0.70022
7.758	0.67772	63.935	0.70572
8.820	0.67761	69.001	0.71132
9.753	0.67750	75.376	0.71869
10.696	0.67743	77.850	0.72166
11.841	0.67735		